Respiratory Patterns Classification using UWB Radar

Zixiong Han

Thesis submitted to the University of Ottawa
in partial Fulfillment of the requirements for the

MASTER OF APPLIED SCIENCE

in Electrical Engineering and Computer Science

School of Electrical Engineering and Computer Science

Faculty of Engineering

University of Ottawa

Abstract

Radar-based respiration monitoring has been increasingly popular among researchers in biomedical fields during the last decades since it is a contactless monitoring technique. It is very convenient for subjects because it does not impose any restrictions on subjects or require their cooperation. Meanwhile, recognizing alternations in respiratory patterns is an important early clue of the diagnosis of several cardiorespiratory diseases. Thus, a study of biomedical radar-based respiration monitoring and respiratory pattern classification is carried out in this thesis.

Radar-based respiration monitoring technology has a shortcoming that the collected respiratory signal will be easily distorted by the body movement of the monitoring subjects or disturbed by environment noise because of the contactless measurement attribute. This shortcoming limits the application of the respiratory pattern classification model, that is, the existing models cannot be applied automatically since the distorted respiratory signal needs to be manually filtered out ahead of the classification. In this study, a new respiratory pattern classification strategy, which can be implemented full-automatic, is proposed. In this strategy, a class “moving” is introduced to classify the distorted signal, and the sampling window length is shortened to reduce the effect caused by the signal distortion. A performance requirement for the continuous respiratory pattern classification is also proposed based on its expected function that can alert the occurrence of the abnormal breathing patterns.

Several models which can meet the proposed performance requirement are developed in this thesis based on the state-of-the-art pattern classification technique and the time-series-based shapelet transform algorithm. The proposed models can classify four breathing patterns including eupnea, Cheyne Stokes respiration, Kussmaul breathing and apnea. A radar-collected respiratory signal database is built in this study, and a respiration simulation model which can generate breath samples for pattern classification is developed in this thesis.

The proposed models were tested and validated in batch and stream processing manner with independently collected data and continuously collected data, respectively.

Acknowledgments

I would like to express my deepest appreciation to Professor Miodrag Bolic for his guidance in the thesis, and his trust, encouragement, support and patience over these three years. He gave me the chance to start my research on health device design, which is my dream in my graduate career, and led me into the field of radar-based health monitoring, which I am enthusiastic about.

I would like to thank Dr. Varun Mehta, who set a good example for me in the comprehensive research. He broadened my horizon, and taught me how to be a professional learner. I would like to thank Shan He, who always shares his experience with me and guides me to build up my research career. I would like to thank Fan Yang, my best friend here, who always cooperates well with me, no matter in the study, research, and life, and he is always willing to help me. I would like to thank Rhajitha Hathurusinghe, who always inspires me to work hard and smarter. He also showed me the skills and the professionalism of an engineer. I would like to thank Cristovao Iglesias, who always trusts me, inspires me, and is willing to share his ideas with me.

Special thanks to the University of Ottawa, who provides me the platform to start my graduate study and the academic resources for my research. Thanks also go to Sarah Plamondon and the University of Ottawa Heart Institute who provides me the platform to collect data and test our devices.

I gratefully acknowledge the assistance of Yao Yang, Yuxuan Li, and the University of Ottawa Makerspace, who helped to design and manufactured the radar enclosure we used in this study.

I would like to acknowledge the help of volunteers who participated in my experiment to perform the respiratory pattern simulation.

Finally, I am extremely grateful to my parents and my girlfriend Jiadi. I would not realize my achievement today without their support, encouragement, and love.

List of abbreviations

AHI	Apnea-hypopnea index
BI-AT-GRU	Bidirectional and attentional gated recurrent unit
BSD	Berkeley Source Distribution
CPAP	Continuous positive airway pressure
CSR	Cheyne Stokes respiration
CTMC	Continuous-Time Markov Chain
CWT	Continuous wavelet transform
CW	Continuous wave
DT	Decision trees
DTW	Dynamic time warping
ECG	Electrocardiogram
FFT	Fast Fourier transform
FMCW	Frequency modulated continuous wave
FS	Fast shapelet
GRU	Gated recurrent unit
ICU	Intensive care unit
IG	Information gain
IR-UWB	Impulse radio ultra-wide band
LNA	Low-noise amplifier
LS	Learned shapelet

MEMS	Microelectromechanical system
PRF	Pulse repetition frequency
PSG	Polysomnogram
RBF	Radial basis function
RF	Radio-frequency
RF	Random forest
SNR	Signal-to-Noise Ratio
SOC	System-on-chip
ST	Shapelet transform
SVM	Support vector machine
TSC	Time series classification
UWB	Ultra-wideband

List of definition

- **Algorithm** is a finite sequence of well-defined, computer-implementable instructions, typically to solve a class of problems or to perform a computation.
- **Breathing signal** is the same as **respiratory signal** in this thesis, indicating the measurement data of respiration.
- **Breath sample** is a segment in the breathing signal
- **Breathing pattern** is the same as **respiratory pattern** in this thesis, including eupnea, Cheyne Stokes respiration, Kussmaul breathing and apnea.
- **Class** is the same as **category** in this thesis. Both of them indicate a group or a collection sharing the same characteristic or attribute.
- **Classification** is an example of pattern recognition, which is attempt to assign each input value to one of a given set of classes.
- **Classifier** is an algorithm that implements classification, especially in a concrete implementation.
- **Feature** is an individual measurable property or characteristic of a phenomenon being observed, which serves as the input for an algorithm.
- **Hyperventilation** is rapid or deep breathing, composed of the crescendo phase and decrescendo phase of the breathing tidal volume. It is a sub-period of Cheyne Stokes respiration.
- **Label** is the name of a **class**.
- **Models** in machine learning are the output of algorithms and are composed of model data and a prediction algorithm.
- **Prediction** refers to the output of a classification algorithm after it has been applied to new data to forecast the likelihood of a particular outcome.
- Pattern **recognition** is the assignment of a label to a given input value.
- **Respiration pulse** refers to the waveform of a cycle of inhalation and exhalation.
- **Ventilation** is the exchange of air between the atmosphere and the lungs which achieved by the physical act of breathing.

Contents

List of Figures

List of Tables

Chapter 1: Introduction and Motivation

This chapter introduces the research objectives and motivations. It also introduces the major contribution of this work and ends by presenting the organization of the thesis.

1.1 Introduction

Nowadays, people pay more attention to their health. Along with the development of science and technology, more and more biomedical instruments become accessible to ordinary people. People start to have more interest to know about their vital signs in daily life, so as to have a better understanding of their physical state. Breathing is one of these signs. It contains physiological information of respiratory rate, tidal volume and blood oxygen level. Medical doctors and researchers also test the breathing functions to monitor, diagnose and treat lung and cardiovascular disease.

The existing respiration monitoring devices can be classified into two categories, contact-based and non-contact based [1]. The contact-based respiration monitoring is mainly based on one of the following parameters: respiratory sounds, respiratory airflow, respiratory-related chest or abdominal movements, respiratory CO_2 emission and oximetry probe SpO_2. There is also technique that can extract breathing information from the electrocardiogram (ECG). The non-contact based respiration monitoring includes radar-based vital signal monitoring technique which detects the respiratory-related chest or abdominal movements, optical-based respiration monitoring technique which detects thoracic movements, and thermal sensor and thermal image based respiration monitoring which analyzes the temperature variation of face area during the respiration.

In this thesis, we used an Ultra Wide Band (UWB) radar to collect the respiratory signal and focus on classifying the breathing patterns of the subjects. We employed machine learning-based classification with traditional statistic feature extraction and the state-of-the-art time-series-based feature extraction to classify four breathing patterns: eupnea, Cheyne Stokes respiration, Kussmaul breathing and apnea. We also proposed a respiration simulation model that can

simulate the above four respiratory patterns to generate high-quality breath samples for the model training.

1.2 Motivation

Breathing patterns, which consists of tidal volume and respiratory rate, are important diagnostic criteria for many diseases [2]. Generally, abnormal breathing patterns are induced by injury of respiratory centers, use of narcotic medications, metabolic derangements, and respiratory muscle weakness [3]. In some cases, it may even be caused by stroke, heart failure [4], and brain damage [5]. Thus, recognition of abnormal breathing patterns is of great importance for health monitoring and disease prognosis. Take the three abnormal breathing patterns, Cheyne Stokes respiration, Kussmaul respiration and apnea as examples: the health status of patients with cardiovascular disease can be assessed based on the occurrence frequency of Cheyne Stokes respiration during sleep; ordinary subjects who have a high risk of cardiovascular disease will be alerted when the Cheyne Stokes respiration occurs in their sleep. Patients with severe metabolic acidosis symptoms can be noticed if Kussmaul breathing occurs and is recognized [3], and subjects with cardiac arrest may also be noticed based on the cessation of respiration [6].

Meanwhile, the most commonly used respiration monitoring instruments are contact-based. Contact-based instruments may make the user uncomfortable, confine the subject with cables, and even influence the breathing pattern of the subject [1]. All situations above may influence the accuracy and credibility of the vital signs measurement. By contrast, non-contact measuring techniques, including radar-based, optical-based and thermal-imaging-based respiration monitoring, do not cause the disturbance listed above. These techniques free the subject from electrodes or straps, which can even be applied in some cases where the contact-based methods are inappropriate, such as the monitoring of infants or subjects with a burn or chemical contamination. Comparing with the optical-based and thermal-imaging-based techniques, the radar-based technique is less affected by the ambient light and surface clothing disturbance, and it raises fewer concerns about privacy violation as well. Therefore, the radar-based respiration monitoring technique is more suitable for long-term respiration monitoring.

Radar has been applied in many scenarios in biomedical fields. In addition to respiration monitoring, it can also be applied in heart rate monitoring [7], fall detection, gait abnormality recognition [8], etc. The non-contact nature of signal measurement, the strong penetration attribute of radar wave, and the advantage of seldomly causing privacy violation issue make the biomedical radar applicable in many fields. Thus the application of biomedical radar has a great development potential. The experience and technology summarized from the respiratory pattern classification research can also be applied to other similar application scenarios and provide more ideas for signal pattern classification.

1.3 Objectives and Contribution

In this thesis, we aimed to develop a radar-based respiratory pattern classification model which can be implemented full-automatically, which means that the respiratory signal collected by radar can be directly input into the model to obtain the respiratory pattern without any human intervention. The possible output of the model include labels of eupnea, Cheyne Stokes respiration, Kussmaul breathing, apnea and others. The label “others” is for the samples whose pattern cannot be clearly identified as the respiratory patterns mentioned above or samples which do not belong to any of them. Most of the samples with the label “others” are breath samples distorted by the random movement of monitoring subjects.

The contributions of this thesis are listed as follow:

1. Developed a respiration simulation model for the radar-based respiratory pattern classification model training. The model is able to simulate samples of four respiratory patterns: eupnea, Cheyne Stokes respiration, Kussmaul respiration and apnea. The output of the simulation model had been verified that they could be used as a substitution for the radar-collected respiratory signal.
2. On the basis of the existing radar-based respiratory pattern classification methods, introduced a new class “moving” for the distorted breath signal and shortened the sampling window length to reduce the impact from the signal distortion.
3. Optimized the existing radar-based respiratory pattern classification models by introducing the time-series-based shapelet transform algorithm and hierarchical classification.

4. Implemented the proposed respiratory pattern classification models in batch and stream processing scenarios, and validated their effectivity according to their performances in the experiments.

1.4 Thesis overview

The thesis consists of seven chapters in total. Chapter 1 introduces the objectives and motivations of this research. Chapter 2 introduces the background of breathing patterns, radar technology, machine learning technique and time series classification. Chapter 3 reviews the state-of-the-art techniques in the respiration simulation model and respiratory pattern classification. Chapter 4 introduces the existing problems in the state-of-the-art study, their potential solutions, and the performance requirements for the proposed model. Chapter 5 demonstrates the respiration simulation model, breathing pattern classification models, and the application of the shapelet transformation algorithm in the respiration study. Chapter 6 is about the implementation of the proposed model in the real environment. After analyzing the performance of the models, we found the most suitable implementation scenarios for each model, including the real-time stream processing and offline batch processing. Chapter 7 concludes this thesis by summarizing the major contents, contributions, faced challenges, and future directions of this research.

Chapter 2: Background

This chapter presents the background knowledge of the topics this thesis is based on. The details of breathing patterns, radar theory, supervised machine learning, and the time series classification are introduced in the following subsections.

2.1 Breathing patterns

In this study, we mainly focus on four breathing patterns: eupnea, apnea, Cheyne Stokes respiration and Kussmaul breathing. They are the most common and most typical respiratory patterns.

Eupnea is the term of normal breathing for an individual at rest. It comprises inspiratory and expiratory phases, with a frequency of 12-20 times per minute [3]. The illustration of eupnea waveform is shown in Fig. 2-1.

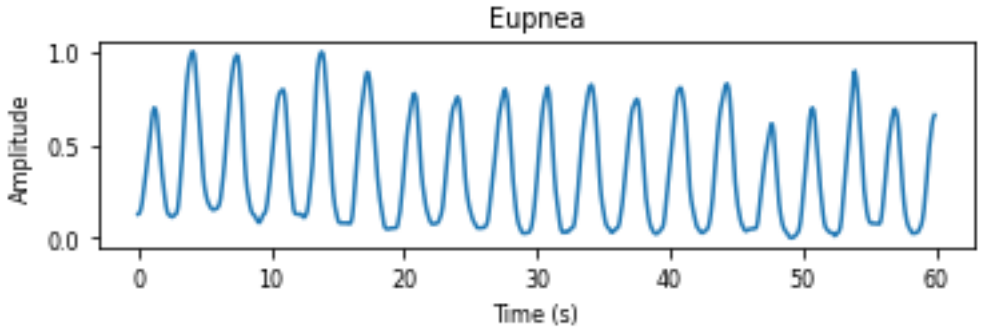

Fig. 2-1 Eupnea

Apnea is a transient breathing cessation characterized by the absence of nasal flow and pressure along with absent chest effort. It can be caused by an injury to the cervical spine or the base of the skull, neurodegenerative illnesses, primary hyperventilation syndrome, and the use of medications like narcotics [3]. An example of apnea is shown in Fig. 2-2.

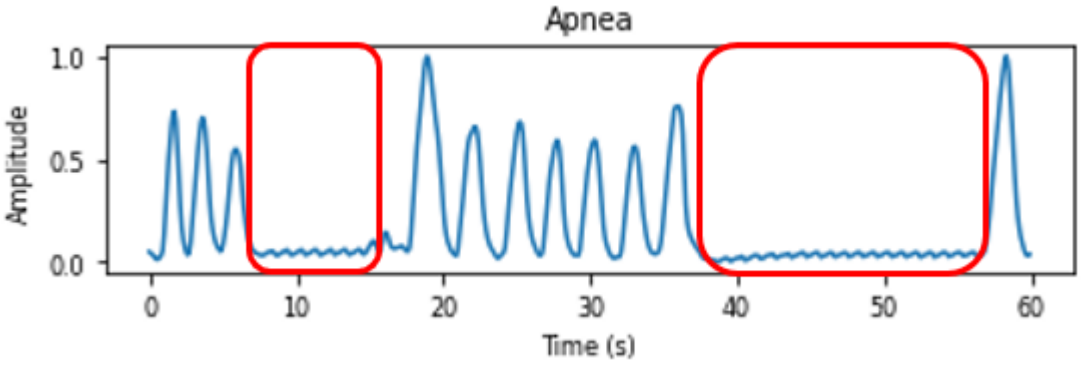

Fig. 2-2 Apnea (Segment in the red box)

Cheyne Stokes respiration (CSR) is an abnormal breathing pattern that often appears in patients with stroke, heart failure, brain tumor, traumatic brain injury. It is also related to carbon monoxide poisoning, metabolic encephalopathy, altitude sickness, narcotics use, etc. [3] A Cheyne Stokes respiration cycle is comprised of a crescendo, decrescendo phase, and a followed apnea phase, as shown in Fig. 2-3. The total length of a Cheyne Stokes respiration cycle is around 45-90 seconds [9]. In each CSR cycle, there is a phase of gradual increase in volume and frequency, following by a phase of gradual decrease in volume and frequency, and a phase of apnea lasting 10 - 30 seconds.

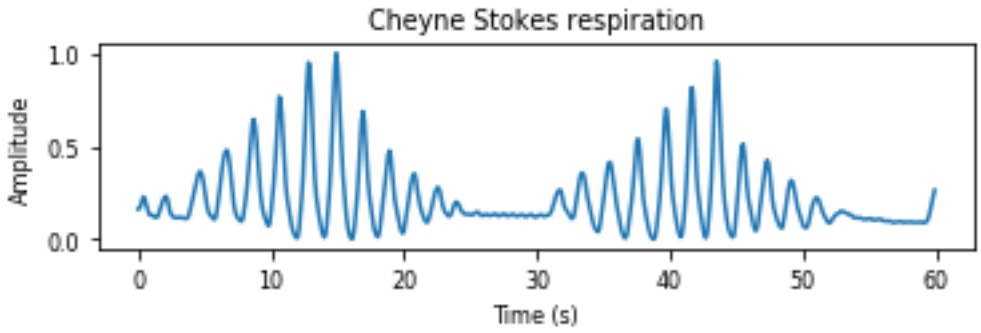

Fig. 2-3 Cheyne Stokes respiration

Kussmaul breathing is a deep and labored breathing pattern characterized by increased breathing rate and depth, as shown in Fig. 2-4. It is a respiratory compensation for a metabolic acidosis, with a breathing frequency over 20 times per minute [10].

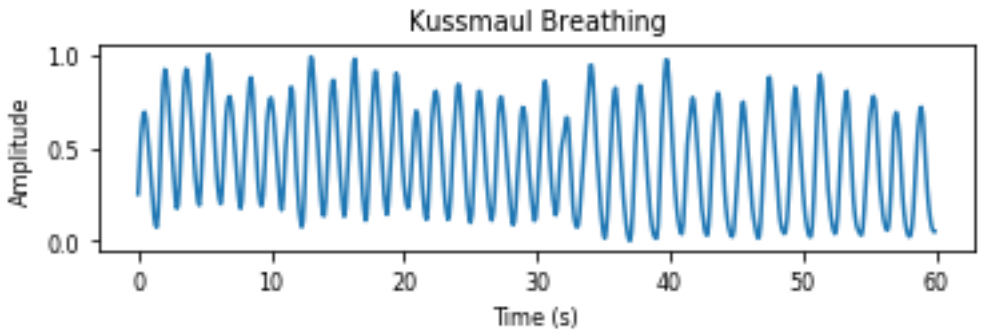

Fig. 2-4 Kussmaul breathing

2.2 Radar technology for medical applications

Biomedical radar is a sensor device that detects or monitors biological subjects with electromagnetic wave. It can acquire the physiological, motion and location-related information of the subjects [11]. It is based on the delay of the received reflected signal time relative to its transmission time, or the phase variation of the reflected signal caused by movements of the target body or organ. It uses the electromagnetic wave which can penetrate dielectric obstacles to detect the movement contactlessly and remotely. Biomedical radars are mostly investigated in contactless sensing of vital movements like respiration and cardiopulmonary activity [7], and they can also be applied in human tumor detection or fall detection [12]. Because of the characteristics of biomedical radars that they do not restrain the subject during the monitoring and less cause issues about privacy violation, they are suitable for long-term health monitoring

The three main categories of biomedical radar are the ultra-wideband (UWB) pulse radar, the continuous-wave (CW) radar, and the frequency modulated continuous wave (FMCW) radar. For remote vital signs monitoring, the radar performance depends on resolution and detecting range. Based on the research from Pisa et al. [13] that reviewed a series of radar-based breath activity monitoring, it concluded that comparing with the CW radar and the FMCW radar, the UWB radar has higher resolution and maximum detection range in the same power consumption level; hence it is more suitable for breath activity monitoring.

2.3 Ultra wideband radar

The biomedical radar employed in this study is ultra-wideband (UWB) pulse radar. The operating period of ultra-wideband pulse radar comprises a short active phase which emits a short pulse and a long pause phase which receives the reflected pulse. The transmission pulse is in a duration of several nanoseconds, and the pause could be in a duration of several milliseconds. Since the transmitting radio-frequency (RF) pulse of UWB radar is in a nanosecond order, the transmitting signal has a very wide bandwidth in the frequency domain (Pulse width is inversely proportional to bandwidth.); hence the radar falls in to the category of ultra-wideband (UWB) radar [14]. According to the definition from FCC, ultra-wideband signals are signals that occupy a 10-dB bandwidth of greater than 500 MHz band-width or larger than 20% fractional bandwidth over the unlicensed frequency range of 3.1-10.6 GHz. The fractional bandwidth is defined as shown in (2-1).

$$Fractional\ Bandwidth = \frac{2(f_H - f_L)}{f_H + f_L} \tag{2-1}$$

where f_H and f_L are the upper and lower frequency limits of the 10-dB bandwidth, respectively.

Compared to the CW radar, the UWB radar has the advantages of fine resolution, long detecting range, high multipath resolution, low interference with other existing signals and reduced signal diminishing [15]. Owing to the superiority mentioned above, UWB radar is also applied in commercial applications of medical imaging, ground penetration detection, and material characterization [16].

2.3.1 UWB radar theory

The UWB impulse radar works by transmitting an impulse signal modulated by carrier frequency. A Gaussian impulse UWB radar is employed in this thesis. The Gaussian impulse can be expressed as shown in (2-2).

$$p(t) = a \cdot \exp\left(-\frac{(t - \frac{T_p}{2})^2}{2\sigma_p^2}\right) \tag{2-2}$$

where a is the maximum amplitude, T_p and σ_p^2 are the duration and the variance of the Gaussian pulse, respectively.

Then the pulse is modulated with a high frequency carrier signal, as shown in Fig. 2-5. A typical UWB pulse transmitter consists of a pulse generator and a digitally controlled modulator circuit which controls the timing or polarization of the transmitted pulse signal. In this research, the Novelda® Xethru radar module X4M03 transmits bi-phase pulses, that is, the input signal from "Data In" alternates between 1 and 0, with 180 degree phase shift between each other. The local oscillator determines the pulse repetition frequency (PRF) of the UWB impulse signal, and the pulse generator produces pulse signal with a desired waveform such as the Gaussian pulse. Each pulse corresponds to one radar scan.

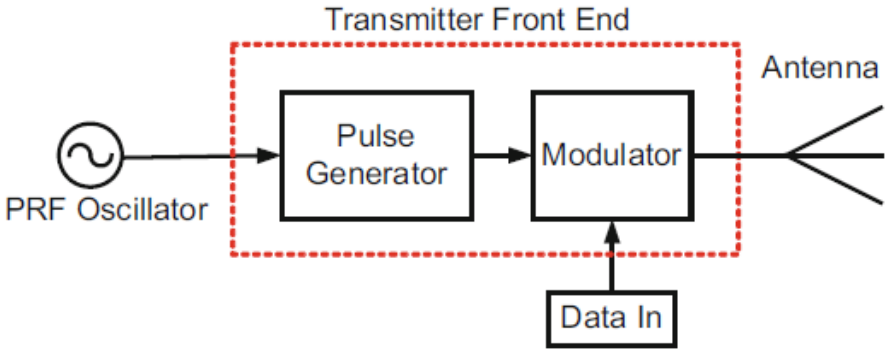

Fig. 2-5 Block diagram of a typical pulse UWB transmitter

The transmitted signal in time domain after these steps for the ith scan is given by (2-3)

$$s_i(t) = p(t - iT_f) \cdot \cos\left(2\pi f_c\left(t - iT_f\right)\right) \tag{2-3}$$

where,

f_c	Carrier frequency
f_p	Pulse repetition frequency
T_f	Duration of scan $T_f = \frac{1}{f_p}$

Let us define a local scan time variable t_f as $t = t_f + iT_f$ with $t_f \in [0, T_f]$ to simplify (2-3). The transmitted signal for scan i can now be written as:

$$s_i(t_f) = p(t_f) \cdot \cos(2\pi f_c t_f) \tag{2-4}$$

A typical UWB receiver circuit consists of a low-noise amplifier (LNA), a correlation circuit and a template pulse generator, as shown in Fig. 2-6. The oscillator drives the pulse generator and determines the pulse repetition frequency (PRF) of the UWB impulse system. After passing the LNA, the received pulse is coherently correlated with the template pulse generated by the pulse generator through the correlator, then the pulse is converted into a baseband signal by the correlator. The returned signal from a single target for the ith scan is given by (2-5) [17].

$$r_i(t_f) = G_{Rx} \cdot L(t_f) \cdot s_i\left(t_f - \tau(t)\right) \tag{2-5}$$

where,

G_{Rx}	Receiver amplifier (LNA) gain
$\tau(t)$	Propagation delay equal to the radar pulse round-trip time
$L(t)$	Free space loss

and,

$$\tau(t) = \frac{2 \cdot R(t)}{c} = \frac{2 \cdot R(t_f + iT_f)}{c} \tag{2-6}$$

where,

$R(t)$	Range to target
c	Speed of light

And the free space loss $L(t)$ is given by $L(t) = \sqrt{\frac{P_r}{P_t}}$, where P_t and P_r are the transmitted power and received power, respectively.

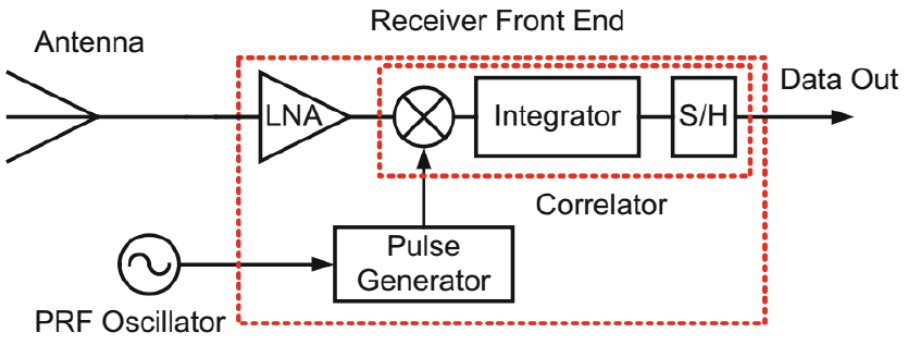

Fig. 2-6 Block diagram of a typical pulse UWB receiver

In the radar-based respiration study, the range $R(t)$ can be written as (2-7):

$$R(t) = d_0 + m_b \sin(2\pi f_b t) \tag{2-7}$$

where d_0 is the distance between the radar and subject, m_b and f_b is the amplitude and the frequency of respiration, respectively.

From the perspective of signal components, the received signal can be presented as the sum of the channel response of the receive antenna and the distance variation caused by respiration [18], as (2-8):

$$r(t,\tau) = \sum_i A_i p(\tau - \tau_i) + Ap(\tau - \tau_d(t)) \tag{2-8}$$

where $p(t)$ is the normalized received pulse, A_i is the amplitude of each multipath component, τ_i is the delay of each multipath and A is the amplitude of the body reflection pulse. The time delay τ_d is modeled as the sum of the time-of-flight τ_0 and sinusoidal delays τ_b associated with respiration, as shown in (2-9).

$$\tau_d(t) = \frac{2d(t)}{c} = \tau_0 + \tau_b \sin(2\pi f_b t) \tag{2-9}$$

There are two important concepts in UWB radar to explain the meaning of the collected signal, slow time and fast time. In a radar scan which stored the received radar signal, slow time is the time between each pulse and fast time is the time between each sampling instance in the receiver [14]. Fast time can be regarded as the traveling time of the electromagnetic wave to a certain distance, and each destination is in the form of a small range. Therefore, each fast time index corresponds to a "range bin". Consequently, fast time corresponds to the distance of a

subject from the radar, and the samples in each range bin records the variation in the certain distance range.

The received signal is in a form of matrix R_{IR}, which is the measurement of the dynamic content in the fast time at the discrete moment of the slow time.

2.3.2 Novelda Xethru X4 UWB radar

This research is conducted on the Novelda® XeThru X4M03 UWB radar. X4M03 is a development kit for the XeThru X4 ultra-wideband (UWB) impulse radar system-on-chip (SoC), as shown in Fig. 2-7. The development programming language of the sensor is Python. The X4 UWB impulse radar SoC combines a transmitter, which can operate at center frequencies of either 7.29 GHz or 8.748 GHz , with a direct radio frequency (RF) sampling receiver and a fully programmable system controller [19]. The radar is equipped with 6-8.5 GHz directional patch antennas with a beamwidth of 65° in both azimuth and elevation axes.

The radar transmits a pulse and samples it with multiple parallel samplers. The X4 SOC generates and transmits the bi-phase pulses (Pulses with 180 degree phase shifts), and after receiving the reflective pulse, it samples, filters and decimates the RF data into a complex base-band data by an optional down conversion processing [14].The radar sampling rate is up to 200 scans per second in slow time. The detection range can be set to up to 25 m by programming the chip [20]. The X4 SOC can communicate with external devices via a USB interface.

Fig. 2-7 Novelda® XeThru X4M03 UWB radar

In this thesis, the X4 chip operated at a center frequency of 7.29 GHz, and the maximum detected range was set to 9.75 m away from the radar. The output data is in the form of a matrix, as shown in Fig. 2-8. The rows represent the radar scan in slow time and the columns represent the samples in fast time (corresponding to range bins). The range resolution of the X4 radar is

approximately 5 cm, hence there are 187 columns in the data matrix. The sampling rate in slow time was set to 17 scans per second.

		Fast time					
	Timestamp(ms)	Distance d1	d2	...	...	d(N-1)	d(N)
Slow time	254.12	7.0195e-06+2.1557e-06i	5.7537e-07+6.0299e-06i	...	...	-0.00021081+0.00019418i	-3.9731e-05+0.000357i
	269.9	6.1373e-08-2.1711e-05i	-2.6851e-07-2.3958e-05i	...	...	-0.00020656+0.00023399i	-2.6444e-05+0.00040573i
	276.64	3.7821e-06+5.3087e-06i	-1.6601e-05+5.3394e-06i	...	...	-0.00020371+0.00024688i	-3.7606e-05+0.0004245i
	281.08	-2.4434e-05-4.8791e-06i	-2.2593e-05-3.8435e-06i	...	...	-0.00021681+0.0002391i	-3.1691e-05+0.00041293i
	311.97	3.4522e-07-2.089e-05i	-9.812e-06-1.1362e-05i	...	...	-0.0001923+0.00022037i	-2.8845e-05+0.00039308i
	357.11	6.6052e-06+1.0679e-05i	-9.8196e-07+1.8542e-05i	...	...	-0.00020202+0.00022329i	-3.4054e-05+0.00038985i
	415.68	-5.5466e-06-2.57e-06i	-2.8431e-05-6.3751e-06i	...	...	-0.00019217+0.00021679i	-1.855e-05+0.00038089i
	...	...	...	...	...	...	...
	...	...	...	...	...	...	...
	65039	-2.4733e-05-2.9689e-06i	-2.7579e-05+4.9712e-06i	...	...	-0.00019696+0.00023495i	-1.5489e-05+0.00039882i
	65097	-3.4752e-06-1.4453e-05i	-1.723e-05-1.7576e-05i	...	...	-0.00016443+0.00021139i	-2.6467e-06+0.00037095i
	65159	-1.0142e-05-1.4162e-05i	-1.9816e-05-2.5777e-06i	...	...	-0.00020235+0.00023793i	-2.6275e-05+0.0003949i
	65222	-1.9946e-07+2.2585e-05i	-2.3467e-05+1.4215e-05i	...	...	-0.00016588+0.00021666i	-1.5059e-05+0.00038757i

Fig. 2-8 Data format used for collecting data from the XeThru X4M03 UWB radar

The distance index shown in Fig. 2-8 is the index of range bin which covering a space around 0.05 m, and each range bin records the reflected wave samples from the corresponding distance range; thus, we can extract the respiratory signal of the biological subject from the range bin corresponding to the distance from the radar to the subject's chest wall. The respiratory signal is obtained by implementing a series of processing on the extracted signal, including calculating the phase angle of the signal to demodulate the signal, unwrapping the phase data to recover the linearity of the measurement to chest movement, and concatenating the phase values according to the time order [11]. A sample of normalized original radar-collected respiratory signal is shown in Fig. 2-9.

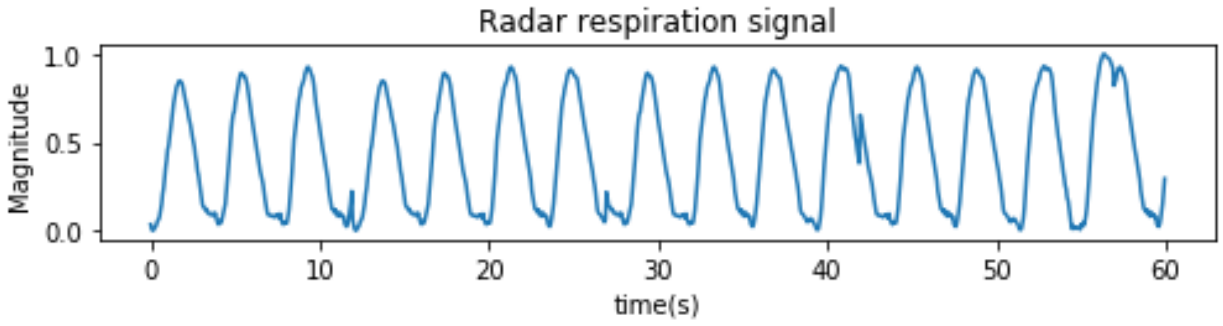

Fig. 2-9 Raw radar collected respiratory signal

2.4 Target localization in the radar-based respiration study

The premise of radar-based respiration analysis is obtaining the exact distance between the radar and the target. The respiratory signal is extracted from the radar range bin corresponding to the radar-target distance. We divided the radar-target distance measuring methods into two categories according to the distance measurement is done, which are 1. the distance-measurement based on the radar signal itself and 2. the external device-based measurement.

The first category is based on radar signal processing, where the range bin index is estimated by eliminating the clutter and highlighting the motion information. Rivera [21] selected the range bin by computing the energy content of all filtered waveforms and identifying the fast-time bin indices where the most significant energy is contained. Chang [22] proposed a CLEAN algorithm to detect the target, and Nguyen [23] modified the CLEAN algorithm to improve its performance. Both of them were developed based on UWB radar data. CLEAN algorithm detects the target by computing the cross-correlation between a scan range bin data and a pre-input template waveform, and if the cross-correlation is larger than a pre-defined threshold, it claims that the target is detected. Gunasekara [14] and Khan [24] in their IR-UWB radar research selected the radar bin data by choosing the column with the highest variance in the radar received matrix (along the fast time axis). Amin [25] used range map technique based on Discrete Fourier Transform (DFT) to measure the target's location and motion information in his FMCW radar research.

For the external device-based measurement, He [26] utilized a Kinect camera to obtain the location information in building a continuous vital signs monitoring system. Most of the radar-based respiratory pattern classification works set up a fixed radar-chest distance in the experiment to ensure the correct radar range bin data is extracted [27] [28] [29]. Both of these categories aim at obtaining accurate and clear respiratory waveforms for further analysis through accurate radar-chest distance measurement.

2.5 Respiratory signal quality

In the study of respiratory rate estimation, a common approach to improve the estimation accuracy is to use a signal quality index (SQI) to identify segments of high quality signals which respiratory rate can be more reliably estimated [30] [31]. This approach also works in the

respiratory pattern classification. In this thesis, the signal quality evaluation criteria are proposed based on the SQI algorithm proposed in [30]. The signal quality evaluation consists of two stages.

At the first stage, a median filter with a kernel size of five is applied to filter the original signal. This filtering process is used to reduce the influence of different signal-to-noise ratio (SNR) on the signal quality evaluation. The signal is then normalized to a range of [0,1] for further processing. After that, the peaks and troughs (local extrema) in the signal segment are detected. The extrema evaluated criterion is that the normalized peak should have a prominence larger than 0.15, so does the trough detection. The segments which have at least one relevant trough between the time spanning consecutive relevant peaks are defined as valid breaths.

At the second stage, the respiratory signal plausibility is assessed based on the valid breaths interval. Respiratory signals with less variable cycle time have higher plausibility [30]. Two criteria were used: (i) the normalized standard deviation of breath intervals is smaller than 0.25, which is used to permit only moderate variation in the durations of detected breaths; (ii) there are at least 3 intervals in a 15-seconds segment, which is set to avoid the misevaluation caused by the randomness from a small sample size. Any segment which did not satisfy these criteria was deemed to be of low quality, and only the respiratory signal segment which satisfies the above criteria can be considered high quality. The illustrations of breath segments which are considered high quality and low quality are shown in Fig. 2-10 and Fig. 2-11, respectively. The red "x" indicates the detected peaks and the blue "x" indicates the detected troughs. The criteria and thresholds were manually chosen based on the experience in the experiment to suit the characteristic of radar-collected respiratory signal, including eupnea, Kussmaul respiration and Cheyne Stokes respiration.

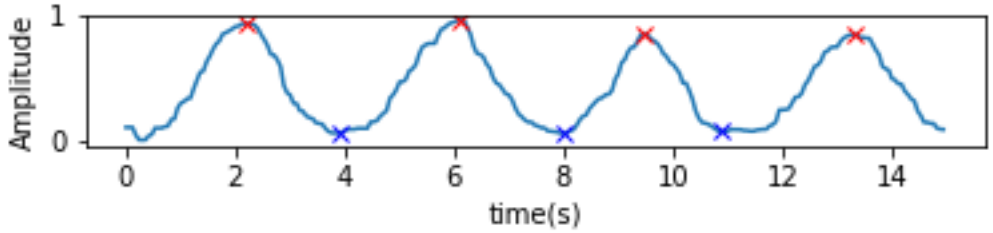

Fig. 2-10 Breath segment be considered high quality

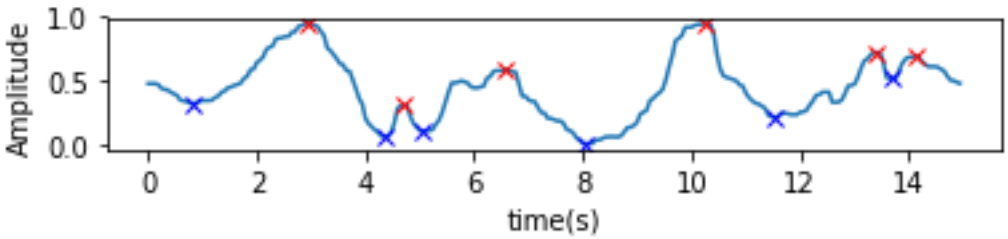

Fig. 2-11 Breath segment be considered low quality

The definition of “high quality” in this thesis only indicates that the inhale and exhale phase of each breath can be unambiguously identified. The major factor that influences the quality of the radar-collected respiratory signal are the random body movements of the monitoring subjects. The random body movement will distort the respiratory signal by adding irregular pulses at any stage of a respiratory cycle, and the distorted respiratory pulse would not be regarded as a valid breath since the duration and amplitude of the inhale and exhale phases cannot be accurately measured. In this thesis, for the distorted breath segment, samples that more than 60% of the duration is occupied by valid breaths are considered "partly distorted", otherwise are considered "completely distorted".

2.6 Radar-based continuous human activity classification

Radar-based human activity classification is a topical area of research in biomedical radar study. From the radar indoor monitoring review written by Amin [12] and Gurbuz [8], the radar continuous monitoring technique has been applied in various aspects, including motion detection, fall detection, gait detection, etc. Human activity classification is essentially continuous motion classification. In practice, human activity is an inherently dynamic time stream of actions, that is, people usually perform motions one after another with varying duration. Therefore, we need to segment the time streams of sensor measurements to implement the motion pattern classification. The sliding-sampling window is the most commonly used segmentation method, which can be implemented in an overlapping or non-overlapping manner depending on the system design requirements [32].

A typical radar-based continuous pattern classification consists of three steps: data acquisition/preprocessing, feature extraction and classification. In the system implementation, high input data throughput and long processing time are the major challenges in the real-time

continuous activity classification [33]. Therefore, we need to consider the model processing time in the development stage.

2.7 Supervised learning

In our study, we employed the supervised machine-learning models to implement the respiratory pattern classification. Machine learning is a method of data analysis that automates analytical model building. It builds a model based on sample data, known as "training data", and the model is used to make predictions or decisions. Supervised learning is a machine learning task of learning a function that maps an input to an output based on the example input-output pairs [34]. The learning algorithm receives a set of inputs along with the corresponding correct outputs, and the algorithm learns by comparing its actual output with correct outputs to find errors. It then modifies the model accordingly. Through methods like classification and prediction, supervised learning uses patterns to predict the values of the label on additional unlabeled data. It is commonly used in applications where historical data can predict future events that likely happens.

2.7.1 Machine learning model

In our study, three common supervised machine-learning models are used to execute the classification. They are support vector machine (SVM), decision trees and random forest, respectively. They are introduced as follows:

Support vector machines (SVM): A binary SVM performs classification by constructing an N-dimensional hyperplane (a plane generalized into N dimensions) that optimally separates the data into two categories. A multi-class classification problem can be realized through breaking down the problem into multiple binary classification problems. The most important parameter of SVM is the kernel function. It is used to transform the raw input data to a higher-dimensional space so that the input data can be better separated by the hyperplane [35]. Typical SVM kernels include linear, nonlinear, polynomial, radial basis function (RBF) and sigmoid function. Each kernel function has a popular application field, which is determined by data attributes.

Decision Trees: Decision Trees learning is operated by building a tree model in which each internal (non-leaf) node is labeled with an input feature, and each leaf of the tree is labeled with a

class. The class label prediction for a record starts from the root of the tree. First, the attribute value of the record is compared with the attribute of the root. According to the comparison, the record is forwarded to the next corresponding node. Then the comparison is implemented again between the node and the record. This process is repeated until the leaf nodes are reached [36]. A sample structure of decision tree is shown in Fig. 2-12.

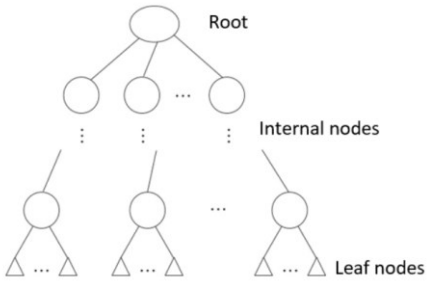

Fig. 2-12 A general decision tree structure

Random forest: Random forest learning model operates by constructing a multitude of decision trees at training time and outputting the class that is the mode of the classes (classification) or mean/average prediction (regression) of the individual trees [37]. The parameter of random forest classifier adjusted in this study is the number of trees. Theoretically, increasing the parameter "number of trees" will improve the accuracy of classification. However, this improvement comes at the cost of increased computational complexity. The increase in accuracy eventually reaches its upper limit, which is determined by the quality of data and features.

In our study, the machine-learning models mentioned above are implemented based on the models in the open-source machine learning library *Scikit-learn*. *Scikit-learn* is a Python module integrating a wide range of state-of-the-art machine-learning algorithms for medium-scale supervised and unsupervised problems [38].

2.7.2 Feature selection algorithm

Relief [39] is a feature selection approach designed for binary classification problems. It calculates a feature score for each feature, ranks them and selects the top-scoring features to realize the feature selection. Relief feature scoring is based on the identification of feature value differences between nearest neighbor instance pairs. If a feature value difference is observed in a

neighboring instance pair with the same class (a “hit”), the feature score decreases. Alternatively, if a feature value difference is observed in a neighboring instance pair with different class values (a 'miss'), the feature score increases. ReliefF is an update of Relif algorithm which is applied to solve multiclass classification problems [40]. In this study, the ReliefF algorithm is used to select the statistic features for the respiratory pattern classification. The outputs of this algorithm are the attribute weights ranging from −1 to 1, with large positive weights assigned to important features. According to the output result, we can remove the features with negative effects to improve the classification accuracy or delete the less important features to reduce the computational complexity.

2.7.3 Model performance evaluation

Confusion matrix is a specific table layout that allows visualization of the performance of an algorithm [41], as shown in Fig. 2-13. In this table, there are two rows and two columns that reports the number of false positives (FP), false negatives (FN), true positives (TP) and true negatives (TN).

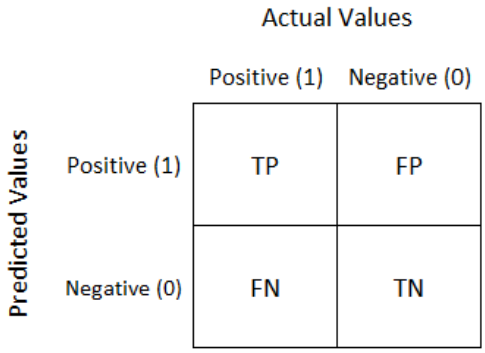

Fig. 2-13 Confusion matrix

There are also four matrices used to evaluate the model performance. They are accuracy, precision, recall and F_1 score. Accuracy is the fraction of correct predictions among all the predictions, as calculated by (2-10). Precision is the fraction of relevant instances among the retrieved instances, as calculated by (2-11). Recall is the fraction of relevant instances that were retrieved, as calculated by (2-12). F_1 score is the harmonic mean of precision and recall, as calculated by (2-13). F_1 score is in a range of $[0,1]$. The highest possible value is 1 indicating perfect precision and recall, and the lowest value is 0 if either the precision or recall is 0.

$$accuracy = \frac{TP + TN}{TP + FP + FN + TN} \tag{2-10}$$

$$precision = \frac{TP}{TP + FP} \tag{2-11}$$

$$recall = \frac{TP}{TP + FN} \tag{2-12}$$

$$F_1\ score = 2 \cdot \frac{precision\ \cdot recall}{precision + recall} \tag{2-13}$$

2.8 Time series classification

Time series data is the data that represents the measurements of a quantity over a period of time. The behavior of the series largely depends on the order of the points, and changing the order of the data points alters the meaning of the entire data set. A traditional classification model classifies the time-series data by extracting its statistic features and inputting the feature vectors into a machine-learning model to obtain the class label, as mentioned in Section 2.7. In the feature extraction phase, it treats each data point as a separate independent measurement.

Time series classification (TSC) is a classification algorithm designed for time series data processing. The implementation of many TSC models, such as those in popular Python libraries like *scikit-learn* [38] and *sktime* [42], consists of feature extraction and machine learning model classification, the same as the traditional statistic-feature-based classification. However, the main characteristic of the TSC is that in the feature extraction phase, the features are extracted based on the ordering of the time-series data, rather than the overall statistical characteristics of the data. Thus, it performs better on average than the traditional classification algorithm over time-series data classification.

There have been a wide range of methods of TSC algorithms developed in diverse research fields. Based on the type of discriminatory features, these techniques are classified into the following categories:

1. **Whole series:** Two series are compared either as a vector (as with traditional classification) or by a distance measure that uses all the data [43].
2. **Intervals:** Rather than using the whole series, this class of technique selects one or more (phase dependent) intervals of the series to measure the similarity [43].
3. **Shapelets:** A family of algorithms focus on finding short phase-independent patterns that define a class. These patterns are commonly called shapelets. A class is then distinguished by the presence or absence of one or more shapelets somewhere in the whole series [43].
4. **Dictionary-based:** Some problems are distinguished by the repetition frequency of subseries rather than by their presence or absence. Dictionary-based methods form frequency counts of recurring patterns and build classifiers based on the counting [43].
5. **Combination:** A further class of algorithms combines two or more of the above approaches into a single classifier [43].

2.8.1 Shapelet transform

Shapelet transform classification is the time series classification method that we employed in this thesis. This selection is based on the following reasoning:

Firstly, according to Bagnall [43], the shapelet-based technique outperforms other four categories of methods in electric device signal classification problems. Secondly, we liked to use a time series classification method that can utilize the shape characteristic of different respiratory pattern. Shapelet-based techniques have an outstanding performance in problems whose characteristic is phase independent; meanwhile, the key feature which can be used to identify a respiratory pattern is also phase-independent.

In the review of shapelet algorithms from Bagnall [43], shapelet transform(ST) classification is significantly better than other 2 algorithms, fast shapelet (FS) and learned shapelet (LS); thus, we eventually selected the shapelet transform (ST) classification.

The shapelet transform classification implemented in our study is based on *sktime*, a Python machine learning toolbox for time series with a unified interface for multiple learning tasks [42].

The whole process of shapelet transform classification consists of shapelet selection, shapelet transform and classification.

2.8.1.1 Shapelet selection

Shapelet selection comprises candidateS generation, shapelet similarity calculation and shapelet assessment. The shapelet selection is described by Algorithm 1 [44].

Algorithm 1. ShapeletSelection($\boldsymbol{T}, min, max, k$)

Input: A list of time series $\boldsymbol{T}$, min and max length shapelet to search for and k, the maximum number of shapelets to find for each class)

Output: A list of k Shapelets

1: $numClasses \leftarrow getClassDistribution(T)$

2: $kShapeletsMap \leftarrow \emptyset$

3: for all T_i in $\boldsymbol{T}$ do

4: $shapelets \leftarrow \emptyset$

5: for $l \leftarrow min\ to\ max$ do

6: $W_{i,l} \leftarrow generateCandidates(T_i, l)$

7: for all $subseries\ S$ in $W_{i,l}$ do

8: $D_s \leftarrow findDistances(S, \boldsymbol{T})$

9: $quality \leftarrow assessCandidate(S, D_s)$

10: $shapelets.add(S, quality)$

11: $sortByQuality(shapelets)$

12: $removeSelfSimilar(shapelets)$

13: $Shapelets \leftarrow ShapeletsMap.get(T.class)$

14: $kShapelets \leftarrow merge(k, Shapelets, shapelets)$

15: $kShapeletsMap.add(kShapelets, T.class)$

16: return $kShapeletsMap.asList()$

Each processing in Algorithm 1 is described below:

- Candidates generation: A time series of length m contains $(m - l) + 1$ distinct candidate shapelets of length l. We denote the set of all normalized subsequences of length l for series T_i to be $W_{i,l}$ and the set of all subsequences of length l for dataset T to be $W_l = \{W_{1,l} \cup W_{2,l} \cup \cdots \cup W_{n,l}\}$. The set of all candidate shapelets for dataset T is $W = \{W_{min} \cup W_{min+1} \cup \cdots \cup W_{max}\}$, where $min \geq 3$ and $max \leq m$. Suppose we have a set of n time series $T = \{T_1, T_2, \ldots, T_n\}$, the set $\boldsymbol{W}$ has $|\boldsymbol{W}| = \sum_{l=min}^{max} n(m - l + 1)$ candidate shapelets.
- Shapelet distance calculation: The squared Euclidean distance between two subsequences S and R, where both are of length l, is defined as (2-14):

$$dist(S, R) = \sum_{i=1}^{l} (s_i - r_i)^2 \tag{2-14}$$

The distance between a time series T_i and a subsequence S of length l is the minimum distance between S and all normalized length l subsequences of T_i, as shown in (2-15):

$$d_{S,i} = \min_{R \in W_{i,l}} dist(S, R) \tag{2-15}$$

We compute distances between a candidate shapelet S and all series in T to generate a list of n distances, $D_S = \{d_{S,1}, d_{S,2}, \ldots, d_{S,n}\}$.

- Shapelet assessment: Shapelet quality is an evaluation index of how well the class values V are separated by the set of distances D_S. The candidate shapelets are those shapelets that have the highest shapelet quality. Binary shapelet transform strategy proposed by Bostrom [45] is the state-of-the-art shapelet quality assessment method for multiclass time series classification. The standard shapelet assessment method measures how well the shapelet splits up all the classes, and binary shapelet transform improves it by focusing on how well the shapelet splits the class of the series it originated from all the other classes. In our study, the standard index information gain (IG) [46] is chosen to evaluates the quality of a shapelet. Based on the D_S distance set generated by the previous process, D_S is sorted, and the IG at each possible split point sp is assessed for S, where a valid split point is the average

between any two consecutive distances in D_s. For each possible split point, IG is calculated by partitioning all elements of $D_s < sp$ into A_s, class of the series it originated, and all other elements into B_s, the collection of the rest of the classes. The IG at sp is calculated as (2-16):

$$IG = H(D_s) - \left(\frac{|A_s|}{|D_s|} H(A_s) + \frac{|B_s|}{|D_s|} H(B_s) \right) \quad (2\text{-}16)$$

where $|D_s|$ is the cardinality of the set D_s, and $H(D_s)$ is the entropy of D_s calculated as (2-17):

$$H(D_s) = -\sum_{v \in V} p_v \log p_v \quad (2\text{-}17)$$

where p_v is the probability mass function of class values V.

The IG of shapelet S, IG_S, is calculated as (2-18):

$$IG_S = \max_{sp \in D_S} IG(D_S, sp) \quad (2\text{-}18)$$

- Self-similar shapelets removal: Since the scheme of candidate generation will generate $(m - l + 1)$ candidates for one time series, and there is a high probability that in the selected shapelets, there will be a shapelet which is the subseries of another shapelet with longer length. Both of them have high shapelet quality but it is redundant. The redundancy may limit the selection of other shapelets for this class, which will decrease the variety in shapelets and influence the shapelet transform performance. The process of removing self-similar shapelets is used to remove the shapelets which are extracted from the same series and reserve the first extracted shapelet.

2.8.1.2 Shapelet transform and classification

The shapelet transform algorithm uses the shapelets extracted from the previous section to transform instances of data into a new feature space; the transformed data can be viewed as a generic feature vector. The transformation process is defined in Algorithm 2.

Algorithm 2. ShapeletTransform (Shapelet S, Dataset $\boldsymbol{T}$)

1: $T' \leftarrow \emptyset$

2: for all T_i in $\boldsymbol{T}$ do

3: for all shapelet s_j in S do

4: $dist \leftarrow subsequenceDist(s_j, T_i)$

5: $T_{i,j} = dist$

6: $T' = T' \cup T_i$

7: return T'

The transformation is carried out with the subsequence distance calculation method described in Section 2.8.1.1(shapelet selection - shapelet distance calculation). A set of k shapelets, S, is generated from the training data $\boldsymbol{T}$. For each instance of data T_i, the subsequence distance is computed between T_i and s_j , where $j = 1, 2, \ldots, k$. The resulting k distances are used to form a new instance of transformed data, where each attribute corresponds to the distance between a shapelet and the original time series. Then, the transformed data of each shapelet composes a transformed dataset. The extracted shapelets are used to transform each instance of the training and test data to create transformed datasets, which can be used as a training feature vector and a test feature vector in any machine-learning classification, respectively.

Chapter 3: Review of the state of the art

This chapter reviews the state-of-the-art techniques in the fields of respiration simulation model and breathing pattern classification. The categories and applications of the respiration simulation model are introduced and the investigation of respiratory pattern classification is presented.

3.1 Review of respiration simulation model

At present, there are numerous types of breathing simulators, which are developed based on different scientific research requirements. IngMar Medical company developed the ASL 5000 Breathing Simulator based on their active servo lung technique which can simulate the breathing airflow. It can be applied in the product development and testing for ventilators, continuous positive airway pressure machine(CPAP), aerosol drug delivery and other respiratory therapy devices [47]. They also developed QuickLung Breather products that can simulate the airflow of several breathing patterns including eupnea, Cheyne Stokes, Kussmaul, Biot's and apneusis [48]. Michigan Instrument company has also developed their Breath Simulation Model with a similar purpose. The model serves as a control module that can simulate airflow combining with their dual-lung simulator [49]. Miron Technologies [50], Radiology Support Devices Inc. [51] developed a breathing phantom torso mannequin that can control the air pressure in the phantoms lung to simulate lung functions along with the chest wall movement. Modus QA company developed a Quasar respiratory motion phantom [52] driven by a motor that can simulate the vertical chest wall movement. All mentioned devices are developed for breathing and tumor research.

There are also several respiration simulation models designed for physiological signals analysis. NeuroKit2 [53] is an open-source Python toolbox developed for neurophysiological signal processing. It also provides simulation models for a series of physiological signals including the respiratory signal. According to the toolbox descriptions, the respiratory signal is collected by the respiratory belt and the signal simulation is based on the characteristic of respiratory belt data.

For the radar-based respiration simulation, the monoharmonic model is the basic and most commonly used model to describe the chest wall motion caused by respiration [54] [55]. Morgan and Zierdt [56] developed the pulse respiration model, which is a further development of the monoharmonic model. Gavrilov et al. [55] proposed a respiration model that can generate samples with high similarity to the human respiratory signals measured by short-range radar. The simulation output of the model developed by Gavriloy is more similar to the real radar-collected data than the output from the monoharmonic model and the pulse respiration model in time domain and frequency domain.

Wang et al. [57] released an open-source respiration simulation model in MATLAB. The model can simulate six breathing patterns including eupnea, bradpynea, tachypnea, Biot's respiration, Cheyne Stokes respiration and Central-Apnea. The model is designed for a depth-camera-based abnormal respiratory pattern classification study. Alinovi et al. [58] developed a breathing pattern simulation model based on Continuous-Time Markov Chain (CTMC) statistical model. This model is designed for their research of video-based monitoring system, which can simulate normal breathing and respiratory pause. The quality of the generated signal is evaluated by comparing the similarity of the feature distribution between the generated signal and the real signal. They proposed a set of features for evaluation, and used the Kullback-Leibler divergence to evaluate the feature similarity. Except for the model from Alinovi [58], none of the other studies mentioned above provide a method for evaluating the signal quality other than visual comparison.

There are also two public respiratory signal databases, CapnoBase Respiratory Event Benchmark [59] and NeuroKit [60], which can provide data for respiration study.

3.2 Review of sensor-based respiratory pattern analysis

The most commonly used technique in respiratory pattern analysis is Respiratory inductance plethysmography (RIP) [61]. It is a method of pulmonary ventilation evaluation implemented by measuring the movement of the chest and abdominal wall, and it can be used to describe various measures of complex respiratory patterns. A respiratory inductance plethysmograph consists of two sinusoid wire coils insulated and placed within two 2.5 cm-wide, lightweight elastic and adhesive bands. Polysomnogram (PSG) [62] can also be used to diagnose abnormal respiratory

patterns like sleep apnea. It includes electrocardiograph, electroencephalograph, continuous oronasal airflow recording (with a thermistor and a pressure transducer), recording of chest wall and abdomen movement (using respiratory inductive plethysmography belts), transcutaneous oximetry and chin electromyography. It diagnoses sleep disorders by investigating the apnea-hypopnea index (AHI). The AHI is defined as the sum of apneas and hypopneas per hour of sleep; apnea is defined as the absence of airflow for ≥ 10 seconds; hypopnea is defined as reduction in respiratory effort with ≥ 4% oxygen desaturation [63]. Comparing with the traditional techniques which classify the breathing pattern with multiple vital signs, this thesis pays more attention to the classification technique with a single sensor in this thesis, especially the classification technique based on univariate respiratory signals.

Costa et al. [64] published a study that introduces breathing monitoring and pattern recognition with wearable sensors. They reviewed the application of breathing sensors, including pressure, acoustics, humidity, oximetry, acceleration and resistive sensors. They also proposed features and classification algorithms that may help measuring and classifying breathing-related activities.

Feker et al. [65] [66] proposed a respiratory pattern classification method based on the signal collected from wearable microelectromechanical system (MEMS) sensors. In the MEMS system, two accelerometer sensors are mounted on the subject's chest and abdomen to record the chest wall and abdomen movement. A support vector machine (SVM) algorithm with seven statistic features was used to classify eight respiratory patterns (eupnea, bradypnea, tachypnea, Kussmaul, apneustic, Biot’s respiration, sighing and Cheyne Stokes respiration).

Wang et al. [57] [67] extracted the respiratory signal with a depth camera, and employed a gated recurrent unit (GRU) neural network with bidirectional and attentional mechanisms (BI-AT-GRU) to classify six respiratory patterns (eupnea, tachypnea, bradypnea, Biot’s respiration, Cheyne Stokes respiration and central-apnea).

There are also studies focusing on respiratory pattern classification based on radar-collected signals. They are presented in the following section.

3.3 Review of respiratory pattern classification with radar collected signal

The radar indoor monitoring technique has been explored in the last decade. One of the attractive research areas is radar-based respiratory pattern classification.

Lee et al. [68] [69] used microwave Doppler radar to record the signal of six breathing patterns, including central apnea, ataxic, Biot's respiration, Cheyne Stokes respiration, dysrhythmic breathing and Kussmaul breathing. They implemented fast Fourier transform (FFT) and continuous wavelet transform (CWT) to process the signals and analyzed their characteristics. An experiment to investigate the correlation between the radar and spirometer in capturing the respiratory function was also conducted, and the results verified the feasibility of radar in capturing different breathing patterns associated with breathing disorders.

Miao et al. [28] proposed a respiratory disorder classification method based on continuous-wave Doppler radar. They extracted three statistic features of the breath signals including the number of signal peaks, minimum short-time energy and variance of short-time energy, and implemented support vector machine (SVM) algorithm to classify four breathing patterns: normal breathing (eupnea), Cheyne-Stokes breathing, dysrhythmic breathing and Kussmaul breathing. They used ten-fold validation to test the method and the best total classification accuracy is 90%, achieved by the linear SVM model.

Feng at al. [29] proposed a Doppler radar based breathing disorder recognition algorithm implemented on FPGA. The usage of FPGA enables a design of a compact breathing disorder classification system with lower computational complexity. They employed a k-nearest neighbor (KNN) classifier with statistic features extracted from the time domain and frequency domain of the signal to classify six breathing patterns: normal breathing (eupnea), Cheyne-Stokes breathing, Cheyne-Stokes variant breathing, dysrhythmic breathing, Biot's breathing and Kussmaul breathing. In the ten-fold validation test, the normal breathing pattern achieves 97% accuracy, Biot's and Kussmaul breathing have accuracy around 80% and the accuracy of Cheyne-Stokes breathing, Cheyne-Stokes variant breathing and dysrhythmic breathing are around 60%.

Zhao et al. [27] applied a 2.4Gz digital-IF Doppler radar to classify six breathing patterns, including normal breathing (eupnea), Cheyne-Stokes breathing, Cheyne-Stokes variant breathing, dysrhythmic breathing, Biot's breathing and Kussmaul breathing. In the classification, the authors proposed thirteen statistic features and selected them with ReliefF algorithm. They also selected the machine learning algorithm according to their performance in the experiment. In the laboratory experiment, the proposed system achieves an accuracy of 94.7 %, and in the hospital environment, it also performs well with the selected breathing data.

3.4 Conclusion

In this chapter, we reviewed the state-of-the-art techniques in respiration simulation and respiratory pattern classification, which are the most relevant study of this thesis. We will further analyze each of the relevant studies in the next chapter to summarize the detailed objectives of this thesis.

Chapter 4: Problem statement

The goal of the thesis is to optimize the existing radar-based breathing pattern classification model to make it applicable for full-automatic implementation. To achieve this goal, there are three major topics that need to be considered, the respiration database for model training, the strategy to implement full-automatic continuous classification, and the performance requirement for the classification model.

4.1 Respiratory signal database

For machine-learning-based pattern classification, sufficient high-quality data is the foundation of model training. Even though we found some public respiration data resources, as introduced in Section 3.1, most of the data from them cannot be used in our study. The reasons are listed as follow.

The first reason is that none of the public abnormal respiration database contains Cheyne Stokes respiration and Kussmaul breathing. They only contain normal respiration data. Besides, most of the open-source respiration simulation models only generate normal breath signal [55] [60]. Therefore, the respiration data we need in this study, including samples of Cheyne Stokes respiration, Kussmaul respiration and apnea, cannot be acquired from the public database and the released simulation models.

The second reason is that the attributes of the accessible respiration data do not meet our requirement, that is, it should be similar to the radar-collected respiration data. Because of the range bin characteristic in the radar-based respiration monitoring, the collected respiratory signal is a one-dimensional time-series signal with a relatively flat baseline. Thus the respiration data which can be used in this study need to have a similar attribute. Meanwhile, the signal waveform should also be similar to a sinusoidal-wave-like signal according to the radar-collected respiratory signal waveform and the respiration model [54]. Although the respiration simulation model released by Wang [57] can generate breath samples of the desired patterns, the attribute of those samples is quite different from what we need. The baseline of the generated samples are not flat, and the waveform characteristic is different from the radar-collected signal we

demonstrated in Fig. 2-9, as shown in Fig. 4-1. A possible reason for the difference is that their model was developed based on the characteristic of the respiratory signal extracted from the depth camera images.

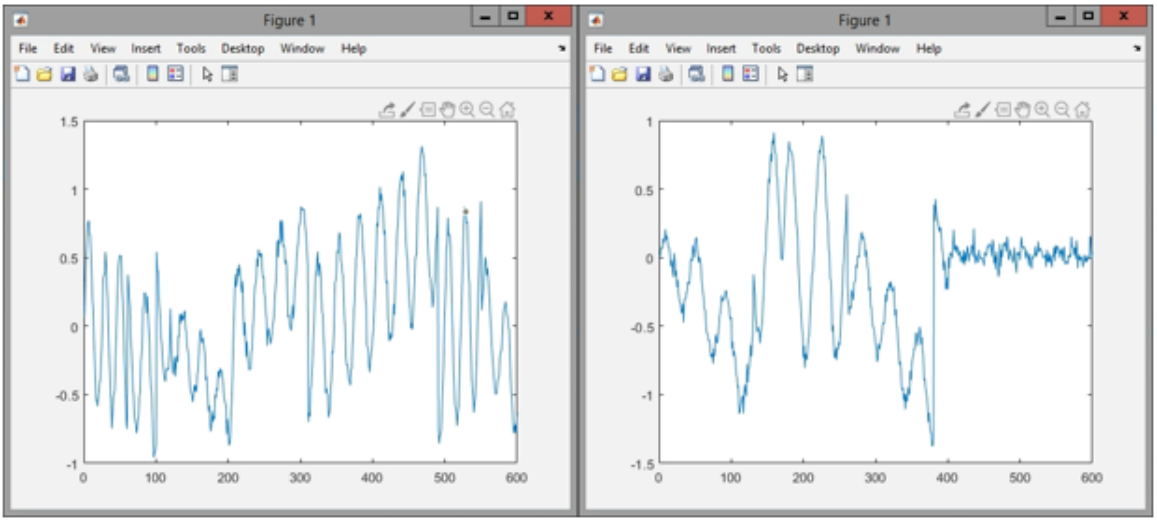

Fig. 4-1 Generated signal from Wang's RSM model: Eupnea (left) and Cheyne Stokes respiration (right)

4.1.1 Proposed solutions

To promote the study of respiratory pattern classification, we need to build a breath sample database. We recruited several healthy volunteers to simulate the four respiratory patterns involved in this study and collected the breath sample from them. During this process, we encountered the third problem, the dataset imbalance for each respiratory pattern. Compared with eupnea, the other three respiratory patterns have much less data. The reason is that the difficulty of the simulation of each respiratory pattern is quite different. For the eupnea, volunteers only need to perform normal breathing; however, for the abnormal breathing patterns, they need to control the tidal volume and rhythm precisely for a period of time. Besides, the human simulation of each abnormal breathing pattern is discomforting and exhausting. Therefore, the number of experiments for conducting the abnormal breath data collection is limited. Meanwhile, there are other accessible eupnea data from the other research in our lab, such as the data from the respiration rate estimation experiment.

There is also a problem that some simulated breathing data cannot be used for classification because the volunteers sometimes cannot simulate the respiratory pattern properly. This problem

mainly existed in the simulation of abnormal breathing patterns. For the above reasons, the dataset capacity of each abnormal respiratory class is much smaller than that of the eupnea dataset.

In order to reduce the impact of the imbalanced dataset, we developed a respiration simulation model to supplement breath data for each pattern to the same level [70]. The model is developed based on the knowledge of the released breathing simulation model and the characteristic of our radar-collected data. The development of the respiration simulation model for our research is crucial since we can obtain sufficient breath samples with precise pattern characteristic and reduce the breathing simulation workload of volunteers.

4.2 Respiratory pattern classification

The radar-based respiratory pattern classification research including patterns of Cheyne Stokes respiration, Kussmaul breathing and apnea started in 2014 [68] [69], and the results have been reported for the experiments performed in the laboratory [27] [28] [29] and in the hospital [27]. Respiratory pattern classification could help medical doctors to better evaluate the patient's condition, especially for cardiovascular disease. However, none of the solutions in [27] [28] [29] [68] [69] cannot be applied to stream processing, and thus they cannot be regarded as a respiratory pattern classification strategy that can be continuously implemented in a full-automatic manner.

The concept of full-automatic respiratory pattern classification is proposed based on the operating mode of radar-based vital signs monitoring systems, which means that the whole process streams, including sections of data collection, respiratory signal extraction and respiratory pattern classification, are automatically and continuously implemented without any human intervention. Under this circumstance, the subjects can be contactless monitored without human caregivers. A full-automatic respiratory pattern classification model which can be continuously implemented is a model that can be implemented in this process stream.

The respiratory pattern analysis from Lee [68] [69] only proved the feasibility of capturing respiration disorder with radar and did not provide any classification solution. Miao [28] and Feng [29] both carried out the respiratory pattern classification study in a batch-processing manner. The breath samples are collected separately and then assembled to implement the

classification. Zhao [27] executed the classification on the basis of the study from Miao [28] and Feng [29] with additional statistic features. He also implemented the model in a new scenario that the respiration data are collected continuously in a long-term experiment. However, the collected signal needs to be manually selected to filter out the respiratory signal distorted by body movement before implementing the classification. It violates the principle of without human intervention, and thus it cannot be regarded as a full-automatic continuous classification strategy. As the evaluation of this study from Kernec [33], the breath signal distorted by body movement makes the result inaccurate.

In fact, not only body movement but also environmental disturbance like obstacles may influence the quality of the collected signal due to the non-contact measurement attribute. It is expected that as a cost of getting rid of the contact-based device which may cause discomfort, we need to bear the risk that the collected signals are easily distorted.

In a full-automatic respiration monitoring strategy, there is a premise that we need to locate the target's chest wall to extract the respiration data from the corresponding range bin. Some of the distance measuring methods which can be implemented continuously and automatically have been introduced in Section 2.4. The distance measuring methods can be divided into two categories according to the implementation device, radar or external devices. However, both of them will introduce a distance measuring deviation. Nevertheless, introducing a ranging technique is necessary for the future development of radar vital signs monitoring since the subject will not be restrained into a certain location. The following problem is that if the distance deviation is too large, it will lead the model to extract the respiration data from an inappropriate range bin, which deeply affects the quality of the extracted breath signal.

4.2.1 Proposed solutions

In this thesis, we proposed two methods to solve the problem of collected breath signal distortion: introducing a new class "moving" to classify the distorted respiratory signal into a certain class and shortening the sampling window length.

The "moving" class includes the respiratory signal distorted by the body movement and the signal extracted from an inappropriate range bin, in other words, the respiration-irrelevant signal.

In the state-of-the-art study from Zhao [27], Miao [28] and Feng [29], their respiratory pattern classification models are based on the samples with a window length of 30 seconds. According to their study, a window length of 30 seconds can sample a whole period of irregular breathing likes Cheyne Stokes respiration. For the respiratory patterns we classified in this study, Cheyne Stokes respiration is the only irregular periodic pattern, and we are able to classify it based on a portion of the complete cycle. Therefore, we shorten the window length to 15 seconds, which is the shortest available length for classifying Cheyne Stokes respiration in our study. This proposal is based on the premise that a sliding sampling window method, a commonly used sampling method in continuous monitoring (mentioned in Section 2.6), is used to sample and segment the stream data. Since the breathing rate and tidal volume are varying, and the breathing rate estimation and respiratory pattern classification are implemented within the sampling window, a sampling window with a shorter length can exclude the episode that occurs much earlier and only sample the latest episodes. Therefore, the sample analysis result can better reflect the latest breathing state.

This reason also applies from the perspective of the sliding window implementation. For example, if the continuous monitoring system is designed with a non-overlapping sliding window, a shorter sample length means it will update the analysis results more frequently; if the system is designed with an overlapping sliding window, the distorted signal segments will appear in more samples if a longer window length is used. Therefore, the influence of the distorted signal on pattern classification will last longer. In other words, the shorter the window length, the less chance the sample to be processed contains a distorted signal.

Meanwhile, shortening the sampling window length would reduce the probability of retrieving the abnormal breathing patterns. As mentioned in the introduction of Cheyne Stokes respiration, its period is usually longer than 30 seconds. However, separating a 30-second

Cheyne Stokes respiration sample into two 15-second samples cannot ensure that both of them can be classified as Cheyne Stokes, as shown in Fig. 4-2 and Fig. 4-3.

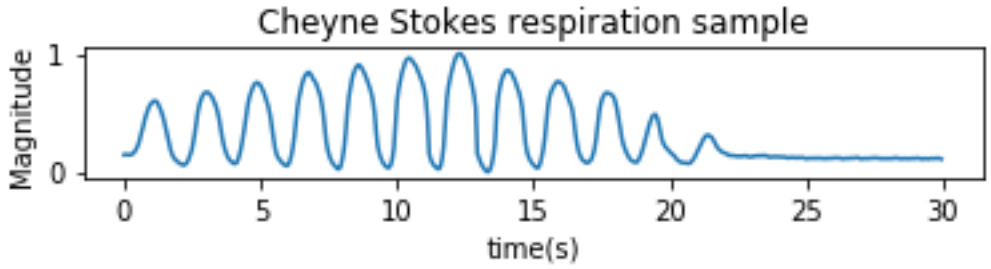

Fig. 4-2 30-second Cheyne Stokes respiration

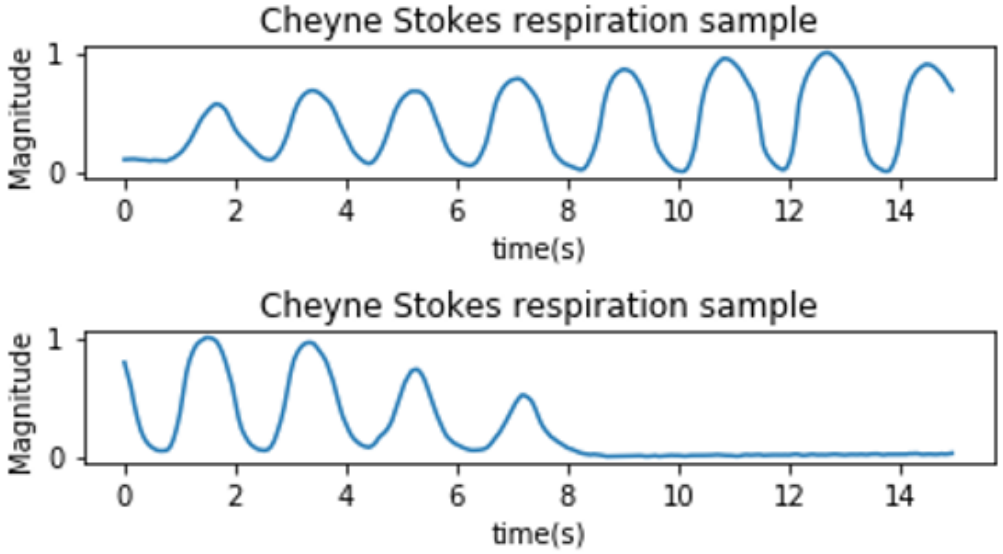

Fig. 4-3 Separated 15-second Cheyne Stokes respiration

Comparing with the sample in the lower picture of Fig. 4-3, the upper sample is more difficult to be classified as Cheyne Stokes respiration since the peak amplitude variation is less obvious and there is not any apnea phase in the sample. Therefore, a shorter respiratory signal than 15-second will lead to severe missing information, which would affects the accuracy of the classification results. A classification model with higher accuracy to differentiate each respiratory pattern is required when the sample length is shortened.

4.3 Performance requirement for the continuous respiratory pattern classification

The last problem that needs to be considered in this thesis comes from the application of the proposed strategy. This full-automatic classification model can be used to implement continuous respiration monitoring, and it is expected to alert or report when the abnormal breathing pattern is detected.

Thus, the model needs to have an attribute of low false alarm ratio, which can make the caregiver pay more attention to the alert. False-alarm ratio is the number of false alarms over the total number of the alarm [71]. In this thesis, Cheyne Stokes respiration, Kussmaul breathing and apnea are the abnormal respiratory patterns that deserve to be noticed when their occurrence is predicted. Therefore, the false alarm ratio is defined as the ratio of the total false prediction of abnormal breathing patterns to the total prediction, written as (4-1).

$$False\ alarm\ ratio = \frac{Total\ false\ prediction}{Total\ prediction} \tag{4-1}$$

The lower the false-alarm-ratio, the more credible the alarm is.

There is another model evaluation index, precision, works in a similar way as the false alarm ratio. As mentioned in Section 2.7.3, precision refers to the fraction of relevant instances among the retrieved instances [72], which evaluates the credibility of the prediction for a specific class only. Hence, we will also pay attention to the model precision in evaluation. The higher the precision of the model, the more credible the prediction.

4.4 Conclusion

In this chapter we introduced the existing problems and the proposed solutions in the radar-based continuous respiratory pattern classification model development. The breath sample distortion is why we cannot implement the existing respiratory pattern classification methods in continuous respiration monitoring. The shortage of breath samples is the major difficulty for us to carry out the study of respiratory pattern classification. The solutions for the problems above are proposed, and the realization scheme will be demonstrated in the next chapter.

Chapter 5: Methodology

This chapter demonstrates the process of building a respiratory pattern classification model which can meet the performance requirements for a full-automatic respiratory pattern classification, as mentioned in Chapter 4. In this chapter, we developed a respiration simulation model to supplement respiration data for the model training, developed several classification models based on the state-of-the-art respiratory pattern classification technique, and explored the application of shapelet transform algorithm in the respiratory pattern classification.

5.1 Respiratory signal database

This section introduces the process of building a respiratory signal database. The respiratory signal database comprises radar-collected respiratory signals from the recruited volunteers and generated signals from the respiration simulation model developed in this thesis.

5.1.1 Radar collected respiratory signal

The radar-collected respiratory signal database is constructed by the radar-collected breath data of 9 healthy human subjects (6 males and 3 females). All subjects were instructed to imitate 3 breathing patterns: eupnea, Cheyne Stokes respiration and Kussmaul breathing. In each experiment, a subject was asked to imitate one of the breathing patterns mentioned above for one minute under a fixed radar-chest distance, and each subject was asked to perform at least 2 sets of measurements. The radar-chest distance varied from 1.25 m to 3 m, and most of them are concentrated in the range of 1.5 m. The distance is measured by a Stanley® laser distance measurer at the start of each experiment to locate the range bin corresponding to the breath signal. Each collected 1-minute signal was segmented into four 15-second samples. Then, by observing the sample waveforms, we manually selected the samples with clear respiratory waveforms and features that match the respiratory pattern. The “moving” signals were also selected from radar-collected signals, they contain signals respiration-irrelevant signals and distorted respiratory signals.

Eventually, there are 425 sets of radar-collected 15-second breath samples in the database, including 137 sets of eupnea, 50 sets of Cheyne Stokes respiration, 50 sets of Kussmaul

breathing and 188 sets of “moving” samples. The experiment protocol was approved by the University of Ottawa Research Ethics Board.

5.1.2 Respiration simulation model

The respiration simulation model (RSM) is used to generate breath samples that can be applied in human respiratory pattern classification. This thesis aims to simulate breath samples of four respiratory pattern, including eupnea, Cheyne Stokes respiration (CSR), Kussmaul breathing and apnea. The respiration simulation model is designed based on the monoharmonic model [55]. The mathematical models for the simulation of each breathing pattern are introduced in this section.

5.1.2.1 Model for respiratory patterns with regular waveform

In this section, three respiratory patterns including eupnea, Kussmaul breathing and apnea are simulated. Both Eupnea's and Kussmaul respiration‘s signal waveforms are similar to sine waves, while the difference lies in respiration frequency and tidal volume. The models of eupnea and Kussmaul breathing are composed of base sine wave and additive white Gaussian noise (AWGN), as shown in (5-1). The models were designed based the following criteria: the signal should be a one-dimensional time series signal with a flat baseline and clear waveform, resembling the non-distorted respiratory signal collected by radar.

$$s(t) = \mathrm{A} \cdot \sin\left(\frac{2\pi}{60/\#bpm} \cdot \mathrm{t} + \mathrm{C}\right) + \mathrm{D} \tag{5-1}$$

where,

A	Breathing amplitude
$\#bpm$	number of breaths per minute
C	Phase shift
D	Additive white Gaussian Noise

The following parameters are chosen for eupnea: the breathing amplitude $A \in [0.6, 0.8]$, the number of breaths per minute $\#bpm \in [12, 20]$ [3], the phase shift $C \in [0, 2\pi]$. For the additive white Gaussian noise [73], the mean is 0 and the variance $E \in [0.05, 0.1]$. For Kussmaul

breathing, the breathing amplitude $A \in [1.0, 1.2]$, the number of breaths per minute $\#bpm \in [28, 40]$ [74] [75], the rest of the parameters are the same as those of eupnea.

For the apnea signal, it is simulated by the additive white Gaussian noise only. The parameter settings are the same as those of eupnea model and Kussmaul model.

The length of the simulated signal is set to 15 second. The outputs of the models are compared to the radar-collected respiratory signals from the subjects simulation experiments in Section 5.1.1, as shown in Fig. 5-1, Fig. 5-2 and Fig. 5-3.

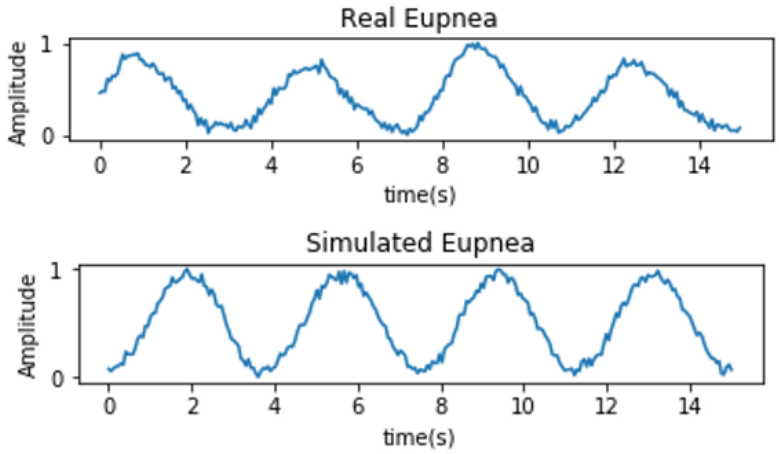

Fig. 5-1 Comparison of radar-collected eupnea and simulated eupnea

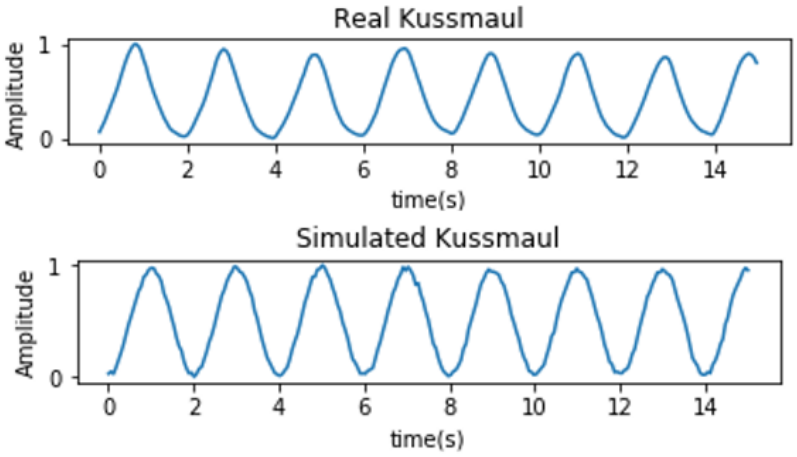

Fig. 5-2 Comparison of radar-collected Kussmaul breathing and simulated Kussmaul breathing

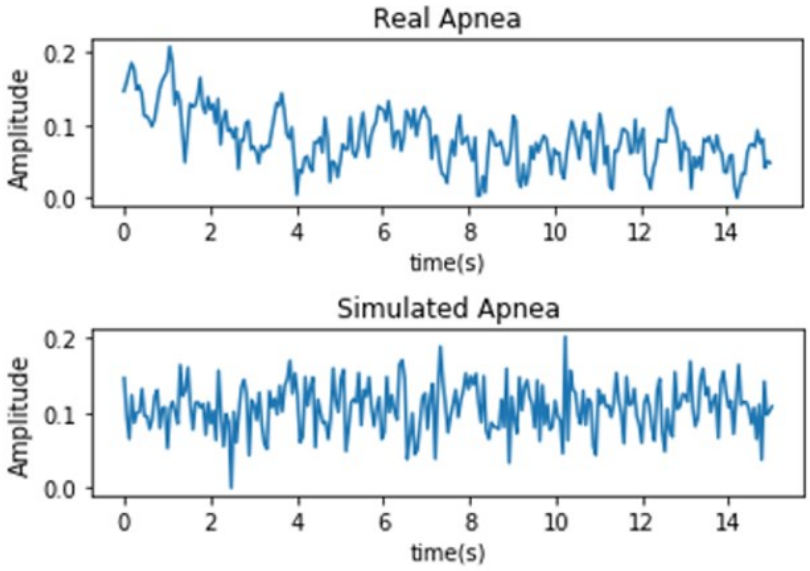

Fig. 5-3 Comparison of radar-collected apnea and simulated apnea

5.1.2.2 Model of Cheyne Stokes breathing

The Cheyne Stokes respiration (CSR) simulation model is developed based on the sinusoidal wave as well, and the sinusoidal wave needs to be amplitude-modulated to simulate the crescendo waveform, decrescendo waveform and apnea. The process of the Cheyne Stokes respiration simulation is shown in Fig. 5-4.

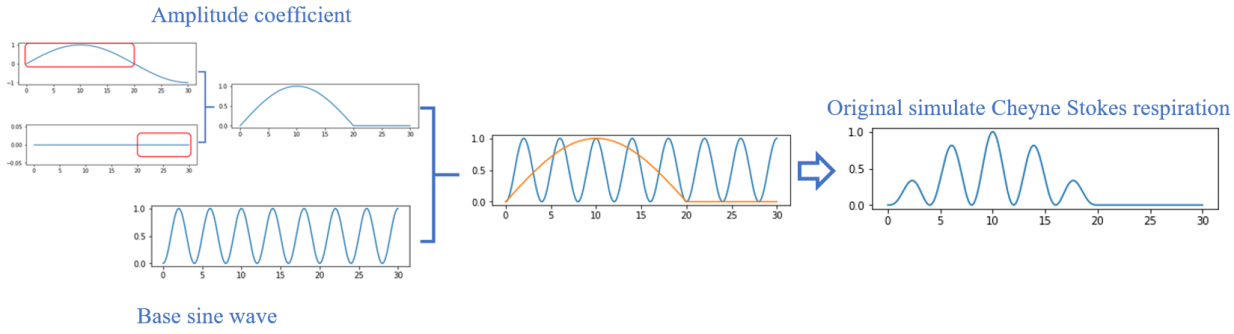

Fig. 5-4 Cheyne Stokes respiration simulation process

Cheyne Stokes respiration (CSR) is a type of breathing disorder characterized by cyclical episodes of apnea and hyperventilation [9]. A complete Cheyne Stokes respiration period includes three phases: crescendo phase, decrescendo phase and apnea phase. The crescendo phase and decrescendo phase are collectively referred to as hyperventilation phase.

The first step in the simulation is to generate a sinusoidal signal as a base signal. The length of the base signal is set according to the length of a cycle of Cheyne Stokes respiration, which is around 45-90 seconds [9]. In this model, the length of the base signal is about the length of 1-2 CSR cycles, and the frequency of the hyperventilation in CSR is determined by the frequency of the base signal. According to the pathophysiology of Cheyne Stokes respiration [6] and the fact that patients with heart failure are normally tachypneic (excessively rapid breathing) [5], the hyperventilation frequency is set to 12-40 breaths per minute. The model of base signal is shown in (5-2).

$$\text{base(t)} = \sin\left(\frac{2\pi}{60/\#bpm} \cdot \text{t}\right), t \in [0, T_{CSR}] \tag{5-2}$$

where,

bpm	Number of breaths per minute
T_{CSR}	Cycle length of Cheyne Stokes respiration (second)

For ranges of the parameters, the number of breaths per minute $\#bpm \in [12, 40]$, and the cycle length $T_{CSR} \in [45, 90]$ were selected. In this stage, we need to scale the base signal to normalize it to a range between [0, 1]. This process makes sure that the apnea phase will be the phase with minimum amplitude values in the CSR sample.

Then, we defined the amplitude modulation function. It is a piecewise function, including the piece of hyperventilation and the piece of apnea. Firstly, we defined the length of hyperventilation phase and apnea phase. The duration of hyperventilation is around 20-30s followed by 10-40s apnea [76], and the relative duration of hyperventilation is longer than the duration of apnea [9]. Thus we set the ratio of hyperventilation R_v to 0.5-0.75, and the rest is for apnea. Considering the physiological characteristic that naturally the inhale or exhale is a complete process, the duration of hyperventilation t_v in seconds can be written as (5-3):

$$t_v = round(\#bpm \cdot \frac{T_{CSR}}{60} \cdot R_v) \cdot \frac{60}{\#bpm} \tag{5-3}$$

The amplitude modulation of hyperventilation is based on another sinusoidal signal. As shown in Fig. 5-4, the amplitude modulation is based on the $[0, \frac{T_v}{2}]$ interval segment of the

sinusoidal signal, where T_v is the period of the sinusoidal signal. The equations of hyperventilation modulation function $H(t)$ are shown in (5-4) and (5-5):

$$T_v = 2 \cdot t_v \tag{5-4}$$

$$\mathrm{H(t)} = \sin\left(\frac{2\pi}{T_v} \cdot \mathrm{t}\right), t \in [0, t_v] \tag{5-5}$$

In the apnea phase, the amplitude modulation function is set to zero.

To sum up, the CSR amplitude modulation function $M(t)$ can be written as (5-6):

$$M(t) = \begin{cases} \sin\left(\frac{2\pi}{T_v} \cdot \mathrm{t}\right), t \in [0, t_v] \\ 0, t \in (t_v, T_{CSR}] \end{cases} \tag{5-6}$$

The CSR simulation model is the product of the base signal model and the amplitude modulation function, as shown in (5-7).

$$CSR(t) = \mathrm{base(t)} \times M(t) \tag{5-7}$$

$$= \begin{cases} \sin\left(\frac{\pi}{30\#bpm} \cdot \mathrm{t}\right) \cdot \sin\left(\frac{\#bpm \cdot \pi}{60 \cdot round\left(\#bpm \cdot \frac{T_{CSR}}{60} \cdot R_v\right)} \cdot t\right), t \in [0, t_v] \\ 0, t \in (t_v, T_{CSR}] \end{cases}$$

Then the additive white Gaussian noise mentioned in the regular respiration model are added to the CSR signal to simulate the signal noise. The simulated Cheyne Stokes respiratory signal is shown in Fig. 5-5. In this example, the simulated data length is set to 90 seconds and there are two cycles of Cheyne Stokes respiration. In this study, all breathing patterns are classified based on a sample length of 15 seconds, so a 15-second sampling window is used to extract samples from a complete cycle of Cheyne Stokes respiration signal. The model outputs are compared to radar-collected respiratory signal, as shown Fig. 5-5, Fig. 5-6 and Fig. 5-7.

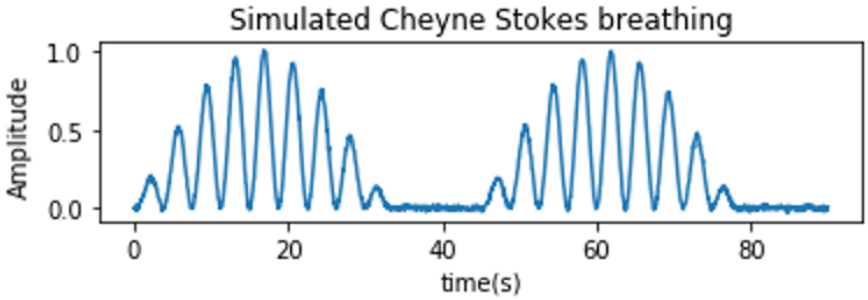

Fig. 5-5 Simulated Cheyne Stokes respiration (90-second length)

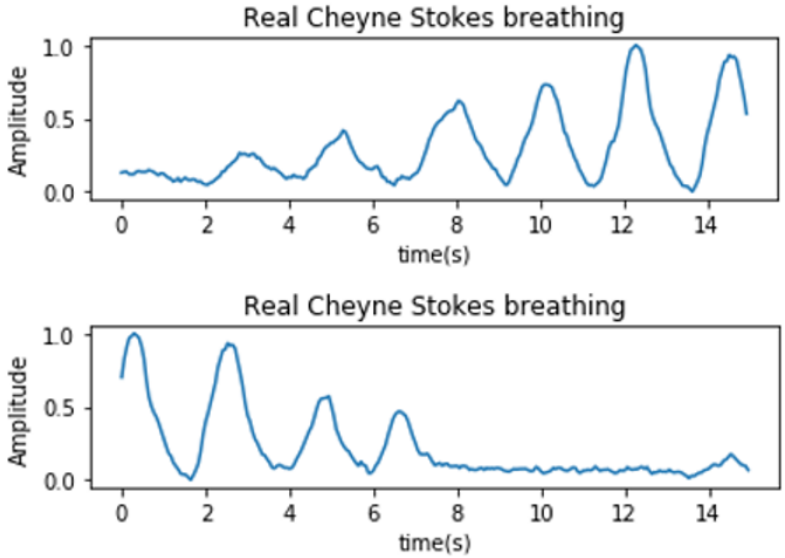

Fig. 5-6 Radar-collected Cheyne Stokes respiration signal (15-second length)

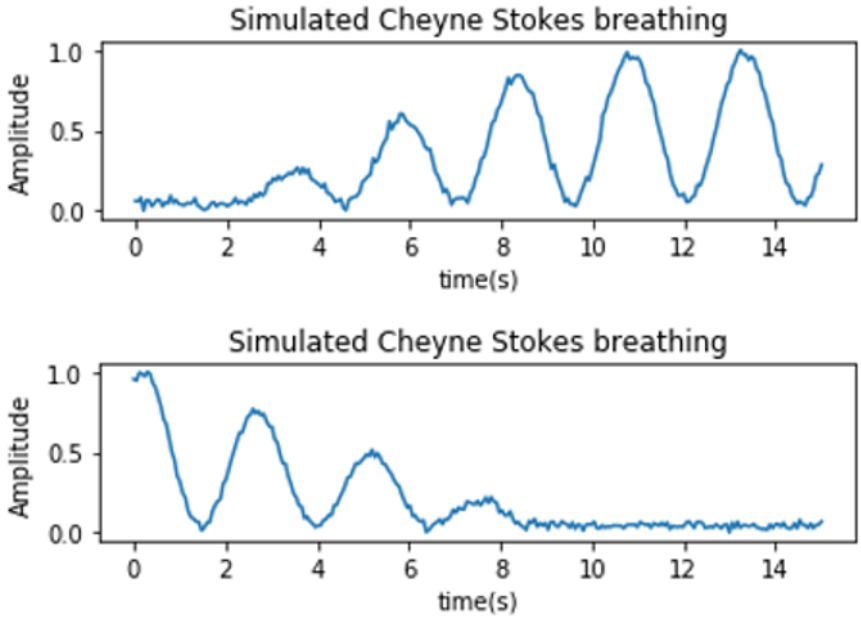

Fig. 5-7 Simulated Cheyne Stokes respiration signal (15-second length)

All the breath samples, including the radar-collected signals and the generated signals, were scaled to a range between [0, 1], which is used to reduce the influence of the different amplitude levels of the signal. The only exception is that if the signal's amplitude range is smaller than 0.3 and the signal variance is smaller than 0.3, it only needs to be translated to a proper range that the minimum value in the signal is zero, and the scaling is not required. The exception is set for the apnea signals which amplitude variation is small. The purpose of this setting is to amplify the characteristic of apnea signals for better classification results. The thresholds are set based on the experiment results.

5.2 Traditional respiratory pattern classification

The basic process of the traditional respiratory pattern classification including statistical feature extraction and classification model training. The category description "traditional" means that the extracted features are statistical features only. The features are independent regardless of the potential internal connection between each data point in the original data. All of the state-of-the-art respiratory pattern classification studies introduced in Section 3.3 belong to this category.

We also proposed a group of features based on the signal peak variation and added them to the feature set of the state-of-the-art breathing pattern classification study to improve the

classification accuracy. The summarized feature set consists of time-domain features, time-frequency domain features and short-term energy domain features..

Time domain features: there are 2 terms need to be pre-defined: peak and amplitude. In this study, the definition of peak in respiratory signal is a signal peak which has a prominence of 0.15 for a normalized signal (signal ranges from 0 to 1) and a minimal horizontal distance of 25 samples (signal sampling rate is 17 scans/second). The peak information includes the peak value and peak location. The method of obtaining the signal trough's information is the same as that of the peak; only the signal needs to be reversed by taking a negative value. The absolute value of difference between the nearest peak and trough is the amplitude. There are 9 time domain features extracted in this study, including amplitude variance, amplitude maximum, amplitude minimum, amplitude range, entropy, peak variance, peak average, peak maximum and number of peaks.

Time-frequency domain features: instantaneous frequency in respiratory signal corresponds to time-varying respiration rate. Hilbert transform is a method of calculating the high-resolution time-frequency domain distribution. The instantaneous frequency $f(t)$ is the temporal rate of the instantaneous phase, which can be calculated by (5-8),

$$f(t) = \frac{1}{2\pi} \cdot \frac{d\varphi(t)}{dt} \tag{5-8}$$

where $\varphi(t)$ is the unwrapped instantaneous phase angle. The instantaneous phase angle is calculated by the Hilbert transform [77]. For a real signal $x(t)$, the Hilbert Transform is defined as (5-9).

$$x_H(t) = -\frac{1}{\pi t} \cdot x(t) = -\frac{1}{\pi} \int \frac{x(\tau)}{\tau - t} dt \tag{5-9}$$

The Hilbert transform shifts the phase of the real signal by $\frac{\pi}{2}$ for negative frequency components and $-\frac{\pi}{2}$ for positive frequency components. Five time-frequency domain features are used, including frequency variance, frequency maximum, frequency minimum, frequency average and frequency range [27].

Short-term energy features: short term energy features are employed to extract the time-varying intensity of the breath signals, especially for the signals of abnormal respiratory pattern,

such as Cheyne Stokes respiration [27]. In this study, a 15-second signal is sliced into four 4-second short-term signal segments with an overlap of 1 second. For a signal $s(i)$ with k samples, where $i = 1,2,\ldots,k$, the energy of signal $s(i)$, E_s, is calculated by (5-10).

$$E_s = \sum_{i=1}^{k} s(i)^2 \tag{5-10}$$

Four short-term energy features are used in this study including energy variance, energy maximum, energy minimum and energy range.

All features introduced above are summarized into Table 5-1. All these features are extracted from the 15-second breath sample.

Table 5-1 Features Summarization

Categories	Indexes	Features
Short-term energy features	1	Energy variance
	2	Energy maximum
	3	Energy minimum
	4	Energy range
Time-frequency domain features	5	Frequency variance
	6	Frequency maximum
	7	Frequency minimum
	8	Frequency average
	9	Frequency range
Time domain features	10	Amplitude variance

	11	Amplitude maximum
	12	Amplitude minimum
	13	Amplitude range
	14	Entropy
	15	Peak variance
	16	Peak average
	17	Peak maximum
	18	Number of peaks

We built a statistic-feature-based respiratory pattern classification model with these features and used this model to test whether the generated signal from the respiration simulation model developed in Section 5.1.2 can be used in the respiratory pattern classification.

5.2.1 Respiration simulation model test

In this section, we aimed to prove the feasibility of using the simulated signals generated by the proposed respiration simulation model in respiratory pattern classification. An iteration classification method proposed by Hernandez-Matamoros et al [78] is used in our study. This method is used to prove that the generated signal can be applied in the pattern classification study. It evaluates the generated signals by using iterative classification: in the first iteration, real biomedical data is used to build a classification model, and the performance of the model is evaluated by 10-fold cross-validation; then, in each following iteration, the generated data is added to the dataset to double the capacity of each class, and build a model based on the expanded dataset. The performance of the model built in each iteration is compared to evaluate the quality of the generated data: if the generated data is so similar to the real data that it can be applied as a substitution of real data in classification, the model performance will at least remain, or slightly improved due to the increase in the training data capacity.

In the respiration simulation model test, we selected 50 sets of radar-collected data from each of eupnea, Cheyne Stokes respiration and Kussmaul breathing datasets. Eighteen features we described at Section 5.1.2 were used for the feature extraction. A random forest classifier with parameter "number of trees" set to 100 was used as the classification model, and we implemented five iterations. The accuracy for each iteration is shown in Table 5-2, and the confusion matrices for each iteration are shown in Fig. 5-8, Fig. 5-9, Fig. 5-10, Fig. 5-11 and Fig. 5-12.

Table 5-2 Accuracy for iteration

Iteration	Samples of each class	Accuracy
1	50	92.0%
2	100	93.6%
3	200	95.2%
4	400	97.6%
5	800	98.5%

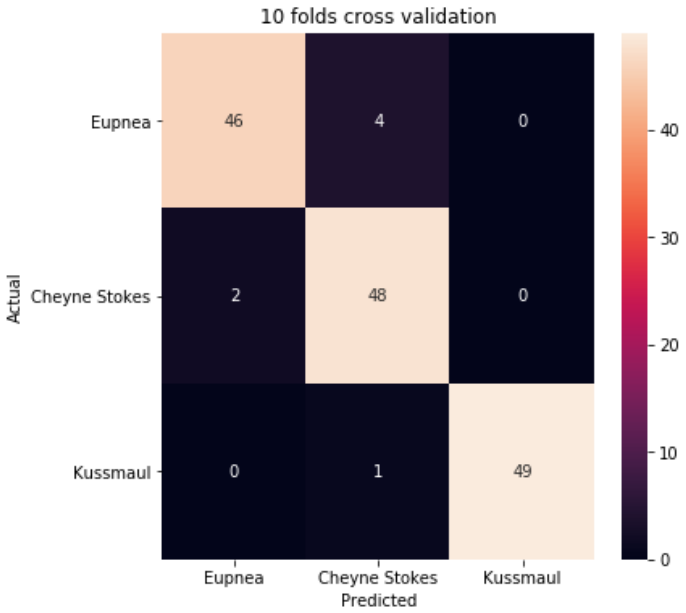

Fig. 5-8 Confusion Matrix-Iteration 1

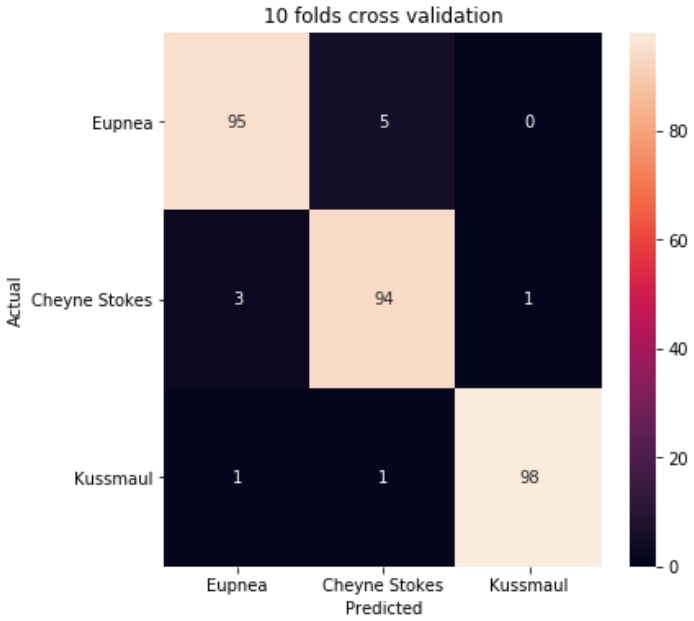

Fig. 5-9 Confusion Matrix-Iteration 2

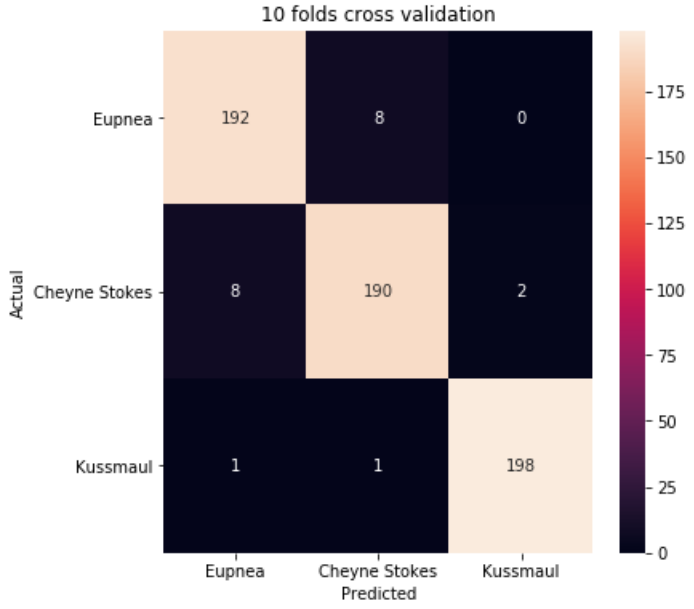

Fig. 5-10 Confusion Matrix-Iteration 3

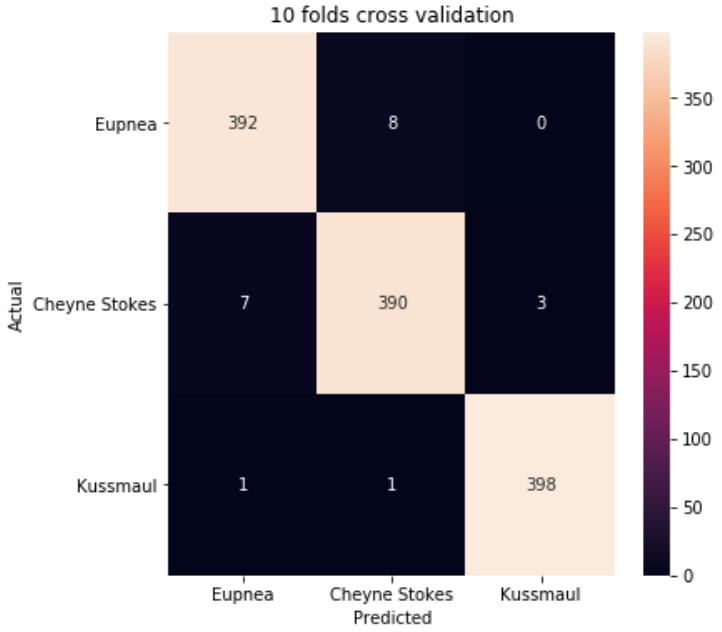

Fig. 5-11 Confusion Matrix-Iteration 4

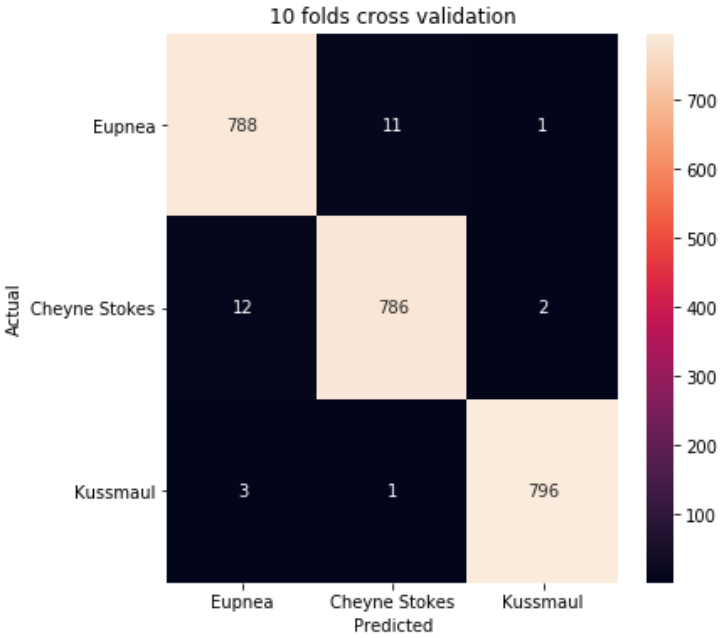

Fig. 5-12 Confusion Matrix-Iteration 5

According to the results shown above, the models are able to successfully differentiate between these three patterns of respiratory signals with accuracy between 92% and 98%. As expected, the model performances remain at a high level in each iteration, and the variation range of accuracy increase is the same as the variation range in Hernandez-Matamoros's study

[78]. The experiment result indicates that the generated simulated signal can be used in respiratory pattern classification.

The apnea data did not present in this test. There are two reasons for the absence. The first reason is that the apnea data is not sufficient for this test. The simulation of apnea may cause severe discomfort, hence we only conducted a limited amount of apnea simulation. The second reason is that the apnea data is more easy to be identified. The apnea signal does not have a sinusoidal waveform, which clearly differentiates it from other respiratory patterns. This characteristic makes the apnea signal easier to be simulated and its similarity is easier to be evaluated. Therefore, we did not include the apnea signal in this test.

5.2.2 Model training

The traditional respiratory pattern classification model is a "flat" classification model, which means that all the class label predictions perform independently at the same level. As shown in Fig. 5-13, all the patterns including eupnea, Cheyne Stokes respiration, Kussmaul breathing, apnea and distorted signal are classified by one classification model.

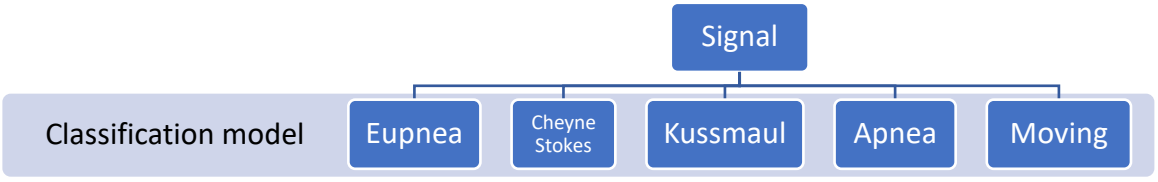

Fig. 5-13 Flat respiratory pattern classification

Since we have proven the feasibility of applying the generated signal from the respiration simulation model for classification in the previous section, we used the generated signal to train the model. The only exception is that the "moving" samples are extracted from the radar-collected signal, which consists of distorted breath samples and respiration-irrelevant samples. This execution is used to prevent that the breath samples collected from the same subject are

used to train and test the model in the same experiment. In that situation, if the model performance is good, there would be a possibility of overfitting [64].

In the classification model training stage, we generated 100 sets of simulated data of eupnea, Cheyne Stokes respiration, Kussmaul breathing and apnea, respectively, and selected 100 sets of data from the moving signal dataset to build a training data set with a total of 500 sets of samples.

5.2.2.1 Classification model selection

Three types of classification method, support vector machine (SVM), decision tree and Random Forest classifier were implemented in this study. Python *scikit-learn* library was used to realize these classification algorithm. To find out the best performance of each classifier, several key parameters of each classifier had been tested, as shown in the Table 5-3. The parameters which are not mentioned in the table were set as *scikit-learn* default values.

Table 5-3 Parameter setting of the classifiers

Classifier	Tested parameters
SVM	Kernels: “linear” , “polynominal”, “Gaussian” , “sigmoid”
Random Forest	Number of trees: 10, 100, 1000

First, 18 features introduced in Section 5.2 were used for generating the feature set. The SVM with linear kernel has the best overall accuracy of 86%, the accuracy of decision tree is 85%, and the Random Forest classifier with 100 trees has the best overall accuracy of 90%.

5.2.2.2 Feature selection

Basing on the feature selection algorithm ReliefF, the feature importance are calculated, as shown in Fig. 5-14.

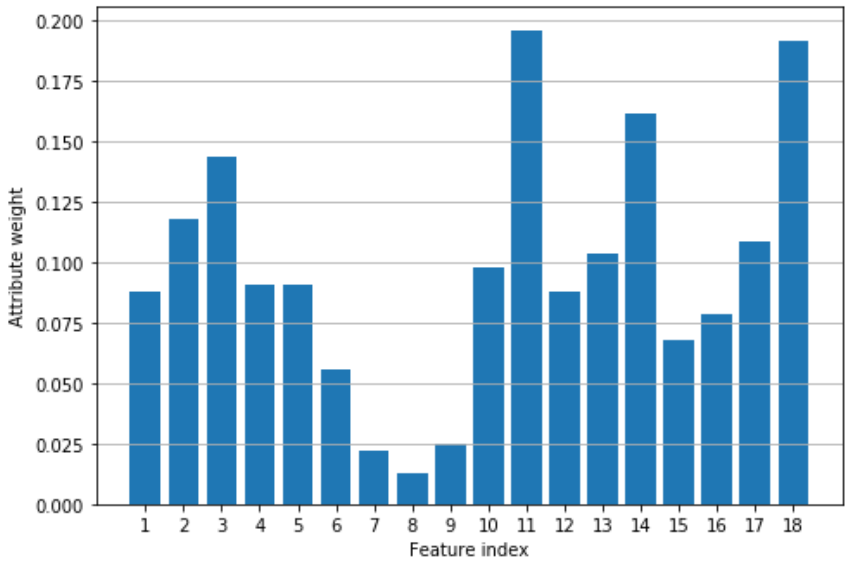

Fig. 5-14 Attribute weights of features in flat classification

According to this figure, all features introduced in this study have positive weights, which means that all of the features have positive effects to the pattern classification.

5.2.2.3 Classification

According to Section 5.2.2.1, the random forest classifier with 100 trees has the best performance, so it was selected as the classifier of this model. We extracted 18 features of the training data mentioned in Section 5.2.2 and used them to train the random forest classifier. The model performance was evaluated by tenfold cross-validation, and the total accuracy is 96.6%.

5.3 Time series-based respiratory pattern classification

Time series-based classification method, which can utilize the characteristic of ordering in a time sequence signal, can provide a new perspective regarding extracting signal features. In the study of time series-based technique, an algorithm based on the shape of time-series signal, shapelet transform algorithm, is considered to be the most suitable algorithm for respiratory pattern classification. In this thesis, a series of trials were carried out to explore the application of shapelet transform in respiration study, and they are incorporated with the traditional respiratory pattern classification technology to build several joint classification models with different performance characteristics.

5.3.1 Shapelet transform algorithm

In Chapter 2, the theory of shapelet transform classification is introduced in details. Briefly speaking, the difference between traditional classification and shapelet transform classification is in the process of feature extraction. In traditional classification, features sets are established based on statistic features, and these features are extracted in a way that regards each data point of the signal as an independent element. However, in shapelet transform classification, the features are extracted in a different way which considers the inner ordering relationship in the scans.

5.3.1.1 Processing flow

Firstly, the algorithm finds patterns in training data which have the highest probability to exist only in the signals with same class label. The patterns and the signals are in a form of time sequences. In other words, these sequences are the most representative sequences of the classes of signal they belong to. These patterns are called shapelets. The shapes of these sequences can be visualized by plotting them with a time axis.

Then, the algorithm calculates the distances between the sub-sequences in each training sample and each shapelet sequence. The more similar the shape of the two, the closer the distance. The sub-sequence can appear anywhere in the sequence of training sample. The closest distance between the sub-sequences and the shapelet sequence is regarded as a feature index of the training sample. The feature set generated by shapelet transform algorithm is an assemble of all the feature indexes. The feature set dimension is determined by the number of shapelets. The more shapelets extracted from the training dataset, the larger the dimension of feature set. A training set contains m samples of time series sequences with n extracted shapelets have a feature set dimension of $m \times n$.

The classification processes of traditional classification and shapelet transform classification are the same. The extracted feature sets are used to train the machine-learning based classifier.

The source code of shapelet transform classification algorithm comes from *sktime* library [79]. In this study, the key to build a good shapelet transform model for respiratory pattern classification is to extract the most representative shapelets for each class.

5.3.1.2 Key factors in model training

The quality of the extracted shapelet depends on four key factors: training data, training time, minimum and maximum shapelet length and maximum number of shapelets to store per class.

The training data needs to have salient features of the respiratory pattern. As an example of the class it represents, it should be a sample with standard waveform. However, most of the respiratory signal collected from radar in the lab cannot meet this criterion. The reason is that it is difficult for human subjects to perfectly perform imitations of respiratory patterns, especially for some breathing patterns which may cause discomfort. In this case, there would be random segments in the samples which may "confuse" the model: the model may extract shapelets from those random segments. In fact, the imitation of all breathing patterns except eupnea will cause varying degrees of discomfort. To avoid random segments in the breath samples, all training data were generated by the respiration simulation model except data from the "moving" class. The randomness and diversity of "moving" samples are difficult to simulate; however, they are easy to be obtained in the experimental data.

Training time is a special factor which does not exist in most of the models, but crucial in this algorithm. In the operation mechanism of the shapelet transformation algorithm in the *sktime* library, the training time needs to be set before performing the shapelet extraction experiment. No matter how many shapelets are extracted or how many pieces of data are analyzed, the experiment will end when the running time reaches the set value. This mechanism is different from that of most models in machine learning. Most machine learning models will analyze all the input training data and will end training after the computed cost function is below the threshold. The purpose of this special design is largely based on the computational complexity of the algorithm: the analysis for one data sample with 255 scans consumes 45-60 seconds by an Intel i7-9750H CPU processor. The analysis time will differ depending on the CPU processor performance and the sample volume. The GPU processor is not used in this algorithm. In this mechanism, the longer the setting time, the more samples will be analyzed. To some extent, the longer the setting time will improve the extracted shapelet quality since more samples are analyzed. However, model performance and training time are not always positively correlated. When the most representative shapelets are extracted, the model performance will reach the top. The upper limit of model performance is still determined by the quality of training data. To

improve the experimental efficiency of model training, the training time needs to be set to a value that is enough for analyzing most of the samples with unique waveform characteristics. According to the data training experiment, we found that the algorithm running on a computer with Intel i7-9750H CPU with 16 GB of RAM spends 1 minute to extract the shapelet from a sample, and thus we set the training time according to the number of training samples.

The minimum and maximum shapelet length set a length range of the extracted shapelet. Sequences shorter or longer than this length range would not be considered as a shapelet candidate. This parameter is used to ensure that the most representative shape features with a required length range can be completely retained in the shapelet library. It can help to distinguish respiratory patterns that have similar local shapes. Meanwhile, the increase of minimum shapelet length value or the decrease of the maximum shapelet length will also shorten the overall analysis time because the number of sub-sequences that meet this criterion in a sample decreases. It can help to improve the model training efficiency. However, the minimum shapelet length cannot be too long to reduce the representativeness of the shapelets. The longer the shapelet, the more difficult to find a similar sequence in the samples. It is important to set a shapelet length range that can balance these two factors.

The maximum number of shapelets to store per class is directly related to the representativeness of the extracted shapelets. In the shapelet extraction, the information gain of each extracted shapelet is sorted, and this parameter determines how many candidate shapelets will be included in the shapelet library of the model. If the maximum number is set to m, only the shapelets with top m highest information gain will be retained. This evaluation principle is based on the assumption that the highest information gain corresponding to the highest representativeness. Contradictory to representativeness is diversity, which means that there is more than one segment waveform that can represent the pattern, such as the decrescendo-apnea phase and apnea-crescendo phase for the Cheyne Stokes respiration. Meanwhile, for this shapelet transform model, there is not a dynamic time warping process which can accept the subtle difference between waveforms of the signal which belong to the same pattern. Hence, increasing the diversity, which can be implemented by increasing the value of maximum number of shapelets, is also important for the model training. In the model implementation, the number of

overall shapelets will also influence the computational complexity: the more the shapelets, the higher the computational complexity.

Other parameters of shapelet transform algorithm in *sktime* not mentioned here will influence the experiment result as well but comparing with these five parameters introduced above, they have less influence on the trained model performance, so they were all set as default value in this study.

5.3.2 Model training

In this section, we demonstrated the process of building two types of joint hierarchical classification models with different strategies. The shapelet transform algorithm plays different roles in these two types of models. The process of training the shapelet transform algorithm model is highlighted in this section. All training data are simulated data generated by the respiration simulation model developed in Section 5.1.2.

5.3.2.1 Joint model I

The classification strategy of joint model I is shown in Fig. 5-15. It is a hierarchical classifier with two levels. In the first level, a traditional pattern classification model was trained to classify the signal into four classes: eupnea, Kussmaul breathing, irregular signal and apnea. In the second level, a shapelet transform classification model was developed to classify signals with irregular waveform patterns, including Cheyne Stokes respiration and the "moving" signal.

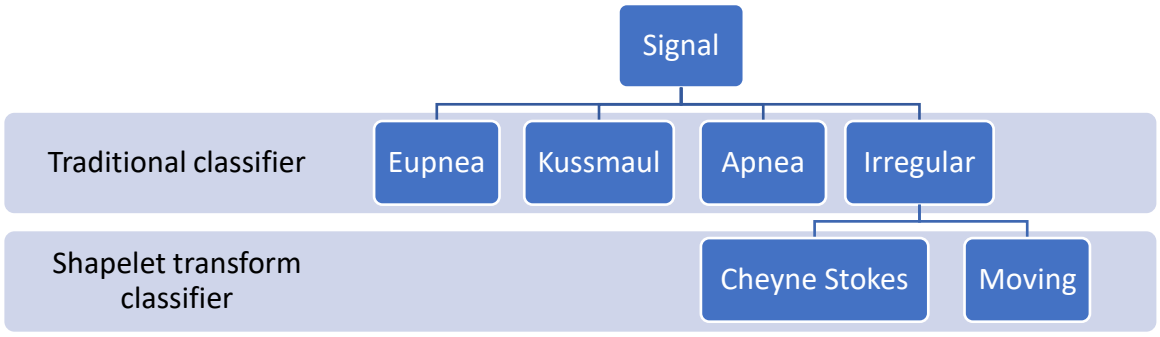

Fig. 5-15 Joint model I classification strategy

The process of developing a traditional respiratory pattern classification model is the same as that in Section 5.2.2. We generated 200 sets of simulated data of eupnea, Kussmaul breathing and apnea respectively, generated 100 sets of Cheyne Stokes respiration, and selected 100 sets of data from the "moving" sample dataset to compose a set of irregular signal, to build a training dataset with a total of 800 sets of samples. We extracted 18 features of the data in the training dataset and used them to train a random forest classifier with 100 trees. The model performance is evaluated by tenfold cross-validation, and the total accuracy is 97.8%.

Then, a shapelet transform classification algorithm was developed to classify two classes of irregular respiratory signals: Cheyne Stokes respiration and the "moving" sample.

The first step to build the shapelet transform model is to prepare training data with salient features. Since there is not a fixed pattern in the moving data, moving data with various kinds of shapes were used to train the model. However, there is an obvious characteristic in Cheyne Stokes respiration. A standard Cheyne Stokes respiration contains three phases: crescendo phase, decrescendo phase and apnea phase. Since the duration of each signal sample is 15 second, and the cycle length of Cheyne Stokes respiration is around 40-90 seconds [9], a sample will not contain a complete cycle of Cheyne Stokes respiration. Therefore, the sampling segments consist of segments of crescendo phase, decrescendo phase, apnea phase, or segments which contain two of the phases mentioned above. Because the apnea phase will be classified into apnea class, and the transition phase of crescendo and decrescendo with smaller peak amplitude variance is hard to be classified even manually, training data with crescendo phase, decrescendo phase, apnea-crescendo transition phase and decrescendo-apnea transition phase were used to train the model. To balance the shapelet number of each class, we divided the Cheyne Stokes respiration samples into two classes, crescendo phase class and decrescendo phase class. The crescendo phase class includes the crescendo phase and apnea-crescendo transition phase, and the decrescendo phase class contains the decrescendo phase and decrescendo-apnea transition phase. All of the samples are manually segmented to make sure the expected waveforms are selected. The features of Cheyne Stokes respiration samples are shown in Fig. 5-16, Fig. 5-17, Fig. 5-18, Fig. 5-19.

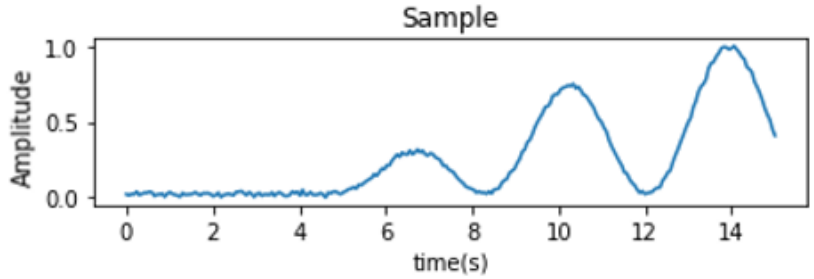

Fig. 5-16 Cheyne Stokes respiration apnea-crescendo transition phase

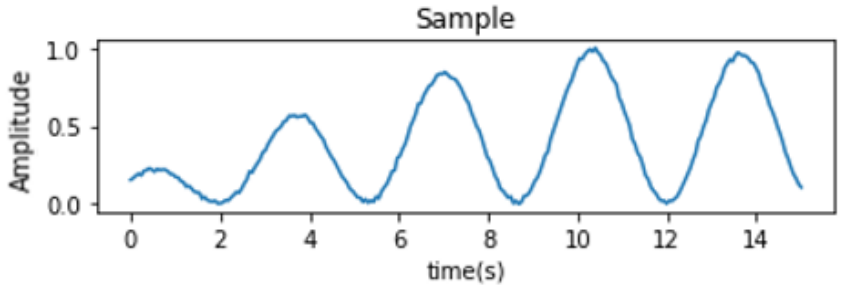

Fig. 5-17 Cheyne Stokes respiration crescendo phase

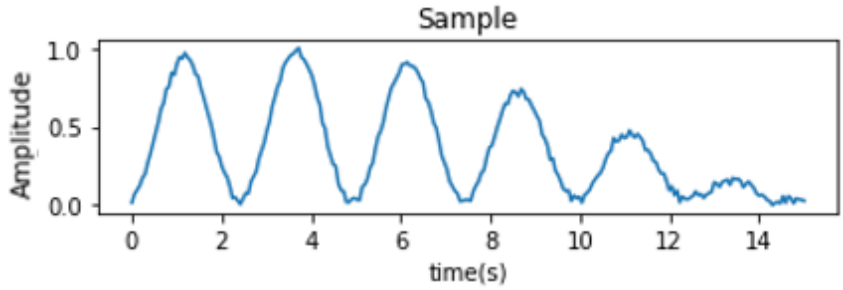

Fig. 5-18 Cheyne Stokes respiration decrescendo phase

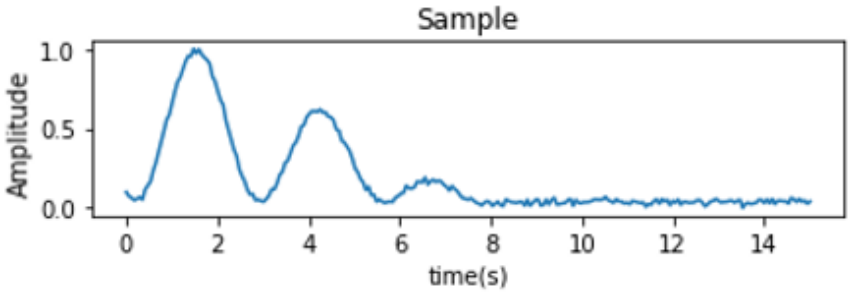

Fig. 5-19 Cheyne Stokes respiration decrescendo-apnea transition phase

In the shapelet extract experiment, the minimum and maximum shapelet length was set to 100 and 255, respectively (the complete sequence length is 255), and the parameter maximum number of shapelets to store per class was set to 5. In this experiment, the expected shapelets are

sequences that can represent those four phases mentioned above. In the model training stage, we selected 10 sets of simulated Cheyne Stokes respiration samples, including 5 sets of crescendo phase samples and 5 sets of decrescendo phase samples, and 10 sets of moving samples to build a training data set with a total of 20 sets of samples. All samples were manually selected and all of them have significant waveform characteristics of their class. The model training time was set to 20 minutes which is enough for analyzing all the samples. The shapelet extraction process extracted 5 shapelets for each class. The examples of shapelet extract results are shown in Fig. 5-20, Fig. 5-21, Fig. 5-22, Fig. 5-23, Fig. 5-24.

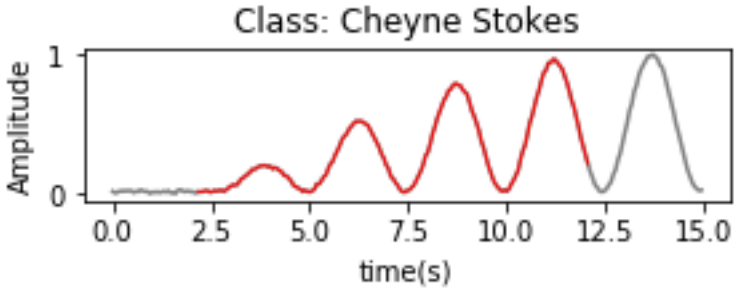

Fig. 5-20 Extracted shapelet for Cheyne Stokes respiration apnea-crescendo transition phase (red line)

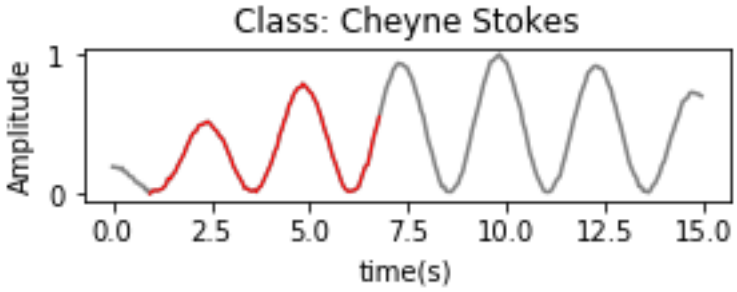

Fig. 5-21 Extracted shapelet for Cheyne Stokes respiration crescendo phase (red line)

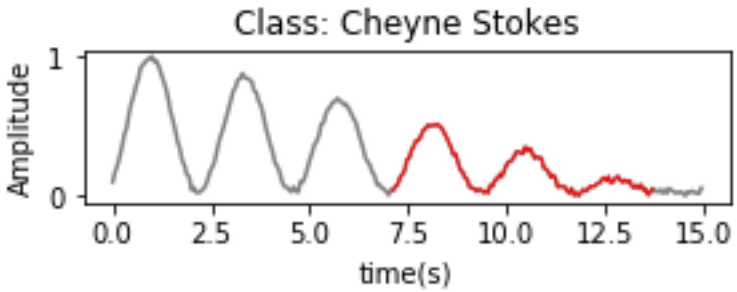

Fig. 5-22 Extracted shapelet for Cheyne Stokes respiration decrescendo phase (red line)

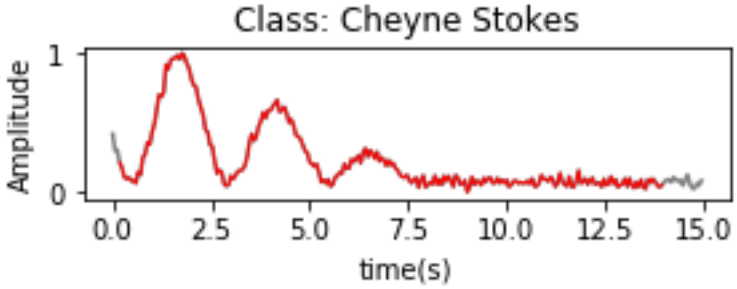

Fig. 5-23 Extracted shapelet for Cheyne Stokes decrescendo-apnea transition phase (red line)

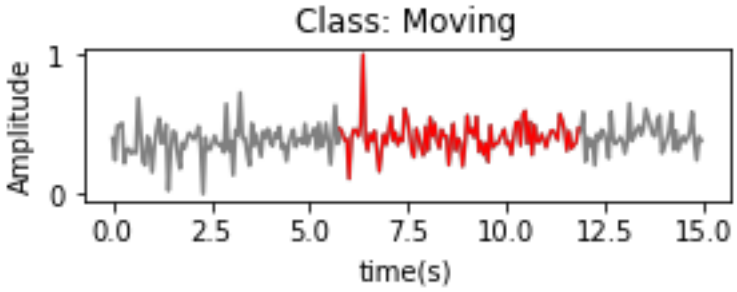

Fig. 5-24 Extracted shapelet for "moving" signal (red line)

In these figures, the grey lines are training samples, and red lines represent the extracted shapelets corresponding to the class of the training samples. According to the figures, the algorithm extracts the required shapelets as expected. Five Cheyne Stokes crescendo phase shapelets, five Cheyne Stokes decrescendo phase shapelets and five “moving” sample shapelets were extracted in the experiment. After the shapelet extraction, the feature set was built by calculating the distances between the input samples and those 15 extracted shapelets. For each sample, a feature vector with 15 dimensions was generated. This feature set was used to train a random forest classifier with 100 trees.

Considering the model is implemented to classify Cheyne Stokes respiration (CSR) and the "moving" sample, and the major difference in the waveform is that the CSR signal has a segment of sinusoidal-wave-like signal while the "moving" sample does not, we also developed another shapelet transform classification model with the minimum and maximum shapelet length set to 30 and 85, respectively, to capture the shapelet containing one sinusoidal wave. We defined this shapelet as "short shapelet", and the shapelet with the length range of 100-255 as "long shapelet". The sample of short shapelet is shown in Fig. 5-25 and Fig. 5-26.

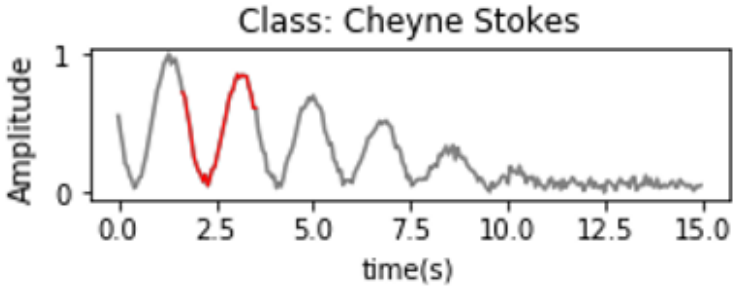

Fig. 5-25 Extracted shapelet for Cheyne Stokes respiration (red line)

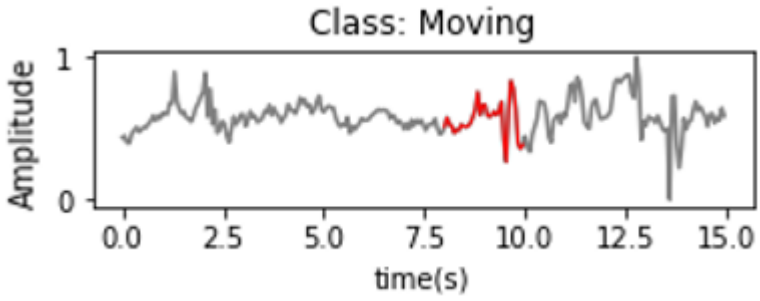

Fig. 5-26 Extracted shapelet for "moving" signal (red line)

The other parameters and training setting are the same as the previous model in this section. To better differentiate these two models, we named them "joint model I with long shapelet" and "joint model I with short shapelet", respectively. In this thesis, the sample window length is 255.

An irregular signal training dataset with 100 sets of Cheyne Stokes respiration samples and 100 sets of moving samples is used to test the performance of the models. The accuracy of joint model I with long shapelet is 85%, and the Joint model I with short shapelet is 97%. The confusion matrices of models are shown in Fig. 5-27, and Fig. 5-28.

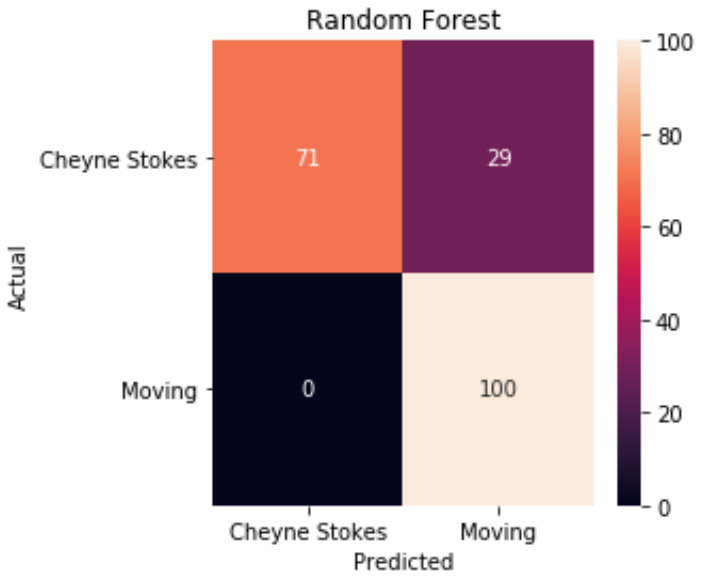

Fig. 5-27 Confusion matrix joint model I with long shapelet

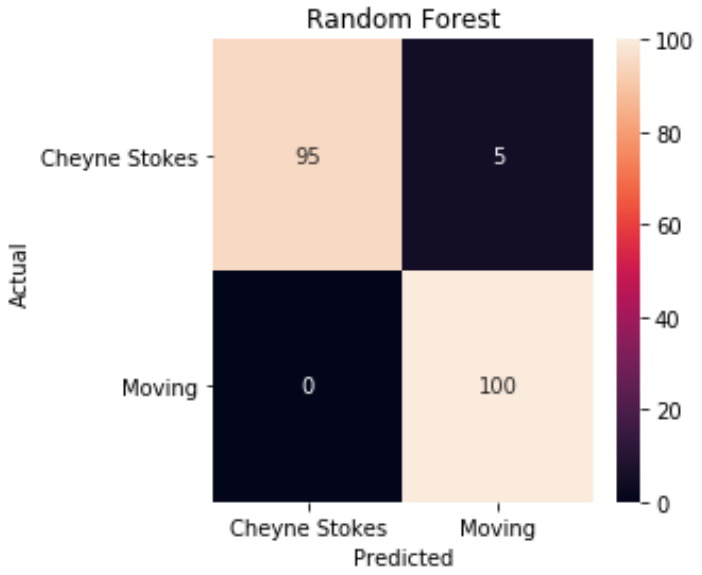

Fig. 5-28 Confusion matrix joint model I with short shapelet

According to the confusion matrices, the shared character of these two models is that even though a portion of CSR samples were classified as “moving”, none of the “moving” samples were classified as CSR. This performance is determined by the characteristic of the shapelet transform algorithm that the classification is based on the shapelet. Only the samples with a sub-sequence similar to a shapelet from the model’s shapelet library can be regarded as the pattern corresponding to that shapelet. For the same reason, the CSR samples are misclassified because

they have no sub-sequence similar to CSR shapelets. The dissimilarity may be caused by a different hyperventilation frequency, a different tidal volume variation or both of them. Also for this reason, a “moving” sample is much harder to be misclassified as a CSR. Therefore, the precision of the classification results is high.

If we define the probability retrieving a CSR sample as the sensitivity to Cheyne Stokes respiration, the longer the shapelet length, the lower the sensitivity. This is because a longer subsequence is more difficult to find someone similar to itself.

This high precision characteristic of the shapelet transform classification is the reason for introducing this technique to the respiratory pattern classification, and we expected this characteristic could help to meet the requirements of low false alarm ratio.

5.3.2.2 Joint model II

Joint model II is another hierarchical classification model we developed in this thesis combing with traditional pattern classification and shapelet transform classification. The classification strategy is shown in Fig. 5-29.

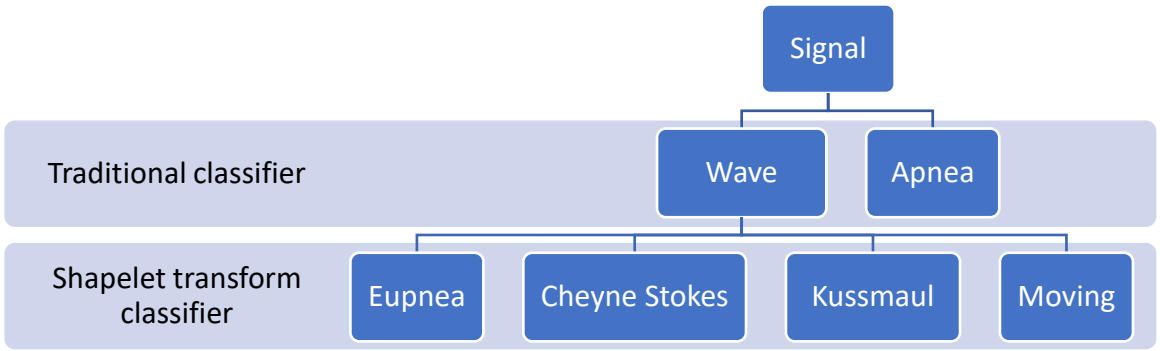

Fig. 5-29 Joint model II classification strategy

In the first level of the hierarchical classification, a traditional statistic-feature-based classification model was trained to classify the signals into 2 classes: signals with obvious amplitude wave and apnea. We simplified the category label "the signal with obvious amplitude wave" to "wave” in the following description. In the second level, a shapelet transform

classification model is trained to classify the “wave” signals into four patterns including eupnea, Cheyne Stokes respiration, Kussmaul breathing and the “moving” signal.

The reason for retaining the traditional classifier in the first level of the model is because the shapelet transform classifier cannot differentiate radar-collected apnea signal and the “moving” signal. Both of the radar-collected apnea samples and “moving” samples are random time series sequences, as shown in Fig. 5-30 and Fig. 5-31. However, the most differentiated feature of the apnea signal is the small amplitude range, which can be easily differentiated by the traditional statistic-feature-based classification model.

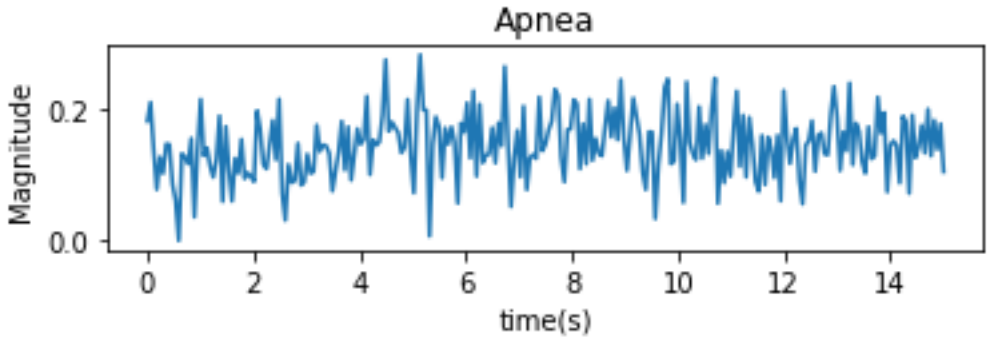

Fig. 5-30 Radar collected apnea signal

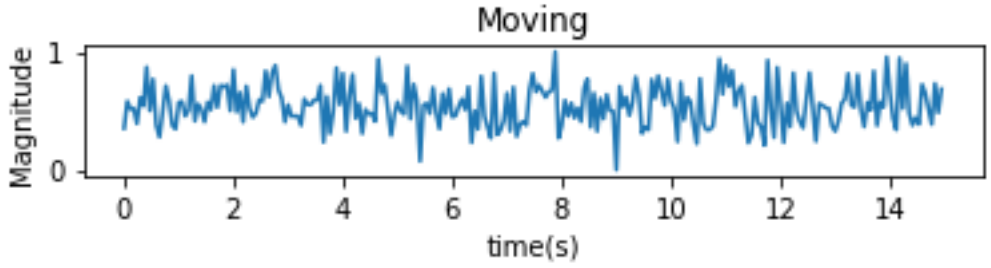

Fig. 5-31 Radar-collected “moving” sample

In Section 5.1.2, we have stipulated that the signals analyzed in this study need to be scaled to a range between [0,1] to reduce the effect caused by different signal amplitude range except for the signals whose amplitude range is smaller than 0.3. This setting prevents the apnea signal from losing the unique amplitude characteristic after being scaled up. However, according to the experiment, this setting did not help the shapelet transform classification algorithm.

Since there are only two classes the traditional classifier needs to classify, it is unnecessary to build a feature set with 18 features. To reduce the computational complexity, we selected 4 features including energy maximum, frequency variance, frequency average and amplitude maximum according to the RelifF algorithm analysis result, which are the four features that have the most significant effect in the classification.

We generated 100 sets of simulated data of eupnea, Cheyne Stokes respiration, Kussmaul breathing, respectively, and selected 100 sets of "moving" signal to compose a set of "wave" signals, and generated 400 sets of apnea signals to build the training dataset with a total of 800 sets of samples. A random forest classifier with 100 trees was trained to build the model. We employed the tenfold cross-validation to evaluate the model performance, and the total accuracy is 99.5%.

In the second level, a shapelet transform classifier is used to classify four classes: eupnea, Cheyne Stokes respiration, Kussmaul breathing and "moving".

In the shapelet extraction stage, the shapelet length range should be larger since the pattern differences between each wave signal cannot be clearly differentiated basing on a short segment. The maximum number of shapelets in each class needs to be reduced to improve the representativeness of each shapelet. After a large number of experiments we eventually set the parameters as follow: the minimum shapelet length is 100 (the complete sequence length is 255) and the maximum number of shapelets to store per class is 5.

In the model training stage, the training database is the same as the one used for training the traditional classifier in the first level of the model. We selected 10 sets of Cheyne Stokes respiration, including 5 sets of crescendo phase samples and 5 sets of decrescendo phase samples, 10 sets of eupnea, 10 sets of Kussmaul breathing, 10 sets of apnea and 10 sets of "moving" samples to build a training data set with a total of 50 sets of samples. All samples are manually selected and all of them have significant waveform characteristics of the corresponding respiratory patterns. The model training time was set to 40 minutes which is enough for analyzing all the samples. The shapelet extraction process extracted 5 shapelets for each class. The example shapelets of each class are shown in Fig. 5-32, Fig. 5-33, Fig. 5-34, Fig. 5-35, Fig. 5-36.

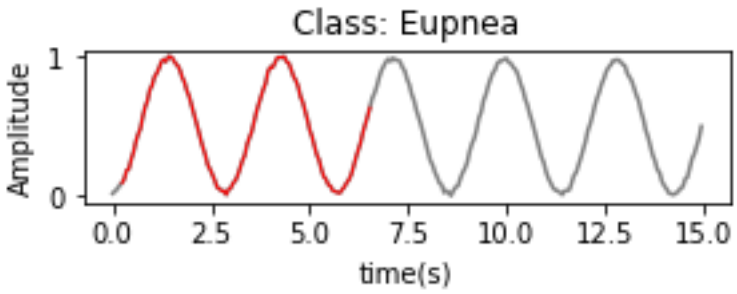

Fig. 5-32 Extracted shapelet for eupnea (red line)

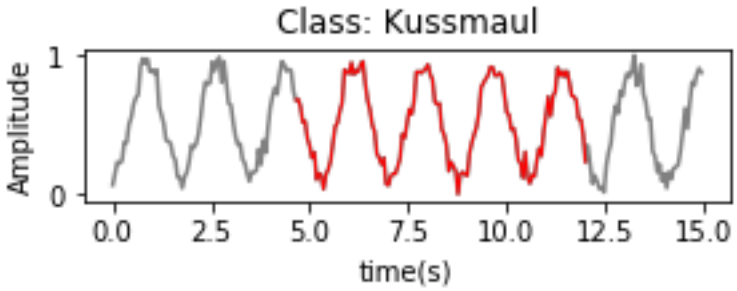

Fig. 5-33 Extracted shapelet for Kussmaul breathing (red line)

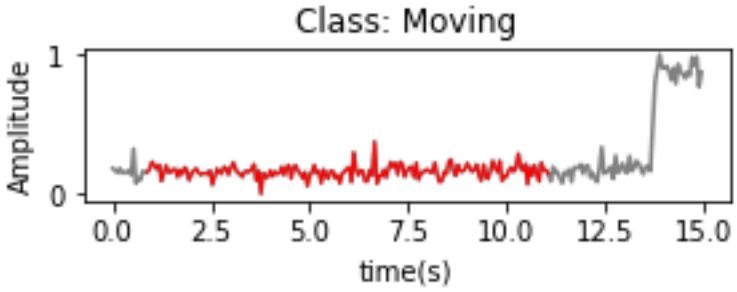

Fig. 5-34 Extracted shapelet for "moving" signal (red line)

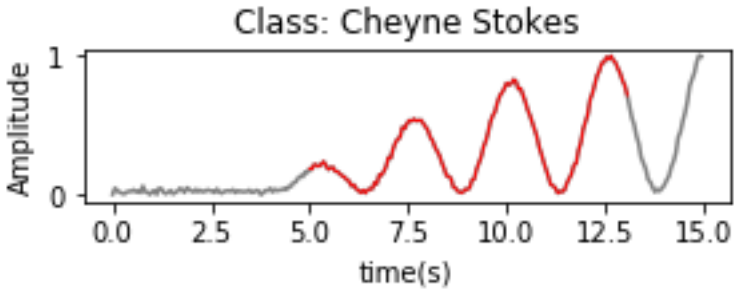

Fig. 5-35 Extracted shapelet for Cheyne Stokes respiration crescendo phase (red line)

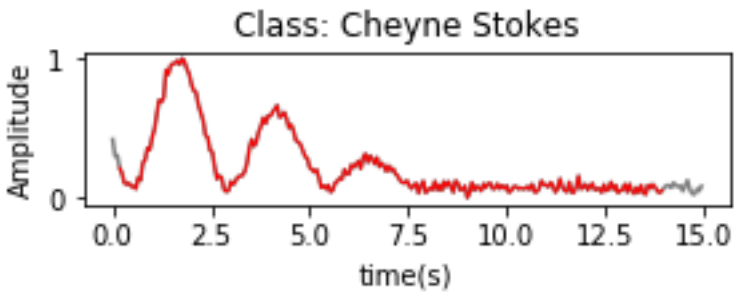

Fig. 5-36 Extracted shapelet for Cheyne Stokes respiration decrescendo phase (red line)

The red lines in the figures are the shapelets extracted from the corresponding classes and the grey lines are the base samples where the shapelets come from. After shapelets extraction, a feature set was built and used to train a random forest classifier with 500 trees.

The “wave” signal training dataset including 100 sets of simulated eupnea, Cheyne Stokes respiration Kussmaul breathing and 100 sets of “moving” samples was used to test the models' performance. The overall accuracy is 97%, and the confusion matrix is shown in Fig. 5-37.

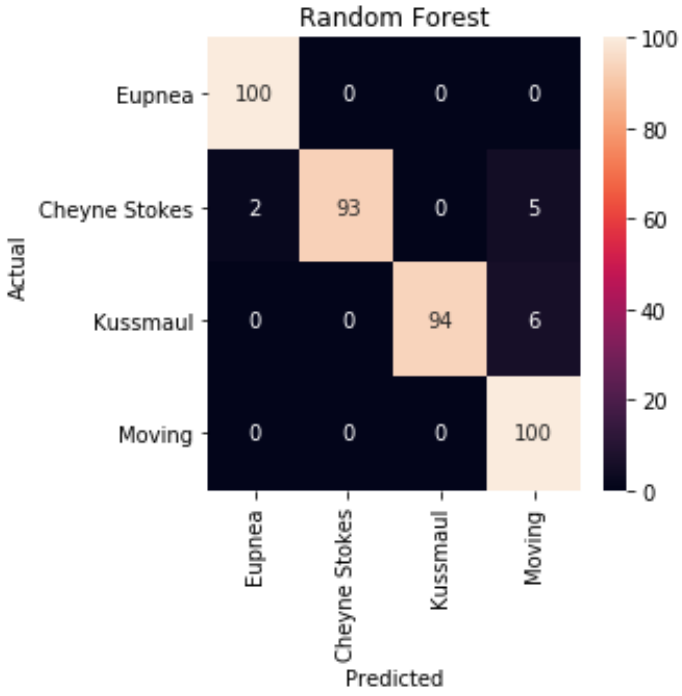

Fig. 5-37 Confusion matrix of Joint model II

According to the results, the precision of each breathing pattern is high, which meets our expectation of the model performance. The reason for the breath samples being misclassified as

“moving” is the same as the reason explained in the section of Joint model I. There are two samples of CSR signal were classified as eupnea, the reason is that the crescendo-decrescendo transition phase in Cheyne Stokes respiration is similar to an eupnea sample, as explained in 4.2.1.

5.4 Conclusion

In this chapter, we demonstrated the process of developing the respiratory pattern classification models. Firstly, we built the respiratory signal database which contains radar-collected breath signals and simulated breath signals generated by the respiration simulation model proposed in this thesis. Secondly, we summarized the feature values used in the state-of-the-art breathing pattern classification study, and used the features to prove the feasibility of applying the generated signal to the respiratory pattern classification study. Then, we used the generated signal to build a classification model based on the summarized features. Thirdly, we introduced the method to train a shapelet transform classification model, and built two types of respiratory pattern classification models based on the traditional classification model and the shapelet transform model. The shapelet transform classification model showed its characteristic of high precision in specific classes, and thus it was expected to meet the requirement of low false alarm ratio for the continuous respiratory pattern classification. The performance of the proposed models will be tested by radar-collected signals in the next chapter.

Chapter 6: Model implementation

In the previous chapter, we introduced the process of developing respiratory pattern classification models based on generated signals and built three types of models. In this chapter, we test these models by radar-collected data. The first test was implemented in a batch-processing manner with data from the respiratory signal database. The second test was implemented in a stream-processing manner with respiratory data collected by a continuous vital signs monitoring system.

6.1 Batch processing: Radar-collected respiratory signal database

The models are firstly tested with data from the respiratory signal database built in Section 5.1.1. Since 100 sets of "moving" signals were used to develop the models, we removed those 100 sets of "moving" samples from the database. Eventually, there are 325 sets of 15-seconds samples, including 137 sets of eupnea, 50 sets of Cheyne Stokes respiration (CSR), 50 sets of Kussmaul breathing and 88 sets of "moving" samples in the database. All the breath samples in the database are collected by radar. The apnea samples were not included in the database, due to the reason mentioned in Section 5.2.1.

6.1.1 Traditional classification model

The performance of the traditional classification model is presents by the classification report and confusion matrix, as shown in Table 6-1and Fig. 6-1, respectively. The overall accuracy is 0.84, and the false alarm ratio is 0.27.

Table 6-1 Classification report of traditional classification model

	precision	recall	f1 score	support
Eupnea	0.98	0.86	0.92	137
Cheyne Stokes	0.57	0.48	0.52	50
Kussmaul	0.94	0.9	0.92	50
Moving	0.76	0.95	0.84	88

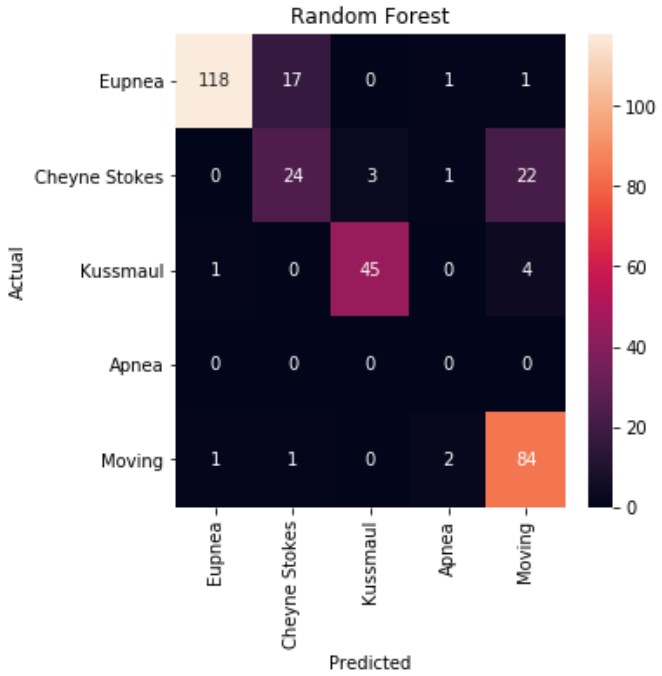

Fig. 6-1 Confusion matrix of traditional classification model

According to the result, there are two major problems in the classification: some eupnea samples were classified as CSR, and some CSR samples were classified as moving. Among the misclassified samples in the first problem, most samples have a common feature, that is, there is a short pause after each respiration pulse, as shown in Fig. 6-2.

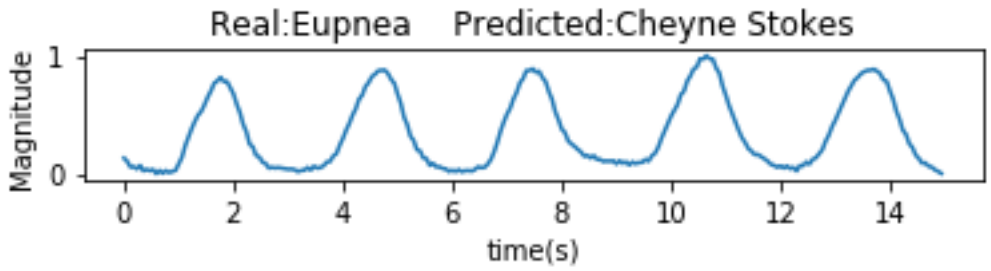

Fig. 6-2 Misclassified eupnea sample

For the second problem, the CSR samples whose peaks are sharp are more likely to be classified as moving, as shown in Fig. 6-3.

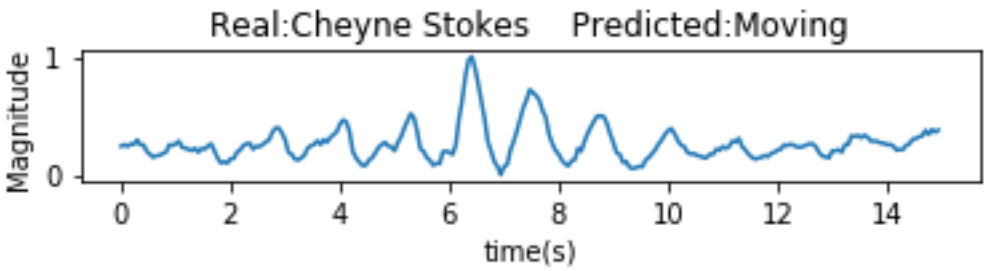

Fig. 6-3 Misclassified CSR sample

In summary, these two problems are mainly caused by the unique breathing habits of different individuals. Since the training data is only composed of sinusoidal-wave-like simulated signals, the monotonicity of the signal waveform is the reason for the misclassification of the model.

6.1.2 Joint model I

The performance of joint model I with long shapelet is shown in Table 6-2 and Fig. 6-4. The overall accuracy is 0.77, and the false alarm ratio is 0.16.

Table 6-2 Classification report of joint model I with long shapelet

	precision	recall	f1 score	support
Eupnea	1	0.8	0.89	137
Cheyne Stokes	0.62	0.1	0.17	50
Kussmaul	0.91	0.96	0.93	50
Moving	0.56	0.97	0.71	88

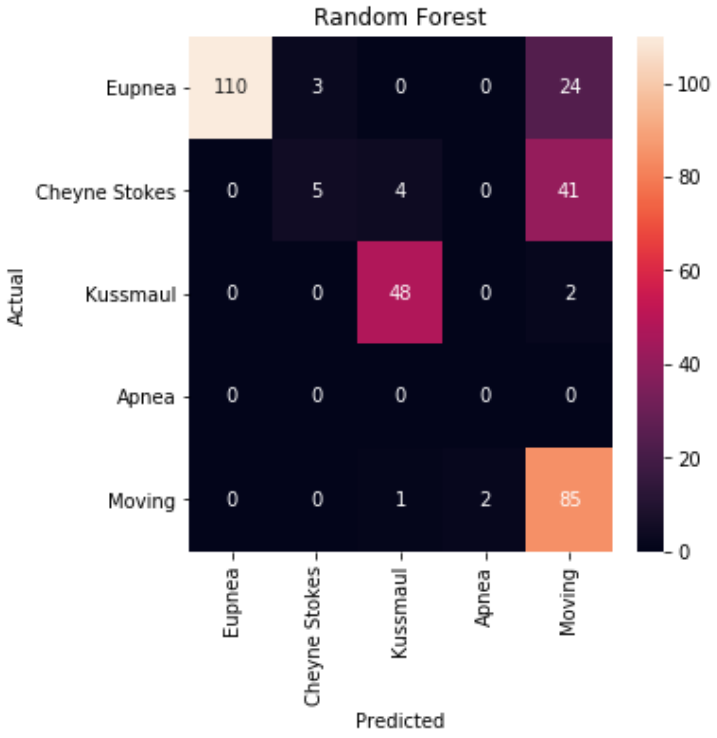

Fig. 6-4 Confusion matrix of joint model I with long shapelet

The major problem of this model is most of the CSR samples were classified as moving. Since the classification of CSR and moving is executed by the shapelet transform classifier, the reason for the misclassification is that the misclassified CSR samples have no sub-sequence similar to the shapelets in the shapelet library, which has been mentioned in Section 5.3.2.1. Because of the samples in the radar-collected database are more diverse than the simulated samples used for shapelet extraction, sub-sequences which similar to the shapelets are more difficult to find in the test samples.

Another problem raising our concern is the misclassification of eupnea. Some of the eupnea samples were classified as moving. The reason is the same as that in Section 5.3.2.1. Those samples classified as CSR in Section 6.1.1 were classified as irregular signal in this model. It is because in these two models, CSR, which belongs to the irregular class, is both classified by a traditional classifier.

The performance of joint model I with short shapelet is shown in Table 6-3 and Fig. 6-5. The overall accuracy is 0.83, and the false alarm ratio is 0.22.

Table 6-3 Classification report of joint model I with short shapelet

	precision	recall	f1 score	support
Eupnea	1	0.8	0.89	137
Cheyne Stokes	0.67	0.56	0.61	50
Kussmaul	0.91	0.96	0.93	50
Moving	0.71	0.95	0.82	88

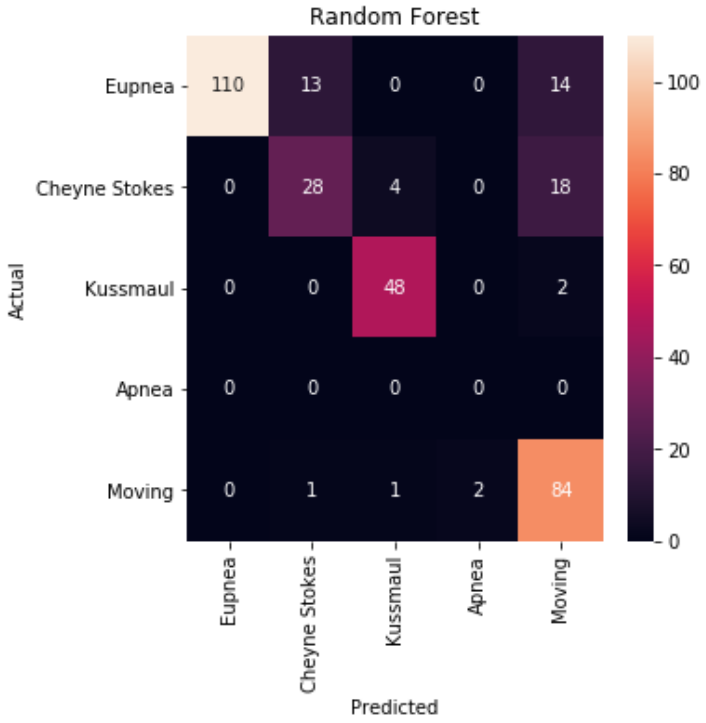

Fig. 6-5 Confusion matrix of Joint model I with short shapelet

The long shapelet model and short shapelet model use the same traditional classifier in the first level which classify the CSR signal and the “moving” signal. The only difference in the results is the amount of predicted CSR. As mentioned in Section 5.3.2.1, models with short shapelet length is more sensitive to CSR. The results in this section confirm this view. Regardless of eupnea samples being classified as CSR caused by the traditional classifier, these

two models, Joint model I with long shapelet and Joint model I with short shapelet, also follow the characteristic of high precision in predicting CSR samples: there is only one moving sample being classified as CSR.

6.1.3 Joint model II

The performance of joint model II with long shapelet is shown in Table 6-4 and Fig. 6-6. The overall accuracy is 0.63, and the false alarm ratio is 0.31.

Table 6-4 Classification report of joint model II

	precision	recall	f1 score	support
Eupnea	0.97	0.5	0.66	137
Cheyne Stokes	0.52	0.22	0.31	50
Kussmaul	0.77	0.72	0.74	50
Moving	0.47	1	0.64	88

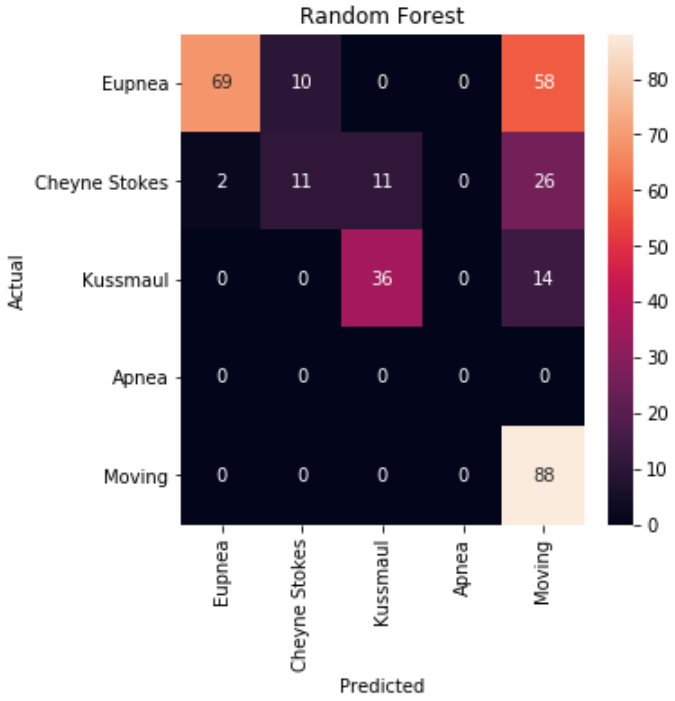

Fig. 6-6 Confusion matrix of joint model II

Joint model II is a hierarchical classification model that most of the classification is implemented by shapelet transform classifier. There is a serious problem in this model that many breath samples are misclassified as moving. This is not the first time this problem occurs. It also showed up in the previous study involving a shapelet transform classifier, and the reason is the same that the misclassified samples have no sub-sequence similar to the shapelets in the shapelet library. The situation in this model is more similar to the situation in Joint model I with a long shapelet. This is because, in both of the study, the parameter of minimum shapelet length was set to 100 in the shapelet extraction phase, which means that all the shapelets are long shapelets. Due to the samples in the radar-collected database are more diverse than the simulated samples, sub-sequences which similar to the shapelets are more difficult to find in the test samples.

There are also problems that some CSR samples were classified as Kussmaul and some eupnea samples were classified as CSR. In the first problem, the hyperventilation frequency of the misclassified CSR samples is high and the tidal volume variation is small and thus they confused the classifier. One example of this situation is shown in Fig. 6-7.

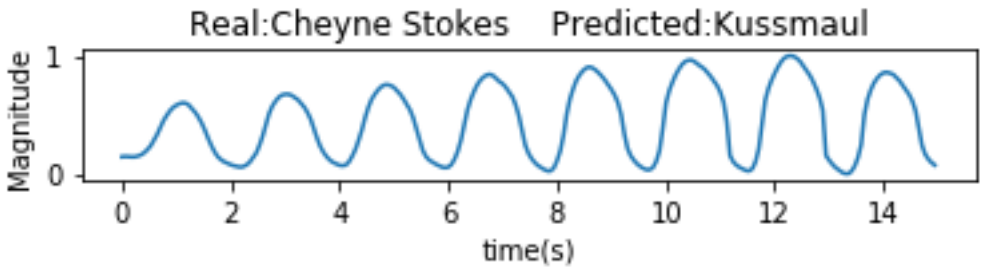

Fig. 6-7 Misclassified CSR sample

For the second problem, eupnea samples with long pauses may also be misclassified as CSR since it has a phase similar to the decrescendo-apnea transition phase of Cheyne Stokes respiration, as shown in Fig. 6-8.

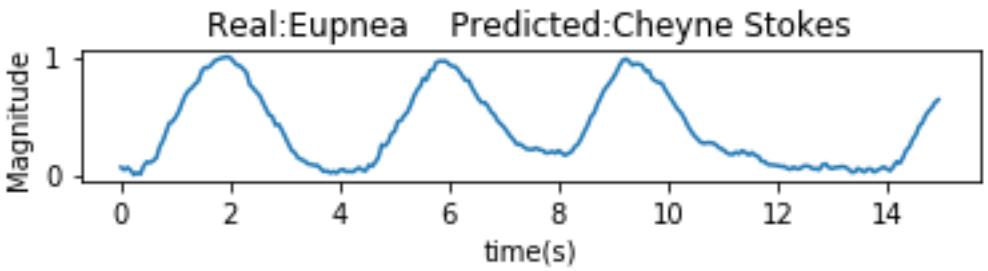

Fig. 6-8 Misclassified eupnea sample

6.1.4 Experiment summary

In the first model test, the traditional classification model and Joint model I with short shapelet have the best overall performance, and Joint model I with long shapelet has the lowest false alarm ratio. All models involving shapelet transform classifier met the same problem, that is, some breath samples were misclassified as "Moving". The reason is that the misclassified samples have no sub-sequence similar to the shapelets stored in the shapelet library. The longer the shapelet length, the more misclassification occurs. The characteristic of high precision of shapelet transform classification still showed up in this test, especially for the Joint model I, but this characteristic is not obvious compared with the traditional classification model.

According to the classification reports, all models had good performance in classifying eupnea and Kussmaul breathing. The CSR is the respiratory pattern that most difficult to be classified, and Joint model I with short shapelet outperformed the other models in classifying the Cheyne Stokes respiration.

6.2 Stream processing: Vital signal monitoring system

The vital signal monitoring system[26] used in this study consists of three Novelda® Xethru X4M03 (IR-UWB) radars that can cover the whole room, a Kinect camera that can track subjects' joints 3D coordinates and a computer which records and processes the data. The experimental setup for this work is shown in Fig. 6-9.

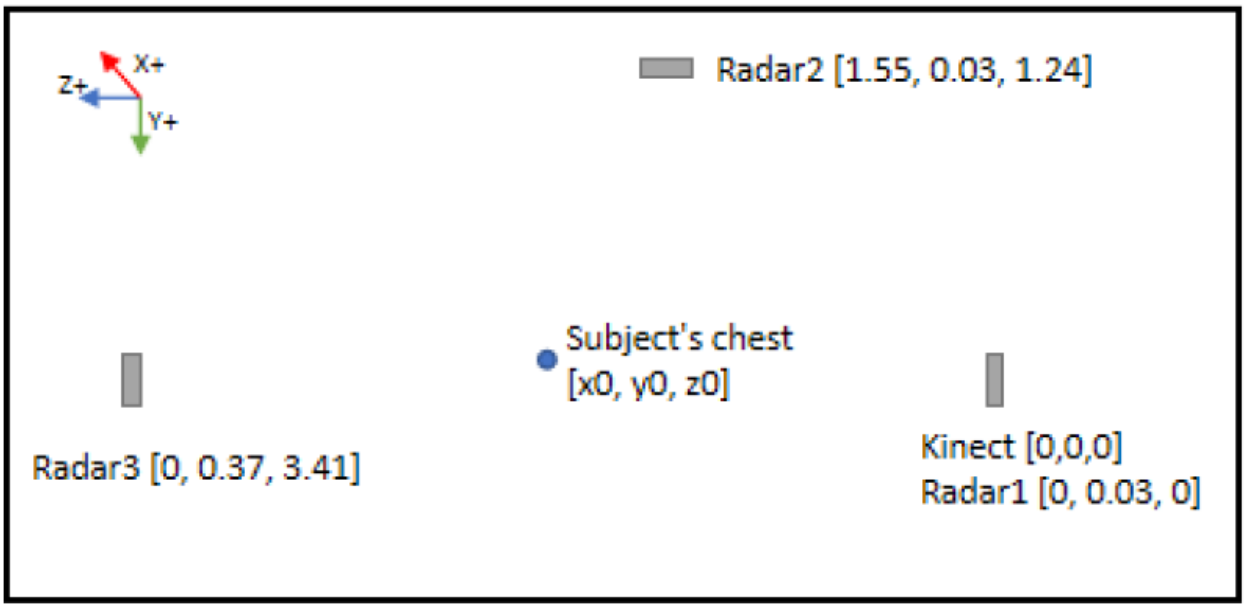

Fig. 6-9 The location of the devices and their coordinates in the reference frame

Three Xethru X4M03 radars are mounted on the poles located at different positions in the monitoring zone, each of the radars is pointing toward the center of the detecting area. The sampling rate of each radar is 17 Hz. The Azure Kinect (Microsoft) has a 12-megapixel RGB camera supplemented by a 1-megapixel depth camera for body tracking. The Azure Kinect camera is placed close to the Radar 1 with a height of 2.11 m. In this system, the Azure Kinect is used to track subject's chest, left and right shoulder and knee's coordinates with the frame rate of 15 frames per second. Two Go Direct respiration belts (®Vernier)[80] were employed to record the respiratory signal as the reference signal of the subject's chest movement. The respiration belt is a force-sensors-based device which can measure the movement of the chest caused by respiration at the sampling rate of 10 Hz.

The work process of vital signal monitoring system is shown in Fig. 6-10. The data is collected by a Kinect camera and three IR-UWB radars. The data is preprocessed by performing data synchronization, resampling and signal denoising [26]. The subject's localization is computed by employing coordinate conversion to Kinect-collected data. The distances between the subject's chest and the radars, the angles between the subject's chest plane and the radars' antenna are also computed based on the Kinect conversion data. According to the angle information, the system selects the radar with the best respiration monitoring angle, the angle between the radar transmission wave and chest plane closest to 90 degrees, to implement the

respiratory signal extraction. The system roughly locates the range bin index according to the distance information from Kinect data, extracts the nearest six range bins data and calculates their variance. The range bin data with the largest variance is selected as the respiratory signal and it is used for the further processing. According to the experiment results, we showed that the system can precisely locate the subjects and extract their respiratory signal. This vital signs monitoring system was designed and developed by the University of Ottawa HEALTH Device Research Group lead by Professor Miodrag Bolic. The thesis author helped to develop the system and took charge of the development of the respiratory pattern classification module.

The collected data stream is time series data and it is segmented by a 15-second overlapping sliding window. The overlap segment length is 12 seconds, which means that it updates the latest 15-second collected signal every 3 seconds. The system runs in real-time to implement the target positioning and breathing rate estimation based on the extracted respiratory signal. After installing the developed respiratory pattern classification model into the system, the system can also output the classification results in real-time.

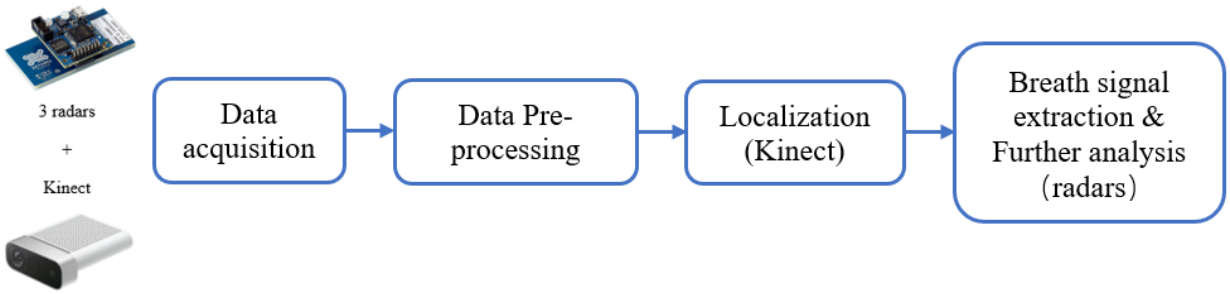

Fig. 6-10 The workflow of vital signal monitoring system

6.2.1 Experiment implementation

In the experiment, the subject was asked to perform eupnea and imitate Cheyne Stokes respiration, Kussmaul breathing and apnea in the monitoring area. The subject was able to move freely during the rest of the time. Two healthy male subjects who did not participate in the experiment mentioned in 6.1 attended this study. Under the circumstance of ensuring that they can complete the experiment task, they determined the duration of the experiment according to the physical conditions. All of the experiment data, including the radar-collected data, Kinect data, respiration belt data, and the system processing outputs like predicted breathing patterns, were recorded. According to the collected data, the experiment duration for one subject was 5

minutes and for the other was 8 minutes. All the data were extracted from the range bin that correspond to the radar-chest distance and the radar which has the best angle to record the chest movement. The radar-collected data had been verified that they are correctly recording the subject's chest movement by comparing the waveform of radar-collected data and the reference respiration belt data, as shown in Fig. 6-11

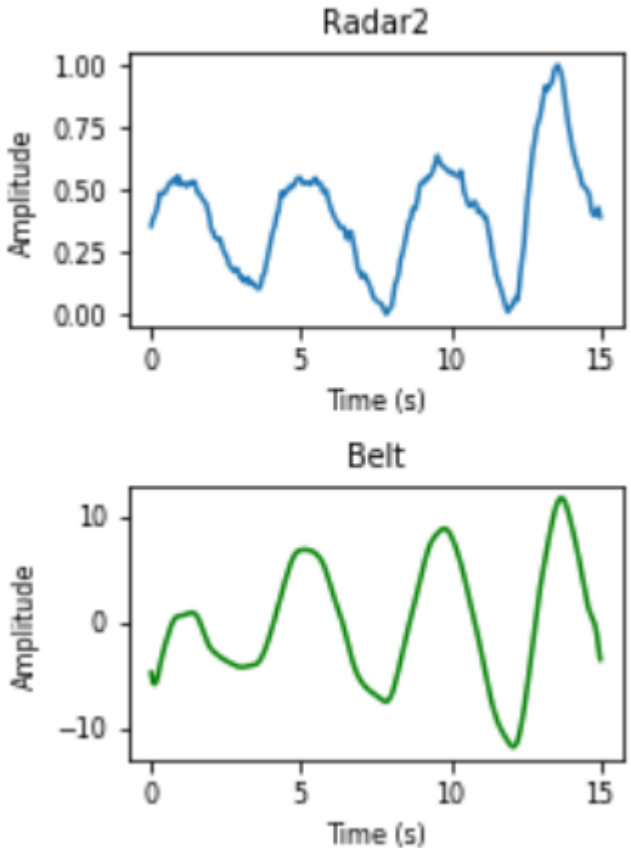

Fig. 6-11 Example of real environment collected radar data verification

According to the data sampling method described in Section 6.2, there were 103 breath samples collected from the first subject and 151 breath samples from the second subject, a total of 254 samples. The respiratory pattern classification is implemented at the moment the collected signal is sampled and transmitted to the model. The experiment protocol was approved by the University of Ottawa Research Ethics Board.

All collected data were manually labeled after the experiment. Comparing with the database test in the previous section, there is a phase of breathing pattern transition in this study. In this study, we labeled those transition phases as "moving" to simplify the labeling.

6.2.2 Traditional classification model

The performance of traditional classification model is shown in Table 6-5 and Fig. 6-12.The overall accuracy is 0.81, and the false alarm ratio is 0.26.

Table 6-5 Classification report of traditional classification model

	precision	recall	f1 score	support
Eupnea	0.86	0.74	0.79	84
Cheyne Stokes	0.55	0.81	0.66	32
Kussmaul	1	1	1	34
Apnea	0.73	1	0.85	11
Moving	0.84	0.77	0.8	93

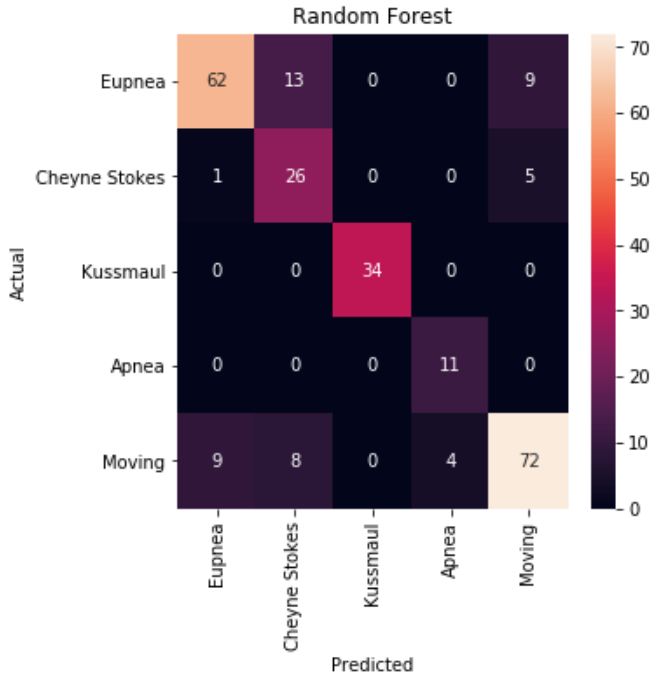

Fig. 6-12 Confusion matrix of traditional classification model

According to the result, the major problems are several eupnea samples were classified as CSR, and some moving samples were classified as apnea. The eupnea samples with large tidal

volume variations are more likely to be classified as CSR. In a real situation, it is normal to have variations in the tidal volume, but only the crescendo or decrescendo variation for a period will be considered to associate with Cheyne Stokes respiration.

For most of the misclassification cases, samples with the “moving” labels while classified as CSR or eupnea belong to the transition phase samples. For the samples with the “moving” label while classified as eupnea, some of them can also be labeled as a breath sample. However, we implemented a strict labeling strategy in this experiment so they were labeled as “moving”, as shown in Fig. 6-13.

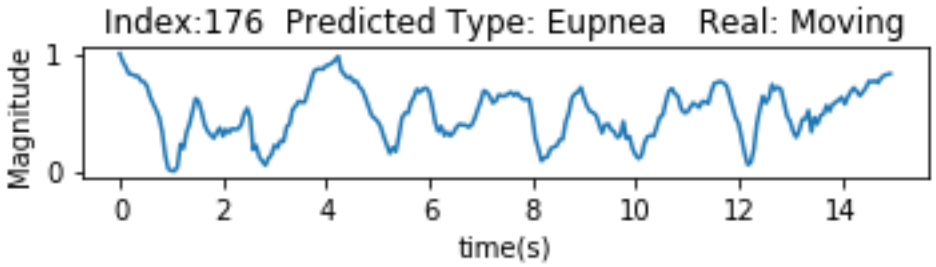

Fig. 6-13 Misclassified moving sample

There are also misclassifications that some moving samples were classified as apnea. The misclassification was caused by the range bin data extraction problem. The problem is that a deviation occurs in the Kinect-based chest-radar distance measuring and the inaccurate distance was sent to the respiratory signal extraction module. If the subject is accurately located, the amplitude of the reflected signal from the subject’s body movement would not be as low as that of the apnea, as shown in Fig. 6-14. This problem occurred in all models because all of them were using the same classification process, which was implemented by the statistic-feature-based classifier.

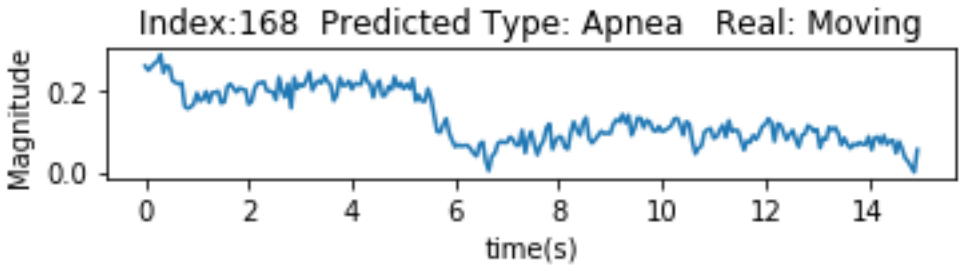

Fig. 6-14 Misclassified moving sample (predicted as apnea)

There is also a small part of the misclassified moving samples as breath samples from the transition phases between each respiratory pattern.

6.2.3 Joint model I

The performance of joint model I with long shapelet is shown in Table 6-6 and Fig. 6-15. The overall accuracy is 0.76, and the false alarm ratio is 0.10.

Table 6-6 Classification report of Joint model I with long shapelet

	precision	recall	f1 score	support
Eupnea	0.87	0.69	0.77	84
Cheyne Stokes	0.8	0.25	0.38	32
Kussmaul	1	1	1	34
Apnea	0.73	1	0.85	11
Moving	0.63	0.87	0.73	93

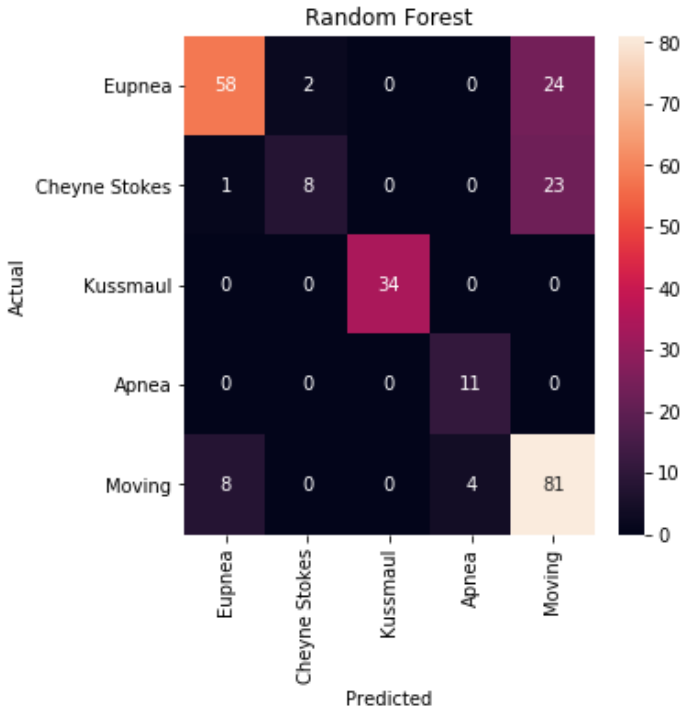

Fig. 6-15 Confusion matrix of Joint model I with long shapelet

In Joint model I, the shapelet transform classifier only classified CSR and the "moving" signal, and the traditional classifier classified the rest of the classes. Therefore, the problems caused by the traditional classifier also showed up in this model. However, comparing with the traditional model, the transition phase samples from CSR are all classified as moving, and the cases of classifying eupnea as CSR are largely reduced because the shapelet transform classifier performs better in recognizing the crescendo or decrescendo phases in eupnea samples with large tidal volume variation. Hence the precision of predicting CSR is significantly improved. There is fewer CSR samples were recognized because models with long shapelets have low CSR sensitivity.

The performance of Joint model I with short shapelet is shown in Table 6-7 and Fig. 6-16. The overall accuracy is 0.77, and the false alarm ratio is 0.28.

Table 6-7 Classification report of Joint model I with short shapelet

	precision	recall	f1 score	support
Eupnea	0.87	0.69	0.77	84
Cheyne Stokes	0.52	0.81	0.63	32
Kussmaul	1	1	1	34
Apnea	0.73	1	0.85	11
Moving	0.76	0.72	0.74	93

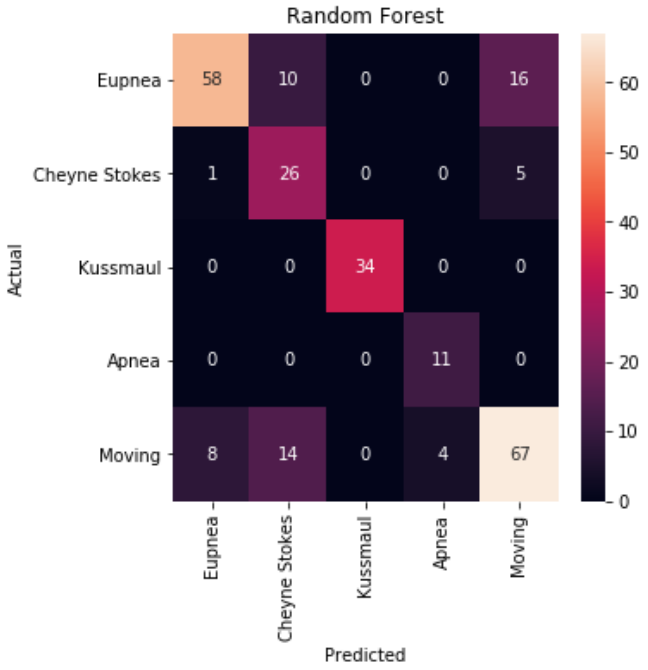

Fig. 6-16 Confusion matrix of Joint model I with short shapelet

Comparing with the Joint model I with long shapelet, this model has lower precision in predicting CSR. This is because short shapelet model is expected to extract samples with at least one respiration pulse, regardless of the overall number of respiration pulses. However, in the continuous monitoring system, most of the samples with the "moving" label are transition phase samples or samples with irregular peaks, as shown in Fig. 6-17, which caused the misclassification. Meanwhile it also retrieved more CSR samples than Joint model with long shapelet, therefore it has a high recall.

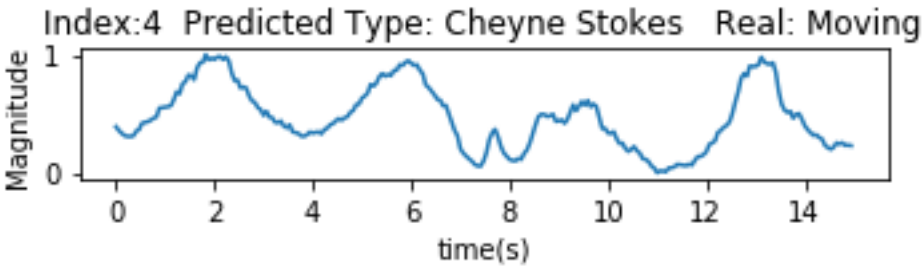

Fig. 6-17 Misclassified moving samples

6.2.4 Joint model II

The performance of Joint model I with short shapelet is shown in Table 6-8 and Fig. 6-18. The overall accuracy is 0.80, and the false alarm ratio is 0.05.

Table 6-8 Classification report of Joint model II

	precision	recall	f1-score	support
Eupnea	1	0.56	0.72	68
Cheyne Stokes	0.95	0.59	0.73	32
Kussmaul	0.97	0.91	0.94	34
Apnea	0.9	0.82	0.86	11
Moving	0.7	0.99	0.82	109

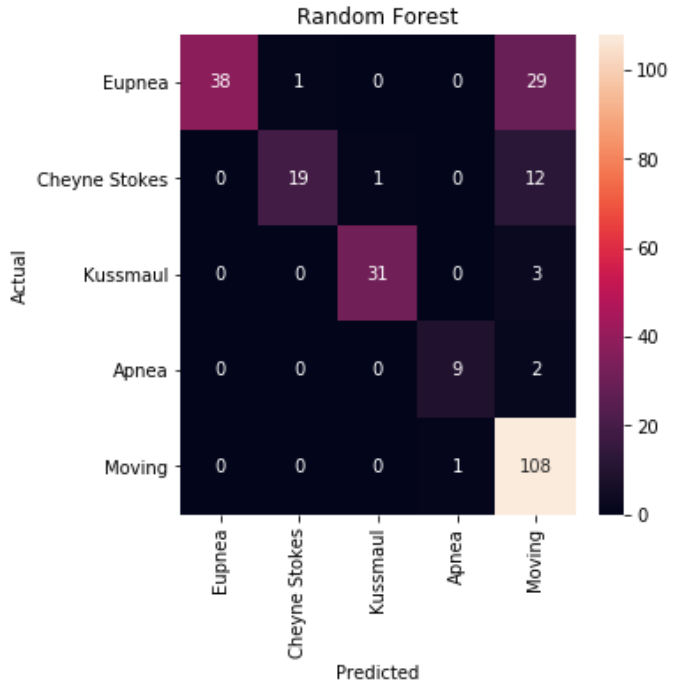

Fig. 6-18 Confusion matrix of Joint model II

In Joint model II, the traditional classifier is only used to recognize apnea samples, and the shapelet transform classifier classified the rest of the classes. Thus, the problem caused by the

shapelet transform classifier that some breath samples were classified as moving also existed. However, comparing with Joint model I with long shapelet, joint model II has a better performance in recognizing CSR. Comparing with Joint model I, which only needs to learn how to distinguish between CSR and “moving” signal, Joint model II needs to learn more types of patterns. Therefore, the model extracts better CSR shapelets to differentiate CSR from eupnea and Kussmaul, which are also sinusoidal-wave-like signals.

Compared with the other models, fewer "moving" samples were misclassified as apnea. Transition phase samples with a large proportion of apneas were all classified as "moving".

6.2.5 Experiment summary

In this model test, the traditional classification model and Joint model II have the best overall performance, and Joint model II has the lowest false alarm ratio. According to the test, the CSR is the respiratory pattern that is most difficult to be classified. The traditional model and Joint model I with short shapelet retrieved more CSR samples but the precision is low. By contrast, Joint model I with long shapelet and Joint model II retrieved less CSR samples, while the precision is high. The advantage of high precision of shapelet transform classification is obvious in the model with long shapelet.

All models had good performance in recognizing eupnea and Kussmaul breathing, but Joint model II outperformed the other models in recognizing apnea. Most of the misclassification of signals with the "moving" label was owing to the breathing pattern transition phase. Considering the number and precision of the classification, Joint model II is the best candidate for continuous monitoring.

6.3 Experiment comparison

This section compares the differences between the experiments in Section 6.1 and Section 6.2 in the perspective of the collected signal to evaluate the performance of the proposed models.

In the database experiment, data samples were collected from independent experiments with a duration of one minute. In the 1-minute experiment, the volunteers were asked to maintain a fixed radar-chest distance and constantly repeat the specific breathing pattern. They also needed

to remain stationary to ensure the quality of the collected data. Each 1-minute data collected in the experiment is divided into four independent 15-second samples with no overlap.

In the continuous monitoring system experiment, the subjects did not have any movement constraints or posture requirements, and because the radar chest distance is measured by the Kinect camera, the subjects could move freely in the monitoring zone. The experimental setup was trying to simulate the model's expected application scenarios. The data collected in this experiment is sampled with a 15-second overlapping sliding window; the overlap segment length is 12 seconds.

The difference of experiment setting leads to 4 significance differences in the collected signal:

1. "Moving" samples: More "moving" samples have breath-like signal segments in the continuous monitoring system than the database. The "moving" class is used to classified the distorted signals or the signals that do not belong to any of the four breathing patterns. Most of the "moving" samples in the database are completely distorted signals, but most of them in continuous monitoring system are samples from pattern transition phase, like "eupnea-CSR", "eupnea-Kussmaul", "eupnea-distorted", as shown in Fig. 6-19.

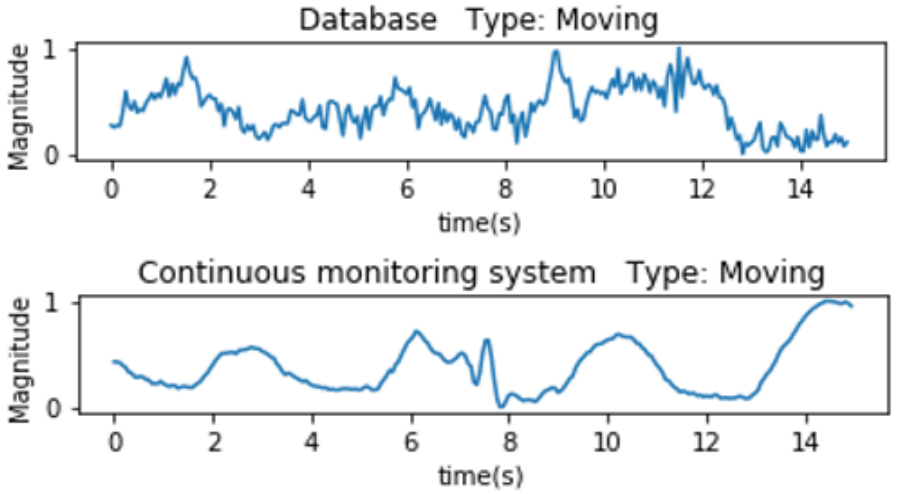

Fig. 6-19 "Moving" samples comparison

There are fewer cases of completely distorted samples in the continuous monitoring system. Only the samples collected in the condition that the subject is continuously moving with a duration longer than 10 seconds are completely distorted. This difference causes the

performance differences of Joint model I with short shapelet in two experiments. This model works in a way that the shapelet transform classifier which implemented the classification of CSR and the "moving" signal was designed to differentiate these two classes based on the respiration pulse only. Meanwhile, the moving samples in the first experiment do not contain respiration pulse, while most of the "moving" signals in the second experiment have respiration pulses. Therefore, the precision of classifying the CSR signal in the first experiment is high and the precision in the second experiment is low.

2. Signal-to-noise ratio: The overall signal-noise ratio (SNR) in the continuous monitoring system is higher than that in the database. In the continuous monitoring system, the respiratory signals are collected from three radars, and the system extracts the respiratory signal from the radar with the best respiration monitoring angle. However, the respiration data in the database are collected by only one radar. In each independent experiment, the experiment environments may vary, and the radar monitoring angles may vary as well. The more the angle variance, the worse the signal quality. Without a setting to automatically select the best reflective signals, some breath samples with low SNR caused by bad monitoring angles are stored in the database. A sample with low SNR in the database is shown in Fig. 6-20. The signal with low SNR is hard to be classified as a breath sample by the shapelet transform classifier with a long shapelet.

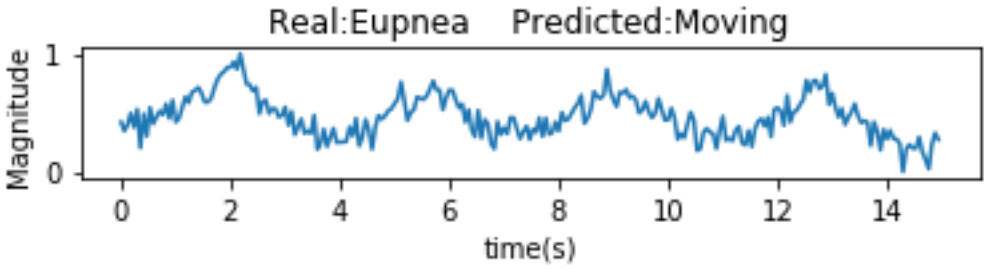

Fig. 6-20 Distorted signal in database

3. Signal waveform diversity: For the respiratory signal database, there are samples from nine subjects; for the continuous monitoring, there are only samples from two subjects. Some subjects have unique breathing patterns that vary from the respiration data in the training database, which may cause poor performance for models with long shapelet. This condition had been described previously. Therefore, the performance of shapelet based models in different types of respiratory signals will vary greatly, especially for Joint model II which

largely depends on shapelet transform classifier. This is the reason why Joint model II performed well in continuous monitoring, but performed bad in database experiment.

4. Signal waveform characteristic: Most of the CSR samples in the database have a waveform characteristic of sharp peak, as shown in Fig. 6-3, which are different from the CSR waveforms in the training data. The hyperventilation frequency of the CSR samples in database are also higher than that in continuous monitoring. The reason is that, in the database experiment, volunteers were asked to imitate each breathing pattern for 1 minute in each experiment set; thus they mainly focused on performing the imitation accurately and completely, regardless of their physical conditions after the experiment. This simulation manner unintentionally makes the breath performing unnaturally. These unnatural breaths are reflected by the sharp peak of the respiration pulse. This situation mainly existed in the simulation of Cheyne Stokes respiration. In the continuous monitoring experiment, this situation did not show up since the subjects were asked to participate as long as possible.

6.4 Model evaluation

This section summarizes the performance of the models according to the performance in each experiment, and evaluates the feasibility of applying them to continuous respiratory pattern classification based on their false alarm ratio report, as shown in Table 6-9. All the models were run on a computer with Intel i7-9750H CPU with 16 GB of RAM.

Table 6-9 Models false alarm ratio report

	Traditional pattern classification	Joint model I with long shapelet	Joint model I with short shapelet	Joint model II
Database	0.27	**0.16**	0.22	0.31
Continuous monitoring	0.26	0.10	0.28	**0.05**

6.4.1 Traditional respiratory pattern classification

The traditional classification model has good overall accuracy in both studies. It has a high F_1 score in each class which indicates its balanced performance in classifying each pattern. The

average classification time per sample is 0.008 seconds, which is the fastest classifier among all. However, it makes a lot of misclassification that it recognizes eupnea samples as CSR, which may cause a high false alarm ratio. To sum up, it is a good candidate for offline classification rather than continuous respiratory pattern classification.

6.4.2 Joint model I with long shapelet

Joint model I with long shapelet also has a balanced performance in the two experiments. The average classification time per sample is 0.054 seconds. The major disadvantage of this model is the low sensitivity to Cheyne Stokes respiration. According to the F_1 score, it has the worst performance in recognizing Cheyne Stokes respiration in this thesis. However, regardless of the influence from its traditional classification components, its implementation of shapelet transform classifier with long shapelet ensures the high precision in classifying Cheyne Stokes respiration. With a high precision in classifying each breathing pattern, it is a good candidate for continuous monitoring.

6.4.3 Joint model I with short shapelet

This model has the best performance in database experiment, but also has the worst performance in continuous monitoring, as the reason explained in Section 6.3. According to the F_1 score, its performance in classifying each breathing pattern is as good as the traditional pattern classification model. The average classification time per sample is 0.057 seconds. It has the highest recall in Cheyne Stokes respiration in the study, so it is the most sensitive model in retrieving Cheyne Stokes respiration. However, it also has a low precision in classifying CSR signals, which leads to high false alarm ratio in the breathing pattern classification. To sum up, it is the best candidate for offline analysis rather than continuous monitoring.

6.4.4 Joint model II

Joint model II performed better than the other models in continuous monitoring experiment, but performed badly in database experiment. The second, third and forth reason in Section 6.3 explained the reason for this difference. The average classification time per sample is 0.105 seconds, which is the slowest model among all in this thesis, but it is still fast enough for implementing the model in real-time.

The major disadvantage of this model is that it cannot accurately recognize the respiratory pattern which waveform is different from that of the training database. One potential solution in this stage is to personalize the model with the respiration data of the monitoring subject, in other words, train the model with the respiratory signal of the subject. For the subjects whose breathing characteristic is similar to that of the simulation data, this model is still the best candidate for the continuous respiratory pattern classification because of the highest precision in recognizing the breath samples.

6.5 Summary

In this chapter, we implemented two experiments to test the models developed in Chapter 5. In the first experiment, we evaluated the model performance based on the radar-collected respiratory signal database built in Section 5.1.1. In the second experiment, we test the model performance by integrating them into a continuous vital signal monitoring system. According to the experiment results, we found that we can utilize the characteristic of shapelet transform classifier that it can achieve a higher precision at the cost of a lower recall, to lower the false alarm ratio in continuous respiratory pattern classification. With the strategy of introducing the “moving” class in classification and implementing the shapelet transform classification model, breath samples with unobvious pattern features will be classified as "moving" signals, thereby improving the precision of respiratory pattern classification.

Chapter 7: Conclusion

This chapter summarizes the major work of the thesis, demonstrates our contribution, and proposes the plan for our future work.

7.1 Summary of work

This thesis aims to propose a full-automatic respiratory pattern classification strategy for biomedical radar. Biomedical radar can collect breath signals remotely without touching the human body, and the breathing pattern can reflect the health status of the subject. This technology is mainly developed for long-term health monitoring.

The research topic of radar-based respiratory pattern classification has recently aroused researchers' interest, and some classification schemes had been proposed. However, the existing studies cannot perform full-automatic classification. The subject’s body movement will distort the collected respiratory signal, making the classification results inaccurate; thus, the distorted signals need to be filtered out manually.

To implement the breathing pattern classification full-automatically, this thesis proposed two solutions, including introducing a “moving” class to classify the distorted signal into a certain class and shortening the window length to reduce the impact of signal distortion. We also proposed a performance requirement for the continuous respiratory pattern classification that the model’s false alarm ratio should be low, which is based on the expectation that the model could alert the appearance of abnormal breathing patterns to raise the subjects’ attention to their health status. A low false alarm ratio means that the alert is more credible and deserves more attention.

To realize the proposed solutions, we developed a respiration simulation model which can generate one-dimensional data of four breathing patterns, and used the generated data to develop the respiratory pattern classification models. We also introduced the time-series-based shapelet transform algorithms into the state-of-the-art respiratory pattern classification model to meet the performance requirement for continuous respiratory pattern classification.

The models proposed in this study are tested by the data in the radar respiratory signal database built in this study in a batch-processing manner, and are tested by continuously collected data in a stream-processing manner. Both of the experiments proved the feasibility of the models.

7.2 Contribution of work

Monitoring the subject's breathing based on biomedical radar in a non-contact way is suitable for long-term health monitoring. The subject's respiratory pattern can be classified based on the collected respiratory signal to evaluate their health status. However, the radar-collected respiratory signal would be distorted by body movement, influencing the accuracy of respiratory pattern classification. Therefore, the distorted signal should be classified during the continuous breathing pattern classification. Meanwhile, the continuous respiratory pattern classification needs to have a low false alarm ratio since it is expected to warn of the appearance of abnormal breathing patterns. A high false alarm ratio will lead to the warning lack of credibility and raise less subjects' concerns about their potential health problems.

The state-of-the-art respiratory pattern classification study cannot provide solutions to both of the problems mentioned above. Thus, they are only available for batch processing. This thesis proposed several strategies to minimize the effect of signal distortion and reduce the false alarm ratio, including shortening the sampling window length, introducing the "moving" class to classify distorted signals, and implementing the shapelet transform technique in the classification. The proposed strategies have been shown to be applicable in full-automatic continuous respiration monitoring by our implementation.

7.3 Faced challenge

We encountered several challenges in this study. The challenges and their walkarounds are explained below.

- The cycle length of Cheyne Stokes respiration is about 30-90 seconds, but the sample window length is 15 seconds in this thesis. Therefore, there is no complete Cheyne Stokes respiration cycle in the sample. The limitation of the length of the sample reduces the uniqueness of the signal characteristics, thus increasing the difficulty of classification. In this study, the training samples were selected from the Cheyne Stokes

respiration segments with the most significant characteristics, including the crescendo phase, the decrescendo phase, the apnea-crescendo transition phase and the decrescendo-apnea transition phase. In the other breathing categories in this study, these phases do not exist.

- Volunteers sometimes cannot simulate breathing patterns correctly. According to the collected signals, some subjects could not control their breath to simulate the crescendo and decrescendo phase of Cheyne Stokes respiration. Some subjects could not hold their breath stably when simulating apnea, and some subjects were unable to maintain high-frequency and high-intensity breathing to simulate Kussmaul breathing. The problems mentioned above are understandable because it is difficult for human subjects to simulate the abnormal breathing like a patient, especially to precisely control the breathing rhythm and tidal volume. Meanwhile, excessive restrictions on the breathing behavior of the subjects will also reduce the diversity of the collected signals, which eventually affect the performance of the breathing pattern classification model. The problems mentioned above reduce the quality of the signal collected in the real experiments. In order to reduce the impact of these conditions, all research volunteers learned the respiratory patterns in advance and implemented the simulation experiment independently, then all data used for model training has been manually screened to ensure that all of them have clear waveforms and characteristics.
- The model training requires a large number of high quality breath samples. In this study, human subjects had to simulate all considered abnormal breathing patterns, including Cheyne Stokes respiration, Kussmaul breathing and apnea, to provide data for training breathing pattern classification models. However, the volunteers had discomfort when simulating these abnormal breathing patterns, such as dizziness. These symptoms would continue for a period of time even after the experiment. Thus, the volunteers could not withstand a large volume of abnormal breathing simulation experiments, so this study faced the problem of lack of samples of abnormal respiratory patterns. The fact that the subjects were uncomfortable also affected the collected respiratory signal quality. To solve this problem, we developed a respiration simulation model to generate a large amount of simulated breath samples as a substitute for the radar-collected data.

- In the radar-collected respiratory signal, some of the samples do not include segments with salient characteristics, especially for the Cheyne Stokes respiration. In the crescendo-decrescendo transition phase of Cheyne Stokes respiration, the peak variance of the waveform is not as obvious as that of the other phases, and thus it has a high similarity to eupnea. Since the classification model predicts the breathing pattern mainly based on the waveform features, for those signal segments which do not include an obvious characteristic of the respiratory pattern it belongs to, the model will classify them based on their phenotype. For example, for a Cheyne Stokes respiration sample with neither apnea phase nor obvious peak amplitude variation, we classified them as eupnea in this study.

7.4 Future work

Several possible work can be done do improve this thesis, they are presented as follow:

Optimizing the respiration simulation model. The respiration simulation model developed in this thesis is a monoharmonic model, which is too rough to perfectly describe the characteristic of the radar-collected respiratory signal. Introducing the high order harmonics to the model can better describe the real circumstance of radar signal collection. This process can also improve the similarity between the output signal of the model and the real collected signal in time domain and frequency domain.

Using the dynamic-time-warping in the distance calculation instead of calculating the Euclidean distance in the similarity evaluation stage of the shapelet transform classification. The similarity of the extracted shapelets and test samples will be evaluated in a more flexible way. This process can improve the efficiency of shapelet transform and the accuracy of the classification.

Using the long short-term memory (LSTM) recurrent neural network (RNN) algorithm to implement the respiratory pattern classification strategy proposed in this thesis. The classification performance of LSTM-RNN can be compared with the models proposed in this thesis to find the best solution for the full-automatic respiratory pattern classification.

Reference

[1] F. Q. AL-Khalidi, R. Saatchi, D. Burke, H. Elphick, and S. Tan, "Respiration rate monitoring methods: A review," *Pediatric Pulmonology*, vol. 46, no. 6, pp. 523–529, 2011, doi: https://doi.org/10.1002/ppul.21416.

[2] "21.5D: Breathing Patterns," *Medicine LibreTexts*, Jul. 22, 2018. https://med.libretexts.org/Bookshelves/Anatomy_and_Physiology/Book%3A_Anatomy_and_Physiology_(Boundless)/21%3A_Respiratory_System/21.5%3A_Mechanics_of_Breathing/21.5D%3A_Breathing_Patterns (accessed May 29, 2021).

[3] G. Yuan, N. A. Drost, and R. A. McIvor, "Respiratory rate and breathing pattern," *McMaster University Medical Journal*, vol. 10, no. 1, pp. 23–25, 2013.

[4] P. Lanfranchi *et al.*, "Prognostic Value of Nocturnal Cheyne-Stokes Respiration in Chronic Heart Failure," *Circulation*, vol. 99, no. 11, pp. 1435–1440, Mar. 1999, doi: 10.1161/01.CIR.99.11.1435.

[5] J. B. North and S. Jennett, "Abnormal breathing patterns associated with acute brain damage," *Archives of neurology*, vol. 31, no. 5, pp. 338–344, 1974.

[6] "Sudden cardiac arrest - Symptoms and causes," *Mayo Clinic*. https://www.mayoclinic.org/diseases-conditions/sudden-cardiac-arrest/symptoms-causes/syc-20350634 (accessed Jun. 11, 2021).

[7] O. Boric-Lubecke, V. M. Lubecke, A. D. Droitcour, B.-K. Park, and A. Singh, *Doppler radar physiological sensing*. Wiley Online Library, 2016.

[8] S. Z. Gurbuz and M. G. Amin, "Radar-Based Human-Motion Recognition With Deep Learning: Promising Applications for Indoor Monitoring," *IEEE Signal Processing Magazine*, vol. 36, no. 4, pp. 16–28, Jul. 2019, doi: 10.1109/MSP.2018.2890128.

[9] M. Rudrappa, P. Modi, and P. C. Bollu, "Cheyne Stokes Respirations," in *StatPearls*, Treasure Island (FL): StatPearls Publishing, 2020. Accessed: Dec. 08, 2020. [Online]. Available: http://www.ncbi.nlm.nih.gov/books/NBK448165/

[10] "Abnormal Breathing Patterns." https://media.lanecc.edu/users/driscolln/RT127/Softchalk/regulation_of_Breathing/regulation_of_Breathing4.html (accessed Jan. 20, 2021).

[11] C. Li, M.-R. Tofighi, D. Schreurs, and T.-S. J. Horng, *Principles and Applications of RF/microwave in Healthcare and Biosensing*. Academic Press, 2016.

[12] M. Amin, *Radar for indoor monitoring: Detection, classification, and assessment*. CRC Press, 2017.

[13] S. Pisa, E. Pittella, and E. Piuzzi, "A survey of radar systems for medical applications," *IEEE Aerospace and Electronic Systems Magazine*, vol. 31, no. 11, pp. 64–81, Nov. 2016, doi: 10.1109/MAES.2016.140167.

[14] A. K. Gunasekara, "Contactless estimation of breathing rate using UWB radar," PhD Thesis, Université d'Ottawa/University of Ottawa, 2017.

[15] C. Nguyen and M. Miao, *Design of CMOS RFIC Ultra-Wideband Impulse Transmitters and Receivers*. Cham: Springer International Publishing, 2017. doi: 10.1007/978-3-319-53107-6.

[16] M. Malajner, D. Šipoš, and D. Gleich, "Design of a Low-Cost Ultra-Wide-Band Radar Platform," *Sensors (Basel)*, vol. 20, no. 10, May 2020, doi: 10.3390/s20102867.

[17] H. Langen, “Ultra-Wideband Radar Simulator for classifying Humans and Animals based on Micro-Doppler Signatures,” 2016, Accessed: Nov. 18, 2020. [Online]. Available: https://ntnuopen.ntnu.no/ntnu-xmlui/handle/11250/2410706
[18] D. Wang, S. Yoo, and S. H. Cho, “Experimental Comparison of IR-UWB Radar and FMCW Radar for Vital Signs,” *Sensors*, vol. 20, no. 22, Art. no. 22, Jan. 2020, doi: 10.3390/s20226695.
[19] “NOVELDA-x4-datasheet-revF.pdf.” Accessed: Jan. 26, 2021. [Online]. Available: https://novelda.com/content/wp-content/uploads/2021/01/NOVELDA-x4-datasheet-revF.pdf
[20] Z. Baird, “Human Activity and Posture Classification Using Single Non-Contact Radar Sensor,” Master of Applied Science, Carleton University, Ottawa, Ontario, 2017. doi: 10.22215/etd/2017-12170.
[21] N. V. Rivera, S. Venkatesh, C. Anderson, and R. M. Buehrer, “Multi-target estimation of heart and respiration rates using ultra wideband sensors,” in *2006 14th European Signal Processing Conference*, Sep. 2006, pp. 1–6.
[22] S. Chang, R. Sharan, M. Wolf, N. Mitsumoto, and J. W. Burdick, “People tracking with UWB radar using a multiple-hypothesis tracking of clusters (MHTC) method,” *International Journal of Social Robotics*, vol. 2, no. 1, pp. 3–18, 2010.
[23] V.-H. Nguyen and J.-Y. Pyun, “Location Detection and Tracking of Moving Targets by a 2D IR-UWB Radar System,” *Sensors*, vol. 15, no. 3, Art. no. 3, Mar. 2015, doi: 10.3390/s150306740.
[24] F. Khan and S. H. Cho, “A Detailed Algorithm for Vital Sign Monitoring of a Stationary/Non-Stationary Human through IR-UWB Radar,” *Sensors*, vol. 17, no. 2, Art. no. 2, Feb. 2017, doi: 10.3390/s17020290.
[25] M. G. Amin and R. G. Guendel, “Radar Human Motion Recognition Using Motion States and Two-Way Classifications,” in *2020 IEEE International Radar Conference (RADAR)*, Apr. 2020, pp. 1046–1051. doi: 10.1109/RADAR42522.2020.9114613.
[26] S. He, V. Mehta, and M. Bolic, “A Joint Localization Assisted Respiratory Rate Estimation using IR-UWB Radars,” in *2020 42nd Annual International Conference of the IEEE Engineering in Medicine Biology Society (EMBC)*, Jul. 2020, pp. 489–493. doi: 10.1109/EMBC44109.2020.9175754.
[27] H. Zhao *et al.*, “A Noncontact Breathing Disorder Recognition System Using 2.4-GHz Digital-IF Doppler Radar,” *IEEE Journal of Biomedical and Health Informatics*, vol. 23, no. 1, pp. 208–217, Jan. 2019, doi: 10.1109/JBHI.2018.2817258.
[28] D. Miao, H. Zhao, H. Hong, X. Zhu, and C. Li, “Doppler radar-based human breathing patterns classification using Support Vector Machine,” in *2017 IEEE Radar Conference (RadarConf)*, Seattle, WA, USA, May 2017, pp. 0456–0459. doi: 10.1109/RADAR.2017.7944246.
[29] C. Feng, H. Zhao, Q. Liu, H. Hong, C. Gu, and X. Zhu, “Implementation of Radar-based Breathing Disorder Recognition Using FPGA,” in *2019 IEEE MTT-S International Microwave Biomedical Conference (IMBioC)*, Nanjing, China, May 2019, pp. 1–3. doi: 10.1109/IMBIOC.2019.8777851.
[30] “An impedance pneumography signal quality index: Design, assessment and application to respiratory rate monitoring,” *Biomedical Signal Processing and Control*, vol. 65, p. 102339, Mar. 2021, doi: 10.1016/j.bspc.2020.102339.
[31] F. Løberg, V. Goebel, and T. Plagemann, “Quantifying the signal quality of low-cost respiratory effort sensors for sleep apnea monitoring,” in *Proceedings of the 3rd*

International Workshop on Multimedia for Personal Health and Health Care, 2018, pp. 3–11.
[32] A. Dehghani, O. Sarbishei, T. Glatard, and E. Shihab, "A Quantitative Comparison of Overlapping and Non-Overlapping Sliding Windows for Human Activity Recognition Using Inertial Sensors," *Sensors (Basel)*, vol. 19, no. 22, Nov. 2019, doi: 10.3390/s19225026.
[33] J. L. Kernec *et al.*, "Radar Signal Processing for Sensing in Assisted Living: The Challenges Associated With Real-Time Implementation of Emerging Algorithms," *IEEE Signal Processing Magazine*, vol. 36, no. 4, pp. 29–41, Jul. 2019, doi: 10.1109/MSP.2019.2903715.
[34] "Artificial Intelligence: A Modern Approach." http://aima.cs.berkeley.edu/ (accessed Jan. 27, 2021).
[35] V. Vapnik, *The Nature of Statistical Learning Theory*. Springer Science & Business Media, 2013.
[36] S. Ben-David and S. Shalev-Shwartz, Eds., "Decision Trees," in *Understanding Machine Learning: From Theory to Algorithms*, Cambridge: Cambridge University Press, 2014, pp. 212–218. doi: 10.1017/CBO9781107298019.019.
[37] Tin Kam Ho, "The random subspace method for constructing decision forests," *IEEE Transactions on Pattern Analysis and Machine Intelligence*, vol. 20, no. 8, pp. 832–844, Aug. 1998, doi: 10.1109/34.709601.
[38] F. Pedregosa *et al.*, "Scikit-learn: Machine Learning in Python," *Journal of Machine Learning Research*, vol. 12, no. 85, pp. 2825–2830, 2011.
[39] R. J. Urbanowicz, M. Meeker, W. La Cava, R. S. Olson, and J. H. Moore, "Relief-based feature selection: Introduction and review," *Journal of Biomedical Informatics*, vol. 85, pp. 189–203, Sep. 2018, doi: 10.1016/j.jbi.2018.07.014.
[40] M. Robnik-Šikonja and I. Kononenko, "Theoretical and Empirical Analysis of ReliefF and RReliefF," *Machine Learning*, vol. 53, no. 1, pp. 23–69, Oct. 2003, doi: 10.1023/A:1025667309714.
[41] "Confusion matrix," *Wikipedia*. Feb. 27, 2021. Accessed: Mar. 01, 2021. [Online]. Available: https://en.wikipedia.org/w/index.php?title=Confusion_matrix&oldid=1009198831
[42] M. Löning, A. Bagnall, S. Ganesh, V. Kazakov, J. Lines, and F. J. Király, "sktime: A Unified Interface for Machine Learning with Time Series," *arXiv:1909.07872 [cs, stat]*, Sep. 2019, Accessed: Nov. 24, 2020. [Online]. Available: http://arxiv.org/abs/1909.07872
[43] A. Bagnall, J. Lines, A. Bostrom, J. Large, and E. Keogh, "The great time series classification bake off: a review and experimental evaluation of recent algorithmic advances," *Data Mining and Knowledge Discovery; New York*, vol. 31, no. 3, pp. 606–660, May 2017, doi: http://dx.doi.org.proxy.bib.uottawa.ca/10.1007/s10618-016-0483-9.
[44] J. Lines, L. M. Davis, J. Hills, and A. Bagnall, "A shapelet transform for time series classification," in *Proceedings of the 18th ACM SIGKDD international conference on Knowledge discovery and data mining - KDD '12*, Beijing, China, 2012, p. 289. doi: 10.1145/2339530.2339579.
[45] A. Bostrom and A. Bagnall, "Binary Shapelet Transform for Multiclass Time Series Classification," in *Big Data Analytics and Knowledge Discovery*, Cham, 2015, pp. 257–269. doi: 10.1007/978-3-319-22729-0_20.
[46] C. E. Shannon, "Communication in the Presence of Noise," *Proceedings of the IRE*, vol. 37, no. 1, pp. 10–21, Jan. 1949, doi: 10.1109/JRPROC.1949.232969.

[47] “ASL 5000 Breathing Simulator,” *IngMar Medical*. https://www.ingmarmed.com/product/asl-5000-breathing-simulator/ (accessed Jan. 22, 2021).
[48] “QuickLung Breather,” *IngMar Medical*. https://www.ingmarmed.com/product/quicklung-breather/ (accessed Jan. 22, 2021).
[49] “Breathing Simulator For Clinical Calibration Testing | Michigan Instruments.” https://www.michiganinstruments.com/lung-simulators/breathing-simulator-module/ (accessed Jan. 22, 2021).
[50] “Breathing Phantom | Mirion Technologies (Capintec), Inc.” https://capintec.com/product/breathing-phantom/ (accessed Jan. 22, 2021).
[51] “RS-1500 Breathing Phantom,” *Radiology Support Devices*. http://rsdphantoms.com/radiology/rs1500/ (accessed Jan. 22, 2021).
[52] “QUASAR™ Respiratory Motion Phantom (pRESP) - Breathing Phantom,” *Modus Medical Devices*. https://modusqa.com/products/quasar-respiratory-motion-phantom-presp/ (accessed Jan. 22, 2021).
[53] D. Makowski *et al.*, “NeuroKit2: A Python Toolbox for Neurophysiological Signal Processing.” PsyArXiv, Jul. 06, 2020. doi: 10.31234/osf.io/eyd62.
[54] S. C. Deshmukh, B. B. Godbole, and R. M. Yadahalli, “Simplistic Simulation for Radar Based Life Signal Detection,” vol. 9, no. 3, p. 6, 2020.
[55] K. Y. Gavrilov and T. Y. Shevgunov, “A New Model of Human Respiration for Algorithm Simulation Modeling in Radar Applications,” in *2020 Systems of Signals Generating and Processing in the Field of on Board Communications*, Mar. 2020, pp. 1–5. doi: 10.1109/IEEECONF48371.2020.9078569.
[56] D. R. Morgan and M. G. Zierdt, “Novel signal processing techniques for Doppler radar cardiopulmonary sensing,” *Signal Processing*, vol. 89, no. 1, pp. 45–66, Jan. 2009, doi: 10.1016/j.sigpro.2008.07.008.
[57] Y. Wang, M. Hu, Q. Li, X.-P. Zhang, G. Zhai, and N. Yao, “Abnormal respiratory patterns classifier may contribute to large-scale screening of people infected with COVID-19 in an accurate and unobtrusive manner,” *arXiv:2002.05534 [cs, eess]*, Feb. 2020, Accessed: Nov. 04, 2020. [Online]. Available: http://arxiv.org/abs/2002.05534
[58] D. Alinovi, “Markov chain modeling and simulation of breathing patterns,” *Biomedical Signal Processing and Control*, p. 10, 2017.
[59] W. Karlen, “CapnoBase Respiratory Event Benchmark.” Scholars Portal Dataverse, Jan. 03, 2021. doi: 10.5683/SP2/B1DDKP.
[60] *neuropsychology/NeuroKit*. École de Neuropsychologie, 2021. Accessed: Jan. 22, 2021. [Online]. Available: https://github.com/neuropsychology/NeuroKit
[61] M. J. Tobin, “Breathing pattern analysis,” *Intensive Care Med*, vol. 18, no. 4, pp. 193–201, Apr. 1992, doi: 10.1007/BF01709831.
[62] S. Sharma, U. Mukhtar, C. Kelly, P. Mather, and S. F. Quan, “Recognition and Treatment of Sleep-Disordered Breathing in Obese Hospitalized Patients May Improve Survival. The HoSMed Database,” *The American Journal of Medicine*, vol. 130, no. 10, pp. 1184–1191, Oct. 2017, doi: 10.1016/j.amjmed.2017.03.055.
[63] Medical Advisory Secretariat, “Polysomnography in patients with obstructive sleep apnea: an evidence-based analysis,” *Ont Health Technol Assess Ser*, vol. 6, no. 13, pp. 1–38, 2006.

[64] T. D. da Costa, M. de F. F. Vara, C. S. Cristino, T. Z. Zanella, G. N. N. Neto, and P. Nohama, "Breathing Monitoring and Pattern Recognition with Wearable Sensors," *Wearable Devices - the Big Wave of Innovation*, Jun. 2019, doi: 10.5772/intechopen.85460.
[65] A. R. Fekr, M. Janidarmian, K. Radecka, and Z. Zilic, "A Medical Cloud-Based Platform for Respiration Rate Measurement and Hierarchical Classification of Breath Disorders," *Sensors*, vol. 14, no. 6, Art. no. 6, Jun. 2014, doi: 10.3390/s140611204.
[66] A. R. Fekr, M. Janidarmian, K. Radecka, and Z. Zilic, "Respiration Disorders Classification With Informative Features for m-Health Applications," *IEEE Journal of Biomedical and Health Informatics*, vol. 20, no. 3, pp. 733–747, May 2016, doi: 10.1109/JBHI.2015.2458965.
[67] Y. Wang *et al.*, "Unobtrusive and Automatic Classification of Multiple People's Abnormal Respiratory Patterns in Real Time Using Deep Neural Network and Depth Camera," *IEEE Internet of Things Journal*, vol. 7, no. 9, pp. 8559–8571, Sep. 2020, doi: 10.1109/JIOT.2020.2991456.
[68] Y. S. Lee, P. N. Pathirana, C. L. Steinfort, and T. Caelli, "Monitoring and Analysis of Respiratory Patterns Using Microwave Doppler Radar," *IEEE Journal of Translational Engineering in Health and Medicine*, vol. 2, pp. 1–12, 2014, doi: 10.1109/JTEHM.2014.2365776.
[69] Y. S. Lee, P. N. Pathirana, and C. L. Steinfort, "Respiration rate and breathing patterns from Doppler radar measurements," in *2014 IEEE Conference on Biomedical Engineering and Sciences (IECBES)*, Dec. 2014, pp. 235–240. doi: 10.1109/IECBES.2014.7047493.
[70] T. Mitsa, "How Do You Know You Have Enough Training Data?," *Medium*, Apr. 23, 2019. https://towardsdatascience.com/how-do-you-know-you-have-enough-training-data-ad9b1fd679ee (accessed Feb. 16, 2021).
[71] L. R. Barnes, D. M. Schultz, E. C. Gruntfest, M. H. Hayden, and C. C. Benight, "CORRIGENDUM: False Alarm Rate or False Alarm Ratio?," *Weather and Forecasting*, vol. 24, no. 5, pp. 1452–1454, Oct. 2009, doi: 10.1175/2009WAF2222300.1.
[72] "Precision and recall," *Wikipedia*. Feb. 22, 2021. Accessed: Feb. 25, 2021. [Online]. Available: https://en.wikipedia.org/w/index.php?title=Precision_and_recall&oldid=1008201122
[73] R. Banstola, R. Bera, and D. Bhaskar, "Review and Design of UWB Transmitter and Receiver," *International Journal of Computer Applications*, vol. 69, pp. 25–28, May 2013, doi: 10.5120/11903-7978.
[74] A. Minagar and W. J. Weiner, "Adolf Kussmaul and His Respiratory Sign," *J Med Biogr*, vol. 9, no. 3, pp. 181–183, Aug. 2001, doi: 10.1177/096777200100900311.
[75] A. R. Fekr, K. Radecka, and Z. Zilic, "Tidal volume variability and respiration rate estimation using a wearable accelerometer sensor," in *2014 4th International Conference on Wireless Mobile Communication and Healthcare - Transforming Healthcare Through Innovations in Mobile and Wireless Technologies (MOBIHEALTH)*, Nov. 2014, pp. 1–6. doi: 10.1109/MOBIHEALTH.2014.7015894.
[76] M. T. Naughton, "Cheyne–Stokes respiration: friend or foe?," *Thorax*, vol. 67, no. 4, pp. 357–360, Apr. 2012, doi: 10.1136/thoraxjnl-2011-200927.
[77] V. Cizek, "Discrete hilbert transform," *IEEE Transactions on Audio and Electroacoustics*, vol. 18, no. 4, pp. 340–343, 1970.

[78] A. Hernandez-Matamoros, H. Fujita, and H. Perez-Meana, “A novel approach to create synthetic biomedical signals using BiRNN,” *Information Sciences*, vol. 541, pp. 218–241, Dec. 2020, doi: 10.1016/j.ins.2020.06.019.
[79] *alan-turing-institute/sktime*. The Alan Turing Institute, 2021. Accessed: Jan. 06, 2021. [Online]. Available: https://github.com/alan-turing-institute/sktime
[80] “Go Direct® Respiration Belt,” *Vernier*. https://www.vernier.com/product/go-direct-respiration-belt/ (accessed Jan. 12, 2021).

Appendix

File Number: H08-17-27 **Date (mm/dd/yyyy):** 11/29/2020

Université d'Ottawa University of Ottawa
Bureau d'éthique et d'intégrité de la recherche Office of Research Ethics and Integrity

Ethics Approval Notice

Health Sciences and Science REB

Principal Investigator / Supervisor / Co-investigator(s) / Student(s)

First Name	Last Name	Affiliation	Role
Miodrag	Bolic	Engineering / Computer Science	Principal Investigator

File Number: H08-17-27

Type of Project: Professor

Title: Contactless Detection of Breathing and Falls of Humans using UWB RADAR and 3D Motion Sensor

Renewal Date (mm/dd/yyyy)	Expiry Date (mm/dd/yyyy)	Approval Type
10/27/2020	10/26/2021	Renewal

Special Conditions / Comments:

Team members:
Fan Yang Engineering / Computer Science Co-Investigator
Zixiong Han Engineering / Computer Science Co-Investigator

550, rue Cumberland, pièce 154 550 Cumberland Street, room 154
Ottawa (Ontario) K1N 6N5 Canada Ottawa, Ontario K1N 6N5 Canada
(613) 562-5387 • Téléc./Fax (613) 562-5338
www.recherche.uottawa.ca/deontologie/ www.research.uottawa.ca/ethics/

Université d'Ottawa University of Ottawa
Bureau d'éthique et d'intégrité de la recherche Office of Research Ethics and Integrity

This is to confirm that the University of Ottawa Research Ethics Board identified above, which operates in accordance with the Tri-Council Policy Statement (2010) and other applicable laws and regulations in Ontario, has examined and approved the ethics application for the above named research project. Ethics approval is valid for the period indicated above and subject to the conditions listed in the section entitled "Special Conditions / Comments".

During the course of the project, the protocol may not be modified without prior written approval from the REB except when necessary to remove participants from immediate endangerment or when the modification(s) pertain to only administrative or logistical components of the project (e.g., change of telephone number). Investigators must also promptly alert the REB of any changes which increase the risk to participant(s), any changes which considerably affect the conduct of the project, all unanticipated and harmful events that occur, and new information that may negatively affect the conduct of the project and safety of the participant(s). Modifications to the project, including consent and recruitment documentation, should be submitted to the Ethics Office for approval using the "Modification to research project" form available at: https://research.uottawa.ca/ethics/forms.

Please submit an annual report to the Ethics Office four weeks before the above-referenced expiry date to request a renewal of this ethics approval. To close the file, a final report must be submitted. These documents can be found at: https://research.uottawa.ca/ethics/forms.

If you have any questions, please do not hesitate to contact the Ethics Office at extension 5387 or by e-mail at: ethics@uOttawa.ca.

Signature:

Marc Alain Bonenfant
Research Ethics Coordinator
For Catherine Paquet, Director of the Office of Research Ethics and Integrity

550, rue Cumberland, pièce 154 550 Cumberland Street, room 154
Ottawa (Ontario) K1N 6N5 Canada Ottawa, Ontario K1N 6N5 Canada
(613) 562-5387 • Téléc./Fax (613) 562-5338
www.recherche.uottawa.ca/deontologie/ www.research.uottawa.ca/ethics/